STRESS-STRAIN RELATIONSHIPS FOR PLASTICS

BY

J. G. Williams, B.Sc.(Eng.), A.C.G.I.

J U L Y 1 9 6 3

Thesis presented for the degree of
Doctor of Philosophy
in the
University of London

Abstract

In Part One the use of the plane strain compression test to determine stress-strain relationships for plastics is described. Factors such as friction and specimen and die geometry are examined in detail. Both total and permanent deformation tests are considered. The stress-strain curves obtained are then used to predict behaviour under other stress systems. The examples of uniform stress systems used are simple tension, a thin walled cylinder under internal pressure, and equal biaxial tension. The non-uniform stress system of the torsion of a solid circular rod is also considered and the prediction of instability points for such a system is illustrated with a thick walled cylinder under internal pressure.

Some aspects of the general problem of complex loading paths are then examined.

Part Two considers the design, calibration and testing procedure of a machine designed to measure the impact strength of polymer film. The results of the impact test, a notch sensitivity test and an impact fatigue test are given. The effect of friction is then analysed by means of methods described in Part One. The impact strength of polyethylene film is interpreted in terms of stress-strain relationships derived from the plane strain compression test and the tension test.

Acknowledgements

The author wishes to thank Professor Hugh Ford for his supervision and encouragement throughout this work. He would also like to thank Mr. A. Donald for his technical assistance in performing the tests.

Contents

Contents (continued) Page

General Introduction

Most of the research work carried out on plastics is concerned with the physics and chemistry of the molecular structure. Such work is valuable but it is considered that there is room for a more practical engineering approach to the understanding of the mechanical properties of these materials. The work described here examines the stress-strain relationships for plastics under various conditions and the derivation from this data of techniques suitable for design work.

The results of this investigation are presented in two parts. Part One deals with fundamental aspects of the problem. An accurate experimental technique for determining stress-strain data is first examined. This is followed by an examination of a method of analysis for using this data to predict the behaviour of various stress systems. It was considered that a more useful purpose would be served at this stage by considering the problem broadly. It is hoped that what has been sacrificed in detail is compensated for by the range of problems considered.

Part Two is concerned with the application

of some of these results to one particular practical problem; the impact testing of polymer film. The testing of this film is of interest to a wide range of users and many problems required solution. A new type of testing machine is examined in detail and the results from several types of film are described. An interpretation of these results in the light of the information obtained in Part One is then given.

PART I

1.0. Introduction

The increasing range of application of plastics in engineering in recent years has involved designers in the stress analysis of plastics. The complex behaviour which plastics exhibit under load is generally outside the scope of existing engineering design procedure developed largely for metals. This is often ignored and much poor design results. This work examines the suitability of certain established techniques when applied to plastics.

The designer in plastics requires a number of mechanical tests, (the fewer the better), to provide the basic mechanical properties of the material and an analytical technique to enable the stresses and deformations under loading conditions to be predicted.

The first essential is to examine the testing methods used and determine their limitations when applied to plastics.

2.0. Testing Methods

The tensile test is the most frequently employed test for metals and it has been freely applied to plastics. It has the advantages that it is easily performed and that equipment, designed for metals, is available. Much work has been done by extending the usual static test to include

the effects of strain rates and temperature but very little to determine the validity of the results obtained. For example a typical load extension curve for polyethylene is shown diagrammatically in Figure 1.

Over the section O - A the load increases and by correcting for area reduction a true stress strain curve may be obtained. The majority of this extension is recoverable but just prior to A flow is instigated, and the load peak results. At some point B after A the load becomes constant and the extension proceeds at constant load to C. The position B is governed by the machine stiffness and is a point of mechanical instability. A neck will often form at A and the material in the neck will work-harden due to orientation until it is harder than that in the shoulder of the neck. The material in the shoulder will then flow into the neck. This is the process represented by BC. When the neck has reached the ends of the specimens the orientated neck section is then extended giving CD. Thus the constant load region BC is a material and machine instability phenomenon and yields no fundamental stress/strain relations.

Such effects are not, of course, found in all tests but their occurrence is not always obvious and they can lead to erroneous conclusions. The test is useful

for fairly small strains, generally up to the onset of flow, but beyond this the difficulties of determining the strains involved are considerable.

Other tests have been devised to overcome these difficulties. Ref. (1) describes a bending test which employs a three point loading system on a beam specimen. This is essentially a small strain test for, although the deflections may be large, the corresponding strains are small. Torsional pendulums have also been employed for visco-elastic tests but these also are for small strains.

Similar problems have been encountered in examining the large strain behaviour of metals and a test designed to overcome them is the plane strain compression test, devised and developed by Ford (Ref. (2)) to investigate the work hardening characteristics of metals. This has not previously been applied to plastics and an investigation was carried out to determine its suitability for testing plastics.

3.0. Plane Strain Compression Test

The specimen in the form of a flat plate is placed between two, parallel, flat, highly polished dies (see Fig. 2) which are forced into the plate from either side. The dies are lubricated to give negligible friction and the specimen suffers no constraint in the direction normal to

to the dies. The deformed material under the tools is restrained from moving parallel to the tools by the constraint of the undeformed material on either side of the deformed section. The test has the advantage that the area under load remains constant and no instability due to reduction in area can occur.

The technique was developed by Watts and Ford (ref. (2)) for determining the permanent deformation curves for metals and has been widely applied to cold rolling and lubrication problems. Thus a great deal of practical and theoretical information is available for its application to metals and appropriate tests were carried out to determine if this information is applicable to plastics.

Plastics are time dependent materials and have complex creep and recovery behaviour. To determine a "permanent" deformation curve it was necessary to fix an arbitrary definition of the deformations which may be regarded as "permanent". It was found that for the materials examined (polyethylene, PVC and Nylon) that any deformations still present 24 hours after unloading does not recover appreciably over any further period. In what follows this deformation is termed "permanent". For some short term tests a deformation after 10 minutes is quoted but this is given only in comparative tests. The interval for which the

load is applied is also important and for the determination of the permanent deformations the loads were applied for a 'dwell' time of 10 minutes. Further discussion of this point will be given later.

The deformation in the tests is defined by means of the ratio λ where,

$$\lambda = \frac{h}{h_o}$$

h = Deformed specimen thickness

h_o = Original specimen thickness.

The permanent deformation test is similar to that used for metals but for plastics a total deformation test may also be performed. This is unpractical for metals as the recoverable, elastic deformations, are of the same order as the deformations of the apparatus and corrections would be large. For plastics however the recoverable deformations are generally much larger than those of the apparatus and the load total deflection curves may be obtained accurately. As the materials are strain rate dependent it is necessary to obtain these curves under continuous loading at a constant speed. A special case, the semi-static test, which arises from this, will be discussed later.

The basic apparatus used in both the total and permanent tests is shown in Figure 3. It consists of a

sub-press with two pillars fitted with ball-bearing sleeves to give low friction. The use of the sub-press ensures that the tools are always rigid and parallel. A high degree of rigidity is required as it is essential that the tools remain parallel throughout the test if plane strain conditions are to be maintained.

Before examining the total and permanent deformation plane strain compression tests in detail separately it is desirable to consider first the most important factors which apply equally to both. These factors are friction and the geometry of the dies and specimens. One or other of the two tests was used for these investigations whichever provided the more convenient method.

3.1. Friction

The most frequent objection to any form of compression test is that the effects of friction are difficult to determine and eliminate. The further problem of buckling encountered in simple compression tests is not present in this test. The two arguments put forward here for assuming that essentially zero friction has been achieved are indirect but are considered to be sufficiently conclusive to warrant the use of the test. Comparison with theoretical solutions (Ref. (3)) and experimental work (ref. (4)) for

metal adds weight to this conclusion.

In the tests performed the values of λ were determined at a constant temperature of 21°C. For the P.V.C., 3 inch wide and 0.25 ins. thick specimens were used with 0.50 in wide tools. A stress of 14,000 lbf/in^2 was applied for 10 minutes and the resulting deformation determined after 24 hours. A low density polyethylene was also used with 4 inch wide and 0.50 ins. thick specimens, 1.00 inch tools and a stress of 3000 lbf/in^2. Specimens were tested with the following lubricants:

a) No lubricant
b) Powdered graphite spread on the specimen
c) A heavy machine oil
d) Powdered graphite covered with machine oil
e) A very soft pencil lead rubbed onto the specimen surface
f) Pencil lead with machine oil added
g) Molybdenum disulphide grease (Molyslip)
h) Petroleum jelly (Vaseline)
i) Graphite grease.

The pencil lead was not applied to the polyethylene as it did not adhere to the surface satisfactorily. The results are shown in Table 1.

TABLE 1

	LUBRICANT TYPE	P.V.C. σ = 14,000 lbf/in^2		Polyethylene σ = 3,000 lbf/in^2	
		λ	λ/λ Molyslip	λ	λ/λ Molyslip
a)	None	.913	1.32	.840	1.21
b)	Powdered Graphite	.951	1.37	.914	1.31
c)	Oil	.741	1.07	.770	1.11
d)	Oil and Powdered Graphite	.713	1.03	.752	1.08
e)	Pencil Lead	.709	1.02	-	-
f)	Pencil Lead and Oil	.672	.97	-	-
g)	Molyslip	.692	1.00	.695	1.00
h)	Vaseline	.696	1.01	.720	1.04
i)	Graphite Grease	.673	.97	.684	.98

The values given for both materials have possible variations of $\pm$ 3% due to material inconsistency. The lubricants e, f, g, h and i all give values within this range for both materials. It is of interest to note that the powdered graphite gives a higher value of λ than no lubricant while the pencil lead gave a much reduced value. This may be accounted for by the powdered graphite penetrating the specimen surface while the pencil lead form was in layers

on the surface due to its method of application. Apart from this exception the addition of the lubricant results in a decrease in the value of λ as the restriction of flow due to friction is reduced. The five lubricants previously mentioned all give an approximately constant minimum value of λ and it is assumed that this corresponds to zero friction. It may be argued that they in fact correspond to an identical minimum value of friction. Apart from the unlikelihood of all five giving the same value it will be shown in a later section that when the results are compared with those of other tests not dependent on friction the agreement is sufficiently good to warrant the conclusion that zero friction exists.

For all the tests described here Molyslip was used as the lubricant. The results indicate, though not conclusively, that graphite grease may be slightly better, a difference of about 1%. As material variations between specimens are generally in excess of this the difference did not justify the adoption of graphite grease in preference to Molyslip. Molyslip has the advantage that it is easy to apply and remove from the specimens.

Many mineral oils and greases are absorbed by plastics and cause swelling and for this reason the period for which they are in contact with the specimen should be kept to a minimum. In these tests the specimen was

thoroughly cleaned immediately after removal from the press. Molyslip tends to dry on the tool surface and results in an increase in friction and to overcome this the tools must be cleaned and polished between each test and fresh grease applied to the specimen.

3.2. Specimen and Die Geometry

a) Die width to specimen thickness ratio (h/b)

The value of this ratio determines whether true plane strain conditions are being obtained. In total deformation tests the ratio changes throughout the course of the test and it is necessary to know the errors incurred. The test has been performed for permanent deformation tests by Watts and Ford (ref. (2)) and the result comparable with a theoretical solution derived by Green (ref. (5)) obtained. The theoretical solution is based on the assumption of a perfectly plastic solid (i.e. constant stress throughout the deformation) which does not apply in the case of total deformation tests on plastics. To obtain a comparison however 0.50 and 1.00 inch tools were used on 0.50 inch thick specimens of low density polyethylene at the same rate of loading. The curves obtained are shown in Fig. 4. The ratio of the $\frac{1}{2}$" into 1 inch tool test stresses at the same values of λ plotted against the specimen thickness to die width ratios is shown in Fig. 5. The theoretical solution

shown is deduced from that of Green to account for the stress ratio not being measured relative to a true plane strain stress (i.e. the 1" local stress varies with h/b). The order of the predicted error is, however, confirmed although the curve is displaced, probably due to the increasing stress not represented in the theory. The higher error of the results h/b $<$ .4 is probably due to an increasing frictional effect at these lower values of (h/b).

The ratios used in these tests were in the range .5 to .25 which results in a maximum error of 3%. No corrections have been made for this, for, as in the previous case, the material inconsistency exceeds the correction and it is not considered necessary.

b) Specimen width to die width ratio (ω/b)

The choice of this ratio is important as the effect of a narrow specimen is to allow movement in excess of that corresponding to plane strain. To determine this effect low density polyethylene specimens, 0.50 ins. thick, were tested with 1.00 inch tools. Values of permanent λ were obtained for various widths of specimen and are shown in Fig. 6. There is a steady decrease in the λ obtained until the curve levels off at (ω/b) greater than four.

The lack of constraint would be expected to give lower not higher values of λ for the narrower specimens but the material has a very large recovery(30%) and is equally unrestrained in recovery which allows the thickness to recover more than in true plane strain resulting in the high values.

Results obtained using P.V.C. are shown in Fig. 7. The recovery of this material is only some 7% and the expected low values are observed. Again the curve is seen to flatten out at ω/b greater than 4 and remain substantially constant, within the limits of material variation thereafter.

From these results it is concluded that a ω/b ratio of four or greater is necessary to ensure plane strain.

A further effect of specimen width is the influence of end spread. The material at the ends of the deformed section is unrestrained and bows outwards. This results in an increase in the effective area in which the load acts and thus an error in the stress calculated. To correct for this it would be necessary to know the pressure distribution and the end regions. The increase in area is approximately constant for all specimen widths and reference to Fig. 7 shows that if these results were corrected on the assumption of uniform pressure an increasing value of λ would result. This and other similar considerations has led to the conclusion that the

pressure distribution is not constant and is in fact so distributed that the effect of the end spread may be ignored. In the work described no corrections have been made and no obvious inconsistencies have arisen. A further point is that materials with large elastic recoveries are often restricted from flowing from between the tools by sharp edges on the tools. This may be overcome by providing slight radii on the edges of the tools when materials of this sort are to be tested.

This concludes the effects which apply to both the total and permanent deformation tests and the two tests will now be considered separately.

3.3. Total Deformation Test

A frequent difficulty in many tests is the necessity of measuring the deformation over some gauge section which is unaffected by end constraints. In the plane strain compression test the required measure of strain is the relative movement of the tools, the measurement of which is less complicated than the use of a gauge length. In the apparatus used in this test (see Fig. 8 a) and b)) this movement was measured by means of two resistance transducers fitted at each end of the press. The deflection recorded is the mean of the two readings and corrects for any tilt of the press during loading. Such tilts are not

more than 0.003 ins. over the tool section in the worst cases.

As these tests are to be carried out at a constant speed the load measuring device must not be subject to dynamic errors likely in many lever and spring systems. The system used was an electrical strain gauge load cell which gave an output of 3 mV. per ton load.

The outputs of the load cell and the deflection transducers were connected to an Ekco X-Y plotter and dynamic load deflection curves were recorded automatically. The response time of the plotter is not adequate for very high strain rates, but the range of the equipment can be extended in future by the use of other recording devices.

A set of curves was obtained for a low density polyethylene using 0.50 inch thick, 4 inch wide specimens and 1 inch wide tools. The load was applied by means of a 50 Ton Denison hydraulic testing machine. The specimen thickness was measured at each end of the test section, to determine a mean value and the specimen width was measured. The specimen was then placed in the press and the load applied with a constant pump setting on the testing machine. The load deflection curve obtained was then converted to a stress versus λ curve by use of the thickness and length values.

Some flexing of the press was evident in an initial displacement of the load deflection curve. This was corrected for by means of a deflection curve for the press obtained without a specimen between the tools.

The speed of the deformation was determined by repeating the test with a 0.2 sec time base instead of the load cell on the y axis of the plotter. This confirmed that, except for a small initial region, the speed was constant and a value was determined for each pump setting of the testing machine.

Examples of the load deflection curves obtained are shown in Fig. 9 and cover a range of strain rate ($\dot{\lambda}$) from .004 to .109 sec^{-1}. The curves indicate an increase of stress with strain rate up to this value but preliminary tests have indicated a decrease for higher values. An investigation of this will be included in future work but the results up to this value will not be affected as they are well within the plotter response times.

The equipment has not been used to investigate fully the effect of strain rate on the stress strain curves of plastics as it is not the purpose of the work at this stage. It would be extremely useful however in any future investigation of this type.

One of the aims of the investigation is to compare

the results of the plane strain compression test with those of other stress systems and it was necessary to develop a technique suitable for the work. The expense and difficulty of instrumenting apparatus to obtain dynamic stress strain curves makes it unpractical in many applications. Many cases are however concerned only with very slow rates of loading. To obtain an approximation to this and to overcome the dynamic recording difficulties a 'semi-static' test was devised. In a semi-static test the load was applied in increments and held constant for each increment while the deflection readings were taken. The number of these increments was governed by the total time span of the test which is kept approximately constant, in this case 10 mins. The lowest strain rate recorded dynamically was .004 sec^{-1} which corresponds to a time span of 1 min for a range of λ from 1 to 0.75. The estimate of strain rate for the semi static test is therefore approximately 10^{-5} sec^{-1} for the same 1 range of λ. The strain range of the test is limited because at higher stresses, around yielding, creep takes place under the constant load. The deformation then varies widely over the period of the load increment and it is difficult to obtain repeatable values.

A curve derived from the plane strain test using the standard time span of 10 mins was obtained for

the polyethylene and is shown in Fig. 9. The relation to the other strain rate curves indicates that this method gives an estimate of the low strain rate properties. The variations of stress over this range of rates are not large and a repeatability of $\pm$ 5% can be expected for the semi-static test.

The apparatus for the semi static test is greatly simplified in that it consists of two dial gauges to replace the resistance transducers and a normal machine weighing device to measure the load. Similar curves were also obtained for P.V.C. and Nylon.

The P.V.C. had a total strain of some 10% which is the minimum range for this test for the loads involved (15,000 lbf) as for strains below this value the correction for the sub-press stiffness is of the same order as the result. The results will be given in a later section.

3.4. Permanent Deformation Test

As has been previously mentioned the definition of permanent deformation is arbitrary. To investigate the effects of the recovery time (t_R) low density polyethylene specimens were loaded with various stresses for a dwell time of 10 mins and the recovery curves of λ after unloading determined. These are shown in Fig. 10

and indicate clearly the constant λ for recovery times of greater than about 10 hrs. Thus the standard convenient time of 24 hrs was chosen to be the period after which a deformation is termed permanent. The 10 min recovery value which is also shown indicates appreciable variation and thus it should be restricted to comparative tests.

The effect of increasing dwell time (t_D) at a stress of 2000 lbf/in^2 is shown in Fig. 11. This is essentially a measure of the permanent creep of the material and λ would go on decreasing with dwell time. The value of λ obtained with $t_D = 0$ is dependent on the strain-rate in the initial loading. This dependence becomes less as t_D is increased and a long t_D eliminates the effect entirely. The value chosen as standard, 10 mins, effectively accomplishes this independence of strain rate and has the advantage of giving extremely consistent results. The permanent deformation curve obtained does, however, include some creep deformation and the value of t_D will always be quoted with the curve. Any future work designed to investigate the effects of strain rate on permanent deformation must of course be performed with low values of t_D.

In carrying out this test the specimen is measured as in the previous case, lubricated, and placed in the press. The appropriate load is then applied and held constant for

10 mins. The load is then removed and the deformation is determined after 24 hours. In the total deformation test the continuous loading made any change of die width when the specimen was reduced in thickness impossible. Such a change is desirable when the die width to specimen thickness ratio is greater than four as errors are introduced due to a stress system which is not plane strain and an increased frictional effect, (see section 3.2). The effect of changing tools at appropriate values is shown in Fig. 12 for polyethylene. Each points corresponds to a separate specimen. The specimen thickness was 0.50 ins which gives a h/b value of 4 at $\lambda = 0.5$. For λ greater than this value the $\frac{1}{2}$ inch tools give a higher stress value than the 1 inch tools as would be expected from previous tests (see section 3.2). For λ less than 0.5 a continuous curve is formed from the 1 inch to the $\frac{1}{2}$ inch die values.

The use of separate specimens for every point on a curve can be wasteful and a convenient method is to reload the specimen in the same place after each recovery. Fig. 13 shows the curve obtained by this method using the same material as in the last test. An identical curve to the one obtained with separate specimens is obtained with a smooth transition from 1 inch to $\frac{1}{2}$ inch.

tool results. Thus material may be saved and the difficulty of inconsistent material overcome by employing this technique. The t_R = 10 min was used for convenience.

A problem encountered in some materials is the formation of cracks. These form in a direction normal to the tool axis, that is, parallel to the direction of orientation introduced by the stress system. The main cause is the residual stress system present after unloading and the cracks can be avoided by reducing the tool widths in stages in obtaining a required deformation. This gives a less severe shoulder between deformed and undeformed material and consequently reduced residual stresses. There does not appear to be any measurable effect on the stress strain curves due to these cracks, probably because they form after unloading and they can be ignored.

For very sharp corners on the shoulders of the reduced sections as when narrow tools are used on thick material (low b/h ratios) in special cases the deformed section of the specimen can be split centrally in a plane parallel to the tool faces, by the residual stresses and if care is not taken high values of λ are recorded. The effect may be avoided by ensuring that severe shoulders are not formed.

The stress versus λ curves were determined for a wide range of plastics to illustrate the use of the method and are shown in Fig. 14.

3.5. Other Tests

a) Creep testing

The stability of this test enables creep curves to be obtained for very high stresses. Certain problems must be overcome such as the elimination of the swelling effect of the lubricant over a long period. The recoverable and permanent parts of the deformation may be separated and recoverable and permanent creep curves may be obtained.

b) Temperature testing

The variation of both total and permanent strains with temperature may also be investigated with this test. Again lubrication problems must first be considered but the method shows promise as is illustrated in Fig. 15 which shows the variation in the polyethylene permanent deformation curve for two temperatures.

The results of this investigation of the testing of plastics by means of the plane strain compression test are incomplete but it gives repeatable and accurate results. Instability does not influence the results and it is possible

to separate permanent and recoverable deformations easily. The measurement of strain is simpler than most test methods and the instrumentation for dynamic recording is readily carried out. The possibility of the application of the test to the investigation of creep and temperature effects is promising.

The remaining problem is to relate these results to other stress systems with the object of predicting behaviour under all stress systems with the results of this test. These predictions are carried out for metals using the work hardening curves obtained in conjunction with the theory of plasticity. This theory and other possible methods will be considered in the next section.

4.0. Application of the Concepts of Plasticity Theory to Stress Analysis of Thermoplastics

The problem encountered in the stress analysis of plastics are best illustrated by considering the established techniques and the behaviour they describe. The analysis of stress in a body at any instant is derived from the equilibrium of the various components and is independent of the deformation process. The analysis of strain is derived from the geometrical relationships of a deforming

continuous body. Some stress strain law must be defined to relate the stresses and strains in order that deformations may be predicted from loads or vice versa.

The strain relationships are of the most simple form for the analysis of infinitesimal strains where strain is defined as:

$$e = \frac{\delta \ell}{\ell_o}$$

where $\delta \ell$ = the deformation

ℓ_o = length over which the deformation occurred.

The combination of infinitesimal strains and a linear relationship between stress and strain (Hooke's law) gives rise to **classical elasticity** (ref. (6)). This has been widely applied as it gives an accurate description of the elastic behaviour of metals. No account is taken of time dependent behaviour and the material is assumed to be 'perfectly' elastic in that all deformations recover immediately on unloading.

The theory has been extended to include time dependence with the development of linear visco-elasticity. This described the material behaviour by means of spring-dashpot models or combinations of linear elastic and viscous elements. Such a model is derived for each material

and from it the strain behaviour, creep, and relaxation may be derived (ref. (7)).

The concepts of these theories have been widely applied to plastics. In the most elementary applications the stress strain curve for rigid plastics is obtained for a small strain range and a value of Young's Modulus derived. For some plastics the stress strain curve is linear but for others it is not, even for small strains, and this is overcome by assigning a mean value of Young's Modulus to the curve. This technique is frequently proposed in the plastics field as adequate for engineering applications involving small deformations.

The lack of linearity in the curves is often ascribed to visco-elastic effects owing to the rate of straining at which the curve was obtained and many investigations have been carried out to describe the behaviour in terms of linear visco-elasticity. In some cases (ref. (8)) this has proved successful while for others (ref. (9)) it has been shown that the material is basically non-linear and the theory is not adequate for its description.

The analysis of large strain, non-linear, elasticity was first developed by Rivlin (ref. 10)) and further extended by Green and Adkins (ref. (11)). The analysis of strain is carried out in terms of extension ratios defined as:

$$\lambda = \frac{\ell}{\ell_0}$$

where ℓ = deformed length

ℓ_0 = original length.

Rivlin showed that any strain state had three tensor invariants in terms of the three principal extension ratios λ_1, λ_2, λ_3, thus

$$I_1 = \lambda_1 + \lambda_2 + \lambda_3$$

$$I_2 = \lambda_1\lambda_2 + \lambda_2\lambda_3 + \lambda_1\lambda_3$$

$$I_3 = \lambda_1\lambda_2\lambda_3$$

Assuming a constant volume deformation

$$I_3 = 1$$

and the stress strain relationship was defined by means of the energy function such that:

$$W = \phi(I_1, I_2)$$

Problems may then be solved in terms of W and it is therefore necessary to determine the form of ϕ for the material under consideration. The theory was developed for rubber and the most frequently used form for this material is:

$$W = C_1 I_1 + C_2 I_2$$

where C_1 and C_2 are constants.

The kinematic theory of rubber elasticity (see ref.(12)) describes the deformation process in terms of the

distortion of the molecular chains and from this basis gives the result

$$W = C_1 I_1$$

where C_1 is a function of the molecular structure and the temperature. No explanation of C_2 appears to be decided upon from this viewpoint. It has been pointed out that C_1, I_1 and C_2, I_2 may be, in fact, the first terms in polynomials describing other functions and other forms have been obtained (ref. (13)) which give good fits to experimental data.

In its present form the theory describes only perfect elasticity and includes no time dependent effects. Some attempts have been made to include these (ref. (14)) but no proven technique is available. The analysis of elastic problems by this method is inclined to be complicated and the possibilities of extending it to anelastic behaviour as encountered in engineering applications of plastics do not appear very great at the moment.

Another technique for the analysis of large strains and non-linearity has been developed for describing the plastic deformation or flow of metals (ref. (15)). The basic definition of strain is in terms of logarithmic strain. In simple tension the increment of this strain is defined as

$$\delta\varepsilon = \frac{\delta \ell}{\ell}$$

where $\delta \ell$ = incremental increase in length

and ℓ = current length.

This may be integrated to give:

$$\varepsilon = \ln.\frac{\ell}{\ell_o} \quad \text{or} \quad \ln \lambda$$

where ℓ_o = the original length.

For a constant volume deformation we have

$$\lambda_1 \lambda_2 \lambda_3 = 1,$$

and hence for the principal strains

$$\varepsilon_1 + \varepsilon_2 + \varepsilon_3 = 0$$

The plastic deformation of a metal is assumed to take place at constant volume and is therefore independent of the hydrostatic component of the stress system. For a stress system defined by three principal stresses σ_1, σ_2 and σ_3 the hydrostatic stress component is:

$$\hat{\sigma} = \frac{\sigma_1 + \sigma_2 + \sigma_3}{3}$$

The plastic deformation is therefore governed by the three principal deviatoric stress components:

$$\sigma_1' = \sigma_1 - \hat{\sigma} \quad \text{etc.}$$

The criterion for plastic deformation to take place or yielding will be governed by the three invariants of the stress system:

$$J_1 = \sigma_1 + \sigma_2 + \sigma_3$$

$$J_2 = -(\sigma_1\sigma_2 + \sigma_2\sigma_3 + \sigma_3\sigma_1)$$

$$J_3 = \sigma_1\sigma_2\sigma_3$$

J_1 is the hydrostatic stress and, it is assumed, does not affect yielding process and it is also assumed (von Mises) that it is also independent of J_3. The yielding criterion is, therefore, a function of the deviatoric stress invariant J_2'

$$J_2' = -(\sigma_1'\sigma_2' + \sigma_2'\sigma_3' + \sigma_3'\sigma_1') = \tfrac{1}{2}(\sigma_1'^2 + \sigma_2'^2 + \sigma_3'^2)$$

such that:

$$\sigma_1'^2 + \sigma_2'^2 + \sigma_3'^2 = 2k^2$$

where k is a parameter depending on the amount of prestrain. The variation of k with prestrain can be described by means of a curve relating $\bar{\sigma}$ an equivalent stress and $\bar{\varepsilon}$ an equivalent strain defined as follows:

$$\bar{\sigma} = \frac{1}{\sqrt{2}}\left[(\sigma_1 - \sigma_2)^2 + (\sigma_2 - \sigma_1)^2 + (\sigma_1 - \sigma_3)^2\right]^{1/2}$$

i.e.

$$\bar{\sigma} = \frac{2}{\sqrt{3}}.k$$

and

$$d\bar{\varepsilon} = \frac{\sqrt{2}}{3}\left[(d\varepsilon_1 - d\varepsilon_2)^2 + (d\varepsilon_2 - d\varepsilon_3)^2 + (d\varepsilon_3 - d\varepsilon_1)^2\right]^{1/2}$$

where $\bar{\sigma}$ and $d\bar{\varepsilon}$ are defined to be the values in simple tension.

The equations governing the plastic deformations are the Levy-Mises equations which may be written as:

$$\frac{d\varepsilon_1}{\sigma'_1} = \frac{d\varepsilon_2}{\sigma'_2} = \frac{d\varepsilon_3}{\sigma'_3} = \frac{d\gamma_{12}}{\sigma'_{12}} = \frac{3}{2}\frac{d\bar{\varepsilon}}{\bar{\sigma}} \quad \text{etc.}$$

or $d\varepsilon_1 = d\lambda\sigma'_1$.

To include the elastic components of strain these must be put into the form of the Prandtl-Reuss equations thus:

$$d\varepsilon'_1 = \frac{3}{2}\frac{d\bar{\varepsilon}}{\bar{\sigma}}\sigma'_1 + \frac{d\sigma'_1}{2G}$$

The deviatoric strain increment is made up of two components, the plastic component in the direction of σ'_1 and an elastic component in the direction of and $d\sigma'_1$. A vector sum is therefore necessary to define the strain behaviour from the imposed stress system.

Considerable success has been achieved in applying this theory to metals. It includes no time dependent phenomenon although some recent work (ref. (16)) has attempted this. No attempts have so far been reported of adopting the concepts of this theory to deal with problems in plastics and a description of such an adaptation will now be given.

For the initial investigation a number of restrictions will be placed on the range of problems to be attempted. These restrictions may be listed as follows:

1) The deformation will take place at constant volume. This appears to be a reasonable assumption for most plastics except for very small strains.

2) The deformations will take place at a constant, very slow, strain rate and at a single temperature. The low strain rate is chosen to eliminate the complication of the effect of strain rates and for the examples given the semi-static test technique will be used (i.e. a constant time span for each test).

3) The material is assumed to be isotropic. For initially isotropic plastics anisotropy only becomes apparent after considerable permanent deformation has taken place. The deformation will only be examined therefore over a limited range after yielding has commenced.

4) Only loading will be considered. Unloading presents special problems which will be discussed later.

5) The principal stress ratios will remain constant (simple loading) throughout the deformation. While this excludes such processes as two part loading systems, e.g. tension followed by torsion, it leaves a large number of common engineering problems.

From these restrictions it will be seen that the problem to be solved is that of large strains with a non-linear relationship between stress and strain for constant conditions of loading, strain rate and temperature.

As the stress ratios remain constant the stress increment and total stress vectors are in the same direction and the Prandtl-Reuss equations can be rewritten:

$$d\varepsilon_1 = \left[\frac{3}{2}.\frac{d\bar{\varepsilon}}{\bar{c}} + \phi\right] \quad c_1' \qquad \text{etc.}$$

ϕ is some measure of the elastic stiffness at this stage of the deformation. The deviatoric strain increment is now replaced by the strain increment as the deformation is at constant volume. The form of this equation implies that there are, in the case of rate sensitive materials, components of strain in the increment and total stress vector directions. This is not necessarily the case as the elastic component could be in some other direction depending on the strain rate. As we are concerned only with loading there is no need to distinguish between recoverable and permanent deformations. Also as we are concerned only with constant stress ratios there is no need to define the directions of the strain increments as they must be in the direction of the increment and total stress vectors, which are coincident.

It is proposed, therefore, that the variable elastic effects denoted by ϕ be incorporated into the $\bar{c}$ versus $\bar{\varepsilon}$ relationship to give:

$$d\varepsilon_1 = \frac{3}{2}.\frac{d\bar{\varepsilon}}{\bar{\sigma}}.\sigma_1'$$

where $d\bar{\varepsilon}$ and $\bar{\sigma}$ now include all forms of deformation. As

the stress ratios are constant the equation of equivalent strain increment may be integrated to give:

$$\bar{\varepsilon} = \frac{\sqrt{2}}{3}\left[(\varepsilon_1 - \varepsilon_2)^2 + (\varepsilon_2 - \varepsilon_3)^2 + (\varepsilon_3 - \varepsilon_2)^2\right]^{1/2}$$

and the stress strain relationships can be re-written:

$$\dot{\varepsilon}_1 = \frac{3}{2}\cdot\frac{\dot{\bar{\varepsilon}}}{\bar{\sigma}}\cdot\sigma_1'$$

Nothing is gained by expressing them in this form and for the purpose of further development they will be left in the incremental form.

The use of the $\bar{\sigma}$ versus $\bar{\varepsilon}$ relationship to describe the deformation process does not imply any dependence on a yield criterion, particularly as it describes deformation below yielding, but that the deformational behaviour of a material under a particular state of stress is governed by the second invariant of the deviatoric stress system as in yielding. Under the particular restrictions imposed in this work this state of stress corresponds to a strain state designated by a similar function of strain and a unique relationship exists between the two functions. This is the basic stress strain curve for these conditions.

To summarise, it is proposed that there exists a unique relationship between the two functions of stress and strain defined as follows:

$$\bar{\sigma} = \frac{1}{\sqrt{2}}\left[(\sigma_1 - \sigma_2)^2 + (\sigma_2 - \sigma_1)^2 + (\sigma_1 - \sigma_3)^2\right]^{1/2} \quad \ldots(1)$$

$$d\bar{\varepsilon} = \frac{\sqrt{2}}{3}\left[(d\varepsilon_1 - d\varepsilon_2)^2 + (d\varepsilon_2 - d\varepsilon_3)^2 + (d\varepsilon_1 - d\varepsilon_3)^2\right]^{1/2} \ldots(2)$$

The relationship between these functions and the stress and strain components in any direction may be expressed in the form:

$$d\varepsilon_1 = \frac{d\bar{\varepsilon}}{\bar{\sigma}}\left[\sigma_1 - \tfrac{1}{2}(\sigma_2 + \sigma_3)\right] \quad \text{etc.} \qquad \ldots..(3)$$

as $\theta_1' = \sigma_1 - \hat{c}$

$$= \sigma_1' - \frac{\sigma_1 + \sigma_2 + \sigma_3}{3} = \frac{2}{3}\left[\sigma_1 - \tfrac{1}{2}(\sigma_2 + \sigma_3)\right]$$

and $d\gamma_1 = \frac{d\bar{\sigma}}{\bar{\sigma}}.\tau_1$ etc. $\qquad \ldots..(4)$

It should be noted that these equations have been presented in terms of the principal components of stress and strain which are defined in terms of the general components as follows:

$$\sigma_1 = \frac{\sigma_x + \sigma_y}{2} \pm \sqrt{\left(\frac{\sigma_x - \sigma_y}{2}\right)^2 + \tau_{xy}^2} \quad \text{etc.}$$

$$d\varepsilon_1 = \frac{d\varepsilon_x + d\varepsilon_y}{2} \pm \sqrt{\left(\frac{d\varepsilon_x - d\varepsilon_y}{2}\right)^2 + d\gamma_{xy}^2} \quad \text{etc.}$$

$$\tau_1 = \frac{\sigma_1 - \sigma_2}{2} \quad \text{etc.}$$

and $d\gamma_1 = d\varepsilon_1 - d\varepsilon_2$ etc.

The equations may, of course, be presented in terms of these general components if required:

$$\text{i.e. } d\varepsilon_x = \frac{d\bar{\varepsilon}}{\bar{\sigma}} \left[\sigma_x - \frac{1}{2}(\sigma_y + \sigma_z) \right] \quad \text{etc.}$$

The application of this technique will now be illustrated by means of a series of examples.

4.1. Uniform Stress Systems

The first of these examples will deal with systems where the stress system is the same throughout the body.

1) Plane Strain Compression

Let σ_1 be the stress applied to the dies being forcedinto the material. The stress normal to the axis of the dies may be assumed to be zero (ref. (5)) and therefore:

$$\sigma_3 = 0.$$

The material undergoing deformation is restricted from moving along the tool axis and there is, therefore, zero strain in this direction

$$\text{i.e. } d\varepsilon_2 = 0.$$

From equation (3) we have:

$$d\varepsilon_1 = \frac{d\bar{\varepsilon}}{\bar{\sigma}}(\sigma_1 - \frac{1}{2}(\sigma_2 + \sigma_3)) \qquad \text{.....(5)}$$

$$d\varepsilon_2 = \frac{d\bar{\varepsilon}}{\bar{\sigma}}(\sigma_2 - \frac{1}{2}(\sigma_1 + \sigma_3)) \qquad \text{.....(6)}$$

$$d\varepsilon_3 = \frac{d\bar{\varepsilon}}{\bar{\sigma}}\left(\sigma_3 - \tfrac{1}{2}(\sigma_1 + \sigma_3)\right) \qquad \text{.....(7)}$$

Now $\sigma_3 = 0$ and $d\varepsilon_2 = 0$

$\therefore$ from equation (6)

$$\sigma_2 = \tfrac{1}{2}\,\sigma_1$$

For constant volume:

$$d\varepsilon_1 + d\varepsilon_2 + d\varepsilon_3 = 0$$

and $\therefore\ d\varepsilon_2 = -\,d\varepsilon_1$ where $d\varepsilon_1 = \frac{dh}{h}$

Substituting in equations (1) and (2) for equivalent stress and strain we have

$$\bar{\sigma} = \frac{\sqrt{3}}{2}\,.\sigma_1 \qquad \text{.....(8)}$$

and $$\bar{\varepsilon} = \frac{2}{\sqrt{3}}.\varepsilon_1 \quad \text{where } \varepsilon_1 = \ln\frac{h}{h_o} \qquad \text{.....(9)}$$

The results of the semi-static test converted to $\bar{\sigma}$ versus $\bar{\varepsilon}$ are shown in Figs. 16, 17 and 18 for polyethylene, P.V.C. and nylon respectively. The results of the permanent deformation test over the same range converted on this basis are also given.

The total deformation curves obtained in this test will be used in the majority of cases for the prediction of the results of other stress systems.

2) Simple Tension

This test is the most generally used in engineering and it is of interest to compare results obtained with those predicted by the plane strain compression test.

For simple tension:

$$\sigma_2 = \sigma_3 = 0$$

∴ From equations (3) $d\varepsilon_2 = d\varepsilon_3$.

For constant volume deformation this becomes:

$$d\varepsilon_2 = d\varepsilon_3 = -\frac{1}{2} d\varepsilon_1$$

and by definition

$$\bar{\sigma} = \sigma_1, \quad \text{and} \quad \bar{\varepsilon} = \varepsilon_1$$

ε_1 is the axial strain defined as:

$$\varepsilon_1 = \ln \frac{\ell}{\ell_o} = \ln \lambda$$

where ℓ = current length

ℓ_o = original length.

For the purposes of comparison the plane strain compression test results were converted to nominal stress and engineer's strain. The nominal stress may be derived from the true strain $\bar{\sigma}$ thus:

$$\sigma_N = \frac{\bar{\sigma}}{\lambda_1}$$

The engineer's strain is defined as:

$e = \frac{\delta \ell}{\ell_o}$ where $\delta \ell$ is the increase in ℓ_o the original length

and $\lambda_1 = \frac{\ell}{\ell_o} = \frac{\ell_o + \delta \ell}{\ell_o} = 1 + e$

The σ_N versus e curve may be regarded as a load deflection curve as σ_N is load per unit original area and e is deflection per unit original length. The converted curves for polyethylene, P.V.C. and nylon are shown in Figs. 19, 20 and 21 respectively.

Tension tests were carried out on the three materials and the results are also given. For tension tests where large strains are involved as in polyethylene and nylon the following technique was used for determining strain. Two gauge marks were made on the specimen and a pair of dividers set to this gauge length. A short arc was then scribed on a strip of aluminium. After the application of each load the dividers were reset to the gauge marks and an arc scribed from the same centre as the original arc. After completing the test the radii of these arcs was measured with a travelling microscope and the strain calculated. For strains up to 20% this was found to give repeatibility of up to $\pm$ 5% of the total which is only slightly worse than the expected variation in the material. For the smaller strains of the P.V.C. a Lindley extensometer was used.

Fig. 19 shows that there is agreement for polyethylene up to the onset of permanent deformation. The tension strains are then larger than those predicted by the compression test. The most likely explanation of this is that the effect of creep during the periods over which the load is held constant is more pronounced in simple tension than in the stress system of the compression test (see section 4.4). This divergence is seen in Figs. 20 and 21 for P.V.C. and nylon and other tests indicate that the simple tension results tend to give a larger creep strain than biaxial stress systems.

All three tests show good agreement up to the onset of the permanent deformation. It is of interest to note that the use of $\bar{\sigma}$ gives an accurate prediction of the rapid increase in strain in the tension test or onset of flow, usually termed yield, from the plane strain compression results. This implies that the criterion for the onset of permanent deformation as defined here is that of von Mises as in metals i.e. is a function of the second deviatoric stress invariant J_2'.

3) Thin Walled Cylinder under Internal Pressure

For a thin walled cylinder under internal pressure, with closed ends, the stresses are:

$$\sigma_\theta = \frac{pD}{2t}, \quad \sigma_z = \frac{pD}{4t}, \quad \sigma_t = 0$$

where p = internal pressure

D = current mean diameter

t = " thickness.

θ denotes the circumferential stress, z the axial stress and t the stress through the thickness.

Hence we have

$$\bar{\sigma} = \frac{\sqrt{3}}{4} \cdot \frac{pD}{t}$$

Therefore $d\varepsilon_\theta = \frac{d\bar{\varepsilon}}{\bar{\varepsilon}}(\sigma_\theta - \frac{1}{2}\sigma_z)$

$$d\varepsilon_z = \frac{d\bar{\varepsilon}}{\bar{\sigma}}(\sigma_z - \frac{1}{2}\sigma_\theta)$$

$$d\varepsilon_t = \frac{d\bar{\varepsilon}}{\bar{\sigma}}(-\frac{1}{2}(\sigma_z + \sigma_\theta))$$

Now $\sigma_z = \sigma\theta/2$ $\therefore$ $d\varepsilon_z = 0$ and $\lambda_z = 1$

$\therefore$ From constant volume:

$$\lambda_\theta \cdot \lambda_t = 1$$

Now $\lambda_\theta = \frac{D}{D_o}$ and $\lambda_t = \frac{t}{t_o}$

$\therefore$ by substitution:

$$\bar{\sigma} = \frac{\sqrt{3}}{2}.\left(\frac{pD_o}{2t_o}\right).\lambda_\theta^2 \qquad .....(10)$$

and $$\bar{\varepsilon} = \frac{2}{\sqrt{3}}.\ln \lambda_\theta \qquad .....(11)$$

and rewriting equation (10)

$$\left(\frac{pD_o}{2t_o}\right) = \frac{2}{\sqrt{3}}.\frac{\bar{\sigma}}{\lambda_\theta^2} \qquad .....(12)$$

For any material for which the stress strain curve is known for any value of λ_θ a value of $\bar{\varepsilon}$ may be calculated from equation (11). By reference to the stress strain curve a corresponding value of $\bar{\sigma}$ may be found and substituted into equation (12) to give the value of the pressure factor $\left(\frac{pD_o}{2t_o}\right)$. Thus a curve may be constructed of this factor versus λ_θ and for any cylinder of known D_o and to the pressure may be found to give any value of λ_θ.

Such a curve, for low density polyethylene, is shown in Fig. 22 together with experimental points obtained for a cylinder of D_o = 1 inch and t_o = .061 ins. The agreement is good and further confirms the validity of this approach.

4) Equal Biaxial Tension

The problem of the analysis of the bulging of a circular membrane subjected to lateral pressure has been solved by several authors. For example a large strain

elastic theory solution is given in ref. (11) and ref. (18) gives a plasticity solution. Both solutions are complicated and a solution will be given here which gives a much simpler solution by means of a number of approximations.

Consider a circular membrane (see Fig. 23) of radius a inflated by a pressure p to give a central deflection δ. Ref. (11) shows that the shape taken by the dome depends on the stress vs. strain curve for the material. For the special case where the dome forms the cap of a sphere of radius R then:

$$\sigma_r = \frac{pR}{2t} \qquad .....(13)$$

where σ_r = radial stress,

t = current thickness.

By symmetry the circumferential stress must equal the radial stress:

$\sigma_\theta = \sigma_r$ and $\sigma_t = 0$ for a thin membrane.

For any given pressure therefore we have

$$\sigma_r t = \text{constant}$$

over the surface of the dome. This implies a stress strain relationship of the form:

$$\sigma = Ae^{\varepsilon}$$

for this condition to hold. This is obviously not generally true and the shape will therefore be other than spherical.

An approximate solution may however be obtained by considering that the shape obtained is equivalent to a uniform, constant thickness spherical cap of the same central deflection. This makes both σ_r and t constant over the dome for each deflection and does not require the particular stress strain relationship to be specified. Any form of this relationship is permissible as each central deflection corresponds to one point in the stress strain curve.

Now as $\sigma_r = \sigma_\theta$ and $\sigma_t = 0$ then $d\varepsilon_r = d\varepsilon_\theta$ and $\therefore \lambda_r = \lambda_\theta$.

For a uniform dome therefore we may write:

$$\lambda_r^2 = \frac{2\pi R\delta}{\pi a^2} \left(= \frac{\text{surface area of cap}}{\text{surface area of original circle}}\right)$$

By geometry:

$$R = \frac{\delta^2 + a^2}{2\delta} \qquad \text{.....(14)}$$

$$\therefore \quad \lambda_r^2 = 1 + \frac{\delta^2}{a^2} \qquad \text{.....(15)}$$

From constant volume

$$\lambda_r \lambda_\theta \lambda_t = 1$$

$$\therefore \quad \frac{t}{t_o} = \frac{1}{\left(1 + \frac{\delta^2}{a^2}\right)} \qquad \text{.....(16)}$$

Substituting equations (14) and (15) into equation (13) we have:

$$\sigma_r = \frac{pa}{4t_o} \cdot \frac{(1 + (\frac{\delta}{a})^2)^2}{(\frac{\delta}{a})}$$

For equal biaxial tension (i.e. $\sigma_r = \sigma_\theta$, $\sigma_\varepsilon = 0$)

$$\bar{\sigma} = \sigma_r$$

and

$$\bar{\varepsilon} = 2\varepsilon_r$$

$$\therefore \quad (\frac{pa}{4t_o}) = \bar{\sigma} \cdot \frac{(\frac{\delta}{a})}{(1 + (\frac{\delta}{a})^2)^2} \qquad .....(17)$$

and

$$\bar{\varepsilon} = \ln(1 + (\frac{\delta}{a})^2). \qquad .....(18)$$

For any value of $(\frac{\delta}{a})$, $\bar{\varepsilon}$ may be calculated from equation (18) and from the basic stress strain curve the appropriate value of $\bar{\sigma}$ obtained. The stress strain curve in this case was obtained from a simple tension test. It is hoped to develop the plane strain compression test using multiple thicknesses of the film in future work. Substituting this in equation (17) gives the value of the pressure parameter required to give this value of $(\frac{\delta}{a})$. A curve derived for low density polyethylene is shown in Fig. 24.

To test this solution the apparatus shown in Fig. 25 was developed. The polyethylene film was held in a circular clamp and pressure was applied through a valve in the base plate. The pressure was measured by means of a water manometer. The central deflection was measured

with a depth micrometer using a bridge over the clamp as shown. A typical set of results are given in Fig. 24 (average of five tests) and show good agreement with the theoretical prediction. At the highest value of pressure the film necked to form local bulges and this was the limit of usefulness of the test. This pressure at which the bulges form corresponds closely to the theoretical maximum of the curve. This apparatus provides a useful technique for determining the stress strain curve for a material in film form where simple tension or plane strain compression tests are difficult.

4.2. Non-uniform Stress Systems

In many applications the stress may vary through a body in any stage in the loading. A common example of this is the tension of a solid circular rod and this will be treated as an example.

Torsion of a Solid Circular Rod

Consider first the torsion of a thin walled circular cylinder of radius r_o, thickness t_o and length ℓ_o. The shear stress in the wall of the cylinder will be constant, say τ and $\sigma_r = \sigma_\theta = \sigma_z = 0$.

$$\therefore \quad \bar{\sigma} = \sqrt{3}.\tau$$

The torque on the tube is given by

$$T = 2\pi r_o^2 t_o \tau.$$

The shear strain increment is:

$$d\gamma = \frac{r_o d\theta}{2\ell_o}$$

where $d\theta$ is the angle of twist. Therefore

$$\bar{\varepsilon} = \frac{2}{\sqrt{3}}.\gamma$$

i.e. $$\bar{\varepsilon} = \frac{2}{\sqrt{3}}.\frac{r_o\theta}{\ell_o} \qquad .....(19)$$

and $$T = \frac{2}{\sqrt{3}}.\pi r_o^2 t_o.\bar{\sigma} \qquad .....(20)$$

Thus the torsion of a thin walled circular cylinder may be solved as before. A solid circular cylinder may be considered to be made up of a series of concentric thin cylinders. If we consider a cylinder of outside radius R_o then the total torque will be given by

$$T_{TOT} = \sum_{o}^{R_o} \frac{2}{\sqrt{3}}\pi r_o^2 t_o.\bar{\sigma}$$

This may be rewritten as:

$$\frac{T}{\pi R_o^3} = \frac{2}{\sqrt{3}} \sum_{o}^{1} \bar{\sigma}\left(\frac{r_o}{R_o}\right)^2.\left(\frac{t_o}{R_o}\right) \qquad .....(21)$$

and $$\bar{\varepsilon} = \frac{2}{\sqrt{3}}\left(\frac{r_o}{R_o}\right).\left(\frac{R_o\theta}{\ell_o}\right) \qquad .....(22)$$

For the examples used here t_o was taken as $0.1R_o$ and hence the rod was divided into ten concentric cylinders. For every value of $\frac{R_o\theta}{\ell_o}$ a value of $\bar{\varepsilon}$ was calculated for each of the ten values of $\left(\frac{r_o}{R_o}\right)$. From these values the values of $\bar{\sigma}$ were calculated and substituted into equation (21) to give the increments of torque. These increments were finally summed to give the total torque factor $\frac{T}{\pi R_o^3}$ corresponding to the twist factor $\frac{R_o\theta}{\ell_o}$. The curve of these two functions for low density polyethylene is shown in Fig. 26, together with practical points for three rods of different diameters of the same material. There is some discrepancy between the practical results and the theoretical prediction which is probably due to bending in the torsion test. The agreement is sufficiently good however to warrant further applications of the technique.

4.3. Instability Predictions

It is frequently of interest to determine the maximum load which a body will support under any given loading system. This maximum load is generally a point of instability as extensions beyond this can be obtained with no increase in load. This leads to the formation of a neck in the tension test and correspondingly this is often taken

as an upper load limit. This load may be predicted in the tensile test as follows:

Let F_1 = load per unit area

$$\therefore \quad F_1 = \sigma_1 \lambda_2 \lambda_3$$

For constant volume $\lambda_1 \lambda_2 \lambda_3 = 1$

$$\therefore F_1 = \sigma_1 / \lambda_1$$

Now $$\frac{dF_1}{d\lambda_1} = \frac{1}{\lambda_1} \frac{d\sigma_1}{d\lambda_1} - \frac{\sigma_1}{\lambda_1^2}$$

For maximum load $\frac{dF_1}{d\lambda_1} = 0$

$$\therefore \frac{d\sigma_1}{d\lambda_1} = \frac{\sigma_1}{\lambda_1}$$

and hence $$\frac{d\sigma_1}{d\varepsilon_1} = \sigma_1$$

For simple tension $\sigma_1 = \bar{\sigma}$ and $e_1 = \bar{\varepsilon}$

and therefore $$\frac{d\bar{\sigma}}{d\bar{\varepsilon}} = \bar{\sigma}.$$

Thus by determining this condition from the $\bar{\sigma}$ vs. $\bar{\varepsilon}$ curve the maximum value of F may be determined.

For a thin walled cylinder under internal pressure from equations (11) and (22) we have

$$\bar{\varepsilon} = \frac{2}{\sqrt{3}} . \ln \lambda_\theta$$

and

$$\frac{pD_o}{2t_o} = \frac{2}{\sqrt{3}} \cdot \frac{\bar{\sigma}}{\lambda_\theta^2}$$

The maximum value of pressure is given when $\frac{dp}{d\lambda_\theta} = 0$ i.e. when

$$\frac{d\bar{\sigma}}{d\lambda_\theta} = \frac{2\bar{\sigma}}{\lambda_\theta}$$

Also $$\frac{d\bar{\varepsilon}}{d\lambda_\theta} = \frac{2}{\sqrt{3}} \cdot \frac{1}{\lambda_\theta}$$

$$\therefore \quad \frac{d\bar{\sigma}}{d\bar{\varepsilon}} = \sqrt{3}\,\bar{\sigma}$$

By substituting the values obtained from this result in the original equations the maximum pressure may be obtained.

As an example containing all the techniques previously described the instability of thick walled polyethylene cylinders under internal pressure, was examined. As in the case of torsion they may be considered as made up of a series of concentric thin walled cylinders. The method used for deriving the pressure, versus radial movement curves for various values of outside to bore diameter ratios (K) was a modification of the Manning method from plasticity theory developed by Ford (ref. (18)). From each of these curves the maximum pressure was obtained and a curve of maximum pressure versus K ratio constructed. This is shown in Fig. 27 together with the prediction

derived from thin walled theory. Cylinders of various K ratios were manufactured by boring out solid rod and their maximum pressures determined. The values obtained are also shown in Fig. 27. The agreement is good and illustrates fully the power of this technique of stress analysis when applied to plastics.

4.4. Some Aspects of the General Problem

In the examples discussed so far the restrictions of loading and constant stress ratios were imposed. To investigate the possibilities of extending the theory to cover unloading and varying stress ratios experiments were performed on thin walled polyethylene cylinders subjected to combined internal pressure and axial load.

The apparatus used (Fig. 28) consisted of two shackles designed to be mounted on a Zwick tensile testing machine. The tube was clamped to the shackles by Jubilee clips and the axial load was applied and measured by the testing machine. The lower shackle was fitted with a flexible hose and water was pumped into the cylinder by a hand pump. The pressure was recorded on a separate pressure gauge. The axial strain was measured on a central two inch gauge length with dividers and the diametral strain by measuring two orthogonal diameters with a micrometer at the central section.

Five tests were performed:

1) Axial load (simple tension)

2) Internal pressure

3) The axial load was applied and then held at a constant value as internal pressure was applied. This was increased and then held constant while the axial load was reduced to zero. The internal pressure was then reduced to zero.

4) The axial load was applied and then held constant while the internal pressure was increased. After reaching the maximum pressure the pressure was then decreased to zero. This was followed by decreasing the axial load to zero.

5) The axial load and internal pressure were increased to the maximum value and decreased to zero in random increments such that the stress ratios varied for each increment.

The maximum points of all systems were chosen to give, as near as possible, the same maximum value of equivalent stress.

As a basis for the investigation it was decided to consider the relationship between $\bar{\sigma}$ and $\bar{\varepsilon}$ throughout the loading systems. The effect of varying the stress ratios is best illustrated by considering the projection of the $\bar{\sigma}$ vector on the deviatoric plane. This plane is

inclined equally to all three orthogonal principal axes and enables the three dimensional stress system to be represented in two dimensions. The hydrostatic, or mean stress, is normal to this plane and as only constant volume deformations are considered its effects are ignored. The axes are chosen such that the angle of the stress vector on this plane is given by (see Fig. 29),

$$\tan \theta = \frac{1}{\sqrt{3}} \cdot \frac{\sigma_z - 2\sigma_\theta}{\sigma_z}$$

The equivalent stress is given by

$$\bar{\sigma} = \left[\sigma_\theta^2 - \sigma_z \sigma_\theta + \sigma_z^2 \right]^{1/2}$$

and by the use of these relationships the stress path may be constructed. The projections of all stresses on this plane should be multiplied by a factor of $\sqrt{\frac{2}{3}}$ (ref. (15)). In the diagrams given the scale was multiplied by this factor and the vectors given their true values. The stress paths for loading systems 3, 4 and 5 are given in Figs. 30, 31 and 32 respectively.

The angle of the strain increment is given by

$$\tan \psi = - \sqrt{3} \quad \frac{d\varepsilon_\theta}{2d\varepsilon_z + d\varepsilon_\theta}$$

If, for any loading conditions, the values of the strains are known then the angle of the equivalent stress vector $\bar{\varepsilon}$ is given by:

$$\tan \psi = -\sqrt{3} \frac{\varepsilon_\theta}{2\varepsilon_z + \varepsilon_\theta}$$

The strain paths corresponding to the stress paths are also given in Figs. 30, 31 and 32.

The two loading systems used to give the stress paths correspond to constant angles on the deviatoric plane. They are:

Simple tension: $\sigma_\theta = 0 \qquad \varepsilon_z = -2\varepsilon_\theta$

$$\tan \theta = \tan \psi = 1/\sqrt{3}$$

Internal pressure: $\sigma_\theta = 2\sigma_z \qquad \varepsilon_z = 0.$

$$\tan \theta = \tan \psi = -\sqrt{3}$$

The results are also presented in the form of $\bar{\sigma}$ vs $\bar{\varepsilon}$ in Fig. 33.

The problem of determining how $\bar{\varepsilon}$ varies with $\bar{\sigma}$ under these conditions of unloading and varying stress ratios must now be considered. If some relationship can be established then it would be possible to determine $\bar{\varepsilon}$ at any point during a complex loading cycle and hence describe the deformational behaviour completely.

The stress level of all these deformations is below that of overall yielding and hence no permanent deformation occurs. The deformation may therefore be considered to consist of two parts; a viscoelastic part and a creep part. As an initial explanation of the behaviour the following empirical relationships are proposed.

The elastic strain component is given by a linear relationship and a lag factor. For a loading process this is given by:

$$d\bar{\varepsilon}_L = \phi(1 - x)d\bar{\sigma}$$

where ϕ = elastic constant

x = lag factor .

For unloading this becomes:

$$d\bar{\varepsilon}_U = \phi(1 + x)\, d\bar{\sigma}$$

This is a vector equation and $d\bar{\varepsilon}$ is in the same direction as $d\bar{\sigma}$.

The basic creep relationship to be used is:

$$\frac{d\bar{\varepsilon}_L}{dt} = A\bar{\sigma}$$

where A = constant.

This may be expressed as:

$$d\bar{\varepsilon}_L = A/\frac{d\bar{\sigma}}{dt}.\bar{\sigma}.d\bar{\sigma}.$$

As each equal load increment is applied for an approximately constant time interval then

$$d\bar{\varepsilon}_L = b.\bar{\sigma}.d\bar{\sigma}$$

where $b = A/\frac{d\bar{\sigma}}{dt}$ which is a constant for a constant loading rate.

This is also a vector equation and $d\bar{\varepsilon}_L$ and $d\bar{\sigma}$ are in the direction of the stress vector $\bar{\sigma}$. The total strain increments are therefore given by:

$$d\bar{\varepsilon}_L = \phi(1 - x)d\bar{\sigma} + b\bar{\sigma}\, d\bar{\sigma} \qquad .....(23)$$

$$d\bar{\varepsilon}_U = \phi(1 + x)d\bar{\sigma} - b\bar{\sigma}\, d\bar{\sigma} \qquad .....(24)$$

The similarity in form with the Prandtl-Reuss equations is of interest as it illustrates the similarity with the creep and the flow functions. Future work will include extending the equation to cover permanent deformation in the form of a non-linear work hardening function.

If we now consider simple loading such as pressure loading then $d\bar{\sigma}$ and $\bar{\sigma}$ are in the same direction and equations (23) and (24) may be integrated:

$$\bar{\varepsilon}_L = \phi(1 - x)\bar{\sigma} + (b/2)\bar{\sigma}^2 + B$$

$$\bar{\varepsilon}_U = \phi(1 + x)\bar{\sigma} - (b/2)\bar{\sigma}^2 + C$$

The end conditions are:

$\bar{\varepsilon}_L = 0$ when $\bar{\sigma} = 0$ $\therefore$ $B = 0$

$\bar{\varepsilon}_L = \bar{\varepsilon}_U = \bar{\varepsilon}_c$, $\bar{\sigma} = \bar{\sigma}_o$ at the unloading point and hence

$$C = b\bar{\sigma}_o^2 - 2\phi x\bar{\sigma}_o$$

Hence:

$$\bar{\varepsilon}_L = \phi(1 - x)\bar{\sigma} + (b/2)\bar{\sigma}^2 \qquad .....(25)$$

$$\bar{\varepsilon}_U = \phi(1 + x)\bar{\sigma} - (b/2)\bar{\sigma}^2 + (b\bar{\sigma}_o^2 - 2\phi x\bar{\sigma}_o) \qquad .....(26)$$

In order to determine the constants from the loading and unloading curves obtained the equations may be expressed as follows:

$$\bar{\varepsilon}_L + \bar{\varepsilon}_U = 2\phi\bar{\sigma} + (b\bar{\sigma}_o^2 - 2\phi x\bar{\sigma}_o) \qquad .....(27)$$

$$\frac{\bar{\varepsilon}_L}{\bar{\sigma}} = \phi(1 - x) + (b/2)\bar{\sigma} \qquad .....(28)$$

$$\frac{\bar{\varepsilon}_U - (b\bar{\sigma}_o^2 - 2\phi x\bar{\sigma}_o)}{\bar{\sigma}} = \phi(1 + x) - (b/2)\bar{\sigma} \qquad .....(29)$$

The results taken from the mean curve drawn to the pressure results (Fig. 33) are given in Figs. 34, 35 and 36 respectively.

Equation (27) is seen to be valid and gives

$$\phi = .0675 \times 10^{-3} \text{ 1/lbf.}$$

and $$b\bar{\sigma}_o^2 - 2\phi x\bar{\sigma}_o = .006.$$

Equation (28) is an acceptable line but there is some evidence of curvature. This may be due to a creep law of the form

$$\frac{d\bar{\varepsilon}}{dt} = A\bar{\sigma}^n$$

In this case it is assumed n = 1 and the variations do not warrant the complication of including the power function. The values from Fig. 35 are:

$$b/2 = .0276 \times 10^{-6} \text{ 1/lbf}^2$$

$$\phi(1 - x) = .045 \times 10^{-3} \text{ 1/lbf.}$$

The value of $b\bar{\sigma}_o^2 - 2\phi x\bar{\sigma}_o$ from equation (27) is substituted into equation (29) and the resulting line is given

in Fig. 36. The constants are:

$$b/2 = .0270 \times 10^{-6} \text{ 1/lbf}^2$$

$$\phi(1 + x) = .088 \times 10^{-3} \text{ 1/lbf.}$$

The constants from the equations are in good agreement and indicate that the forms of the equations are valid. The mean values taken from these results are as follows:

$$\phi = .067 \times 10^{-3} \text{ 1/lbf.}$$

$$b = .054 \times 10^{-6} \text{ 1/lbf}^2.$$

$$x = 1/3.$$

The curves for the set of sample of tension results are also shown in Figs. 34, 35 and 36. The predicted linearity is not obtained here and it is assumed that this arose mainly from material inconsistencies which were considerable. Simple tension values up to the first change over point gave good agreement. Some variation in x and a more pronounced non linearity in the creep function may also occur in this type of loading (see section 4.1.).

It is noted that x and b are related in that $x = 0$ when $b = 0$ for a non time-dependent process.

For complex loading systems where $\bar{\sigma}$ and $d\bar{\sigma}$ are not in the same direction the strain path on the deviatoric plane may be constructed from the stress path. Consider a stress vector $\bar{\sigma}$, OA shown in Fig. 37, changing to OB. The line DE is then constructed parallel to AB the stress

vector (OD is the strain vector $\bar{\varepsilon}$). The length DE is $\phi(1 - x)AB$ for loading. EF is then constructed parallel to OB and EF is of length $b/2.\bar{\sigma}.CB$. The total strain increment is then given by DF and the new $\bar{\varepsilon}$ corresponding to OB is OF.

The strain paths for the stress paths given in systems 3 and 4 are shown in Fig. 38. System 3 consists of following the rectangular stress path and system 4 by retracing the stress path from station 12 back to zero. The experimental points obtained for these two paths are also given. Both loading systems show good agreement on the loading path (i.e. up to station 12). System 3 gives reasonable agreement on unloading although there is some displacement of the curves. System 4 gives poor agreement in that the experimental results give an unloading line parallel to the stress path indicating no creep. This is improbable and it is considered that the discrepancies are due to the imposed loading system. The tensile force is applied by imposing an axial extension while for the pressure the load is imposed and the extension results. This is not the theoretical condition of applying the stress system and measuring the strain resulting from this.

The $\bar{\sigma}$ vs $\bar{\varepsilon}$ relationship derived from the theoretical strain paths are shown in Fig. 39. There is

considerable difference between these and the simple unloading curve. The experimental points are in much better agreement, probably owing to the loading systems used. The implications of these results are not clear and more accurate experiments are required to draw a clear conclusion.

The analysis does provide a method for predicting simple loading and unloading curves for below yield stresses. The technique for dealing with complex loading systems shows some promise but a great deal more work is required to draw any firm conclusions. The relation of the empirical equation to linear viscoelastic theory will also be considered when more evidence is obtained.

4.5. Conclusions

The plane strain compression test provides a method of overcoming the stability and measurement difficulties inherent in the simple tension test. The problems of friction and of die and specimen geometry have been fully investigated and an accurate and valuable testing method has been developed. It is also possible to separate recoverable and permanent deformations easily and thus a powerful tool for investigating flow properties is made available. The semi-static test gives repeatable and easily obtained curves for the total deformational behaviour and gives a good measure of the low strain rate properties.

The use of this curve to predict the behaviour of other stress systems under simple loading (i.e. constant stress ratios) by means of equivalent stress and strain has been successful. The cases examined were not treated in great detail as it was considered that a broad examination would be more profitable at this stage. The agreement with experimental results for the cases examined is excellent. The problems of dealing with more complex problems such as the stress varying throughout a body and the calculation of instability loads have also been examined and good agreement with experimental results obtained. This analytical technique provides a useful method of carrying out design calculations in the engineering applications of plastics.

The problem of dealing with complex loading (i.e. varying stress ratios) and unloading has been examined and a solution using a deviatoric plane construction proposed. This shows some promise but doubts as to the loading systems employed in the experiments prevent any firm conclusion being drawn. A full examination of this problem will require the development of sophisticated apparatus which could not be attempted in the time available. The solution presented is therefore a proposal on which future work may be based.

PART II

5.0. Introduction

Plastics film is widely used in packaging where it is required to withstand impact loading. The problem of devising a suitable test for estimating strength under these conditions has been attempted by several workers. To be successful the test must include loading systems similar to those met in practice and give accurate and easily reproducible values. The conditions usually adopted are some measure of the energy required to produce penetration of the film by a projectile. The ball and dart drop tests (refs.19,20) are widely used and consist of dropping a ball or hemispherical headed dart onto a clamped film from increasing heights or with increasing weights until a 50% failure rate of samples is attained. The height or weight at which this occurs is quoted as the 'dart drop' impact strength. The test is easily performed but the reproducibility is doubtful. Attempts to correlate the results with other tests (ref.21) have met with little success.

A more refined type of test consists of measuring the actual energy absorbed on penetration. These are generally of the dropping ball or ballistic pendulum type (ref.22). A machine described by Elmendorf (ref.23) is an example of the latter and the excess energy after penetra-

tion by the striker pendulum is measured by means of a timing device and the energy absorbed by difference with the initial value. Some correlation with practical applications such as bag dropping are reported. The test would appear to be the most satisfactory available but its general adoption has presumably been limited by the complexity of the calibration and energy measurement which is the usual objection to this type of test. The machine used in this work is of a similar type but has the advantage that the complexity is eliminated. The design was carried out by R.S.Collingwood (ref.24) and is based on a principle suggested by Professor H. Ford.

6.0. Machine Design

The principle of operation of most pendulum impact machines such as those used in the Charpy and Izod tests is that the pendulum is released from a known height, fractures the specimen at the bottom of the swing, and the height to which it rises is determined. The difference in potential energy corresponding to the original and final heights gives the energy absorbed in fracturing the specimen. The nature of the film requires that it be supported in a ring and thus the pendulum, with the striker head attached, cannot complete the swing. This can be overcome by mounting

the striker head on a very long extension piece (ref.25) but the mechanical difficulties make the idea unpractical. The alternative is to mount the striker head on a short extension piece, long enough to complete the penetration of the film and then absorb and measure the excess energy. In this design this is done by allowing the striker head to contact an abosrber pendulum which rises to a measurable height, and by suitable calibration the fracture energy may be determined.

The striker pendulum (see Fig.40) has a two inch diameter hemispherical striker head on a six inch extension piece and is capable of delivering 25 in. lb_f at 17 ft/sec. The absorber pendulum rests against a step behind the clamp and has a light head located in line with the striker head. On impact the absorber pendulum rises carrying with it a lazy pointer enabling its angle of rise to be determined.

The clamping device should give a uniform, low, initial tension with reasonable ease. The design consists of three rings, a backing ring, a clamping ring and a locking ring. The film is placed between the backing and clamping rings which have curved mating surfaces with slightly different radii to give line contact. When the locking ring is screwed down the clamping ring is prevented from rotating by locating pegs. The free aperture of the

specimen is six inches in diameter.

It is generally desirable to have the centre of percussion of the striker pendulum at the point of impact as this gives zero reaction at the supports. Even with this condition errors of up to 40% have been reported on large Charpy machines owing to energy absorbed by the support. In this design the shape of the pendulum prevented this being achieved but as the forces involved are small compared with machine rigidity the effect is not considered important.

7.0. Calibration and Accuracy

The initial energy of the striker pendulum is absorbed in the following ways:

1) Windage and friction losses on the downward swing.

2) Fracture and distortion of the film.

3) Loss on impact with absorber pendulum.

4) Energy imparted to the absorber pendulum.

If the case of the pendulums colliding without a specimen being interposed is considered then for every initial position of the striker pendulum there is a corresponding height to which the absorber pendulum rises. Thus any

value of the angle of rise θ of the absorber pendulum corresponds to a particular energy for the striker pendulum. If, after fracturing a film, the striker pendulum gives a reading of θ, the energy left in the striker pendulum after fracturing may be found. The energy corresponding to the initial position is then found and hence by difference the energy absorbed in fracture may be calculated. The calibration curve relating θ to the initial position of the striker pendulum accounts for both the energy transferred to the absorber pendulum and that lost on impact as the impact is between essentially rigid bodies and hence depends only on the striker pendulum energy.

Fig.41 shows the calibration curve where θ is plotted against an angular measure of the striker pendulum initial position ϕ which is measured from an arbitrary zero displaced 42.5° from the true zero. The repeatability of this curve was investigated by taking forty readings for each of three values of ϕ. Histograms of the distribution of these values, read to 0.1° with the scale calibrated in 0.5° divisions are shown in Fig41. The values group around the scale marks indicating that the distribution is due to observer choice. The machine may therefore be taken to be repeatable to within $\pm 0.25^{\circ}$, i.e. $\pm$ 0.08 in.lb_f

at $\phi = 65^{\circ}$ and $\pm$ .06 in lb_f at $\phi = 0^{\circ}$.

The windage and friction losses on the downward swing must be subtracted from the initial potential energy value used in the calculations. They are brought about by friction in the bearings and the drag of the surrounding air. As the pendulum has a large surface area to weight ratio the bearing friction losses would be expected to be low compared with the air friction losses. These would be in the form of viscous damping and would result in the following relationship

$$\log_e x = A - BN$$

where x = angle of swing

N = number of swings

and A ; B = constants.

Fig. 43 shows results taken from a test where the striker pendulum was allowed to swing freely and x was measured every ten swings. The assumption of viscous damping is confirmed. This corresponds to a loss of 0.1 in.lb_f for the maximum downward swing at $\phi = 65^{\circ}$ which is less than the calibration accuracy and may be neglected. Thus the energy before impact may be taken as the potential energy corresponding to the initial value of ϕ.

To summarise the calibration procedure;

a) The initial energy is determined from the

initial value of ϕ,

b) A value of θ from the absorber pendulum is found from the impact test,

c) The corresponding value of ϕ may then be determined from the calibration curve and hence the residual energy calculated,

d) The difference between the initial and the residual energy is the energy absorbed in fracturing the film. The value may be quoted to an accuracy of $\pm$ 0.1 in.lbf.

In some tests film adheres to the striker head and a test was carried out with the striker head covered with polyethylene film. No variation of greater than 0.5% in the calibration curve was found and the effect may be ignored.

8.0. Testing Procedure

When testing a film it is necessary to examine a set of specimens taken from the batch for which the impact strength is required. Plastics film is subject to wide variation, even within a batch, and it is necessary to know the expected accuracy of any value determined. To investigate the effect of sample size, fifty specimens* were tested from a clay-flat polyethylene film (E 2069) of density

* The code numbers are those of Polymer Services Laboratory, U.S.I. who kindly provided the material and definitions are given in Table 2.

.923, melt index 5 and a nominal thickness of 1.2×10^{3} ins. Histograms of the results as taken from each side of the lay-flat tubing are shown in Fig. 44. The shading directions in-indicate the values from each side and the cell size is taken as 0.5 in lb_f.

There is a marked difference between the two sides and considerable variation within each set. Such variations are brought about by manufacturing errors resulting in material inconsistencies and localised variations in thickness. Attempts to measure thickness variation were unsuccessful as the techniques available, such as comparators and micrometers, were not capable of measuring local thickness variations. When defining a mean value for the film both sides of the tube must be included. The fifty specimen mean is not a statistically true mean as this is a sample of a larger population but as the distribution is bimodal and therefore statistically complex it is considered, that for practical purposes, it is a sufficiently accurate measure of the mean energy.

The mean calculated from smaller sample sizes will differ from this value. To estimate this effect the fifty values were considered in samples of one, five, ten and twenty five in the order in which they were taken from the tubing. The means for each of these samples were then calculated and the average variation of the means of each set of samples from the fifty specimen mean was determined. These are shown plotted as a percentage against the number of

specimens per sample in Fig.45. The largest or worst variation from the fifty sample mean for a given sample size is also given. Thus for a sample of ten specimens the likely variation from the fifty specimen mean is ± 3.5% with a possible maximum of ± 6.5%. This is considered to be a more realistic estimation of accuracy than a standard deviation as the distribution is not normal as is required by the calculation of the standard deviations. The variations obtained depend on the particular film and Fig. 46 shows the expected variation for another polyethylene (E 2066) film. The mean variation for ten specimens in this case is ± 8.0%. In the tests to be described the ten specimen means were determined and the variation from a fifty specimen mean is expected to be less than ± 10% with a possibility of up to ± 15% variation for the worst case. These values refer to specimens taken from one section of the lay-flat tube. Slightly better accuracy would be expected if the specimens were taken from widely separated sections if it is ensured that an approximately equal number is taken from each side of the tube. The values quoted here refer to polyethylene film as this is the major concern of this work. Further tests of this type are necessary for other plastics.

The velocity at impact can affect the energy absorbed as plastics are rate sensitive materials. This may

be varied by means of varying the initial angle of the striker pendulum. To investigate as large a range of velocity as possible a loaded pendulum was used as well as the normal one as the energy available varies with initial angle and to achieve fracture at the lower velocities extra weight was required. Fig.47 shows the curves obtained for two polyethylene films E2181 and E2185. The continuity of the curves over the normal machine characteristic indicates that the fracture energy is essentially independent of the energy available. There is, however, considerable variation with velocity, particularly with the higher energy values and it is necessary to define the velocity of testing. The tests carried out in this programme were at 17 ft/sec which corresponds to an initial energy of 25 in lb_f for the normal pendulum.

The initial tension in the film may also affect the energy value obtained. The consistency of tension in the clamping arrangement used depends largely on operator skill and in the tests performed care was taken to ensure uniformity between specimens. A test was carried out with a polyethylene film E2068 in which one sample of ten specimens was clamped as tightly as possible and a second sample with approximately $\pm$ 1 inch slack at the centre. The former gave a mean of 13.4 in lb_f and the latter 13.5 in lb_f

indicating that in this clamping technique it is difficult to obtain anything other than zero tension. Thus with careful mounting of the specimens no appreciable error should result.

When the fracture energy is low a more accurate value may be obtained by testing several thicknesses at once. This is illustrated in Fig.48 where the fracture energy is shown plotted against the number of thicknesses for polyethylene film E 2185 of thickness 0.7×10^{-3} inches. Numbers greater than about six are undesirable as those thicknesses furthest from the striker head tend to be subjected to a different stress system. Up to this value there is a simple additive process.

The temperature of a film affects the fracture energy and in applications such as frozen food packaging variations in impact strength of this nature are important. It is hoped to carry out some work on this topic later but the present tests were all at 23°C with variations not greater than $\pm$ 1°C.

The standard procedure used, unless otherwise stated, may be summarised as follows:

1) The specimen is clamped with zero tension.

2) The pendulum delivers 25 in lb_f at 17 ft/sec.

3) The temperature is constant at 23°C.

4) The mean of ten specimens is quoted, which, for polyethylene films is within ± 10% of the fifty specimen mean. This variation is due to the material and not the machine.

5) The specimen has an effective diameter of six inches and the striker head is a two inch diameter hemisphere of polished aluminium.

The effects of friction over the striker head are also of importance and are discussed fully in a later section.

9.0. Test Results

9.1. Impact Test

a) Polyethylene

Fourteen different types of polyethylene film were tested and the results, together with details of density, melt index, and thickness, are given in Table 2. Also given are tensile test results and Elmendorf tear test and Dart Drop values as determined by Polymer Services Laboratories. The impact values are divided into three columns each corresponding to a type of fracture which are defined as follows:

Split: See Fig. 49a. This is a single break usually two or three times longer than the striker head

diameter. There is little or no evidence of permanent deformation around the break.

Tear: See Fig. 49b. This type of fracture consists of a break somewhat smaller than the striker head diameter with significant permanent deformation around the break.

Hole: See Fig. 50a. The film breaks in a circular ring with large permanent deformation.

Most of the fractures obtained could be divided into these three categories and in some cases two types occurred within one sample of ten specimens. The numbers of the type found in the sample together with the mean energy are given in Table 2. Fig. 51 shows the mean energies plotted against film thickness and three lines corresponding to the three fracture types are indicated. The 'weak' points are those of means of less than five specimens with expected errors of greater than $\pm$ 10%. All points except the 'weak' values and one split value (E 2066) lie within the limits of $\pm$ 10% of the mean line. The energies per unit thickness (W) for the three types of fracture are as follows:

Split 6.0×10^3 in $lb_f/in.$, Tear 8.3×10^3 in lb_f/in,

Hole 12.7×10^3 in $lb_f/in.$

Certain fractures such as that shown in Fig. 50b

are difficult to classify on appearance but reference to the value of W will give a definite classification.

b) Polypropylene

Ten specimens of E 1964 of density 0.9108 and thickness 0.5×10^{-3} ins were tested. The values ranged from 1.0 to 23.2 in lb_f. with wide variations in the type of fracture obtained. The fractures where made up of straight, highly localised, splits parallel and normal to the machine direction. The higher energies were found to be proportional to the length of the parallel fractures and independent of the normal fracture. The lower energies bear no relation to either fracture length. Further testing would be required to determine the cause of the low energy types of fracture and at present all that can be said is that the film is prone to wide variations, in some cases with values as low as 1.0 in lb_f, and care should be taken in its application.

c) Melinex

Two to three inch long splits were obtained with a mean of 15.6 in lb_f.

d) M sat. (Nitro-cellulose coated cellulose)

A very distinctive radial fracture pattern formed resulting in very large numbers of streamers at a radius

of about two inches. One blow was found to be insufficient and two blows were used. This results in a high value as some energy is absorbed by recovery between the blows. The value is quoted for comparative purposes and is approximate. The mean value obtained was 39.5 in lb_f.

e) Saran Wrap No. 7

The number of blows required varied from one to five with variations in values of 9.5 to 114 in.lb_f. As in the previous case these can only be taken as approximate indications. The mean value was 70 in lb_f and the fractures varied from straight splits (low energy) to numerous radial splits (high energy).

9.2. Notch Sensitivity

Many impact failures of film in practice take place at much lower energies than anticipated because of flaws or breaks already present in the film. It is desirable to have a measure of the sensitivity of film to the presence of these flaws or notches and this test was developed for this purpose. In the case of breaks in the film it was considered that a razor blade slit would be the most severe case and was therefore adopted. The position and size of the slit would determine its effect and a series of tests were carried out to determine the worst cases i.e.

that which produces the largest decrease in energy from the unnotchedvalue. As the principal concern is polyethylene this was used for the exploratory work and the results applied to other materials. Modification may however be required as experience is gained.

a) The Effect of Notch Length

Four materials were tested; E2184 and 2186 split materials, E2069 a tear material and E2182 a hole material. Two curves were determined for each material, the first with the slits normal to the extrusion direction, and the second with the slits parallel to the extrusion direction. The results are shown in Figs. 52, 53,54 and 55. For both split and tear materials the fractures formed along the extrusion direction while for the hole material they formed in the direction of the slits.

The split and tear materials show a marked initial drop for the parallel slits which may be taken as a measure of notch sensitivity. The normal slits gave a more gradual decrease and for the hole material a gradual decrease was obtained for both parallel and normal slits.

The test must be defined in terms a single notch length if the test is to be used for routine determinations. The length chosen was 0.5 inches and the notch sensitivity

is defined by the ratio of the energy absorbed by the notched specimen to that of an unnotched specimen. The suffices p and n refer to slits parallel and normal to the extrusion direction. The values for the materials tested are given in Table 3.

Table 3

Code No.	Type of Failure	Unnotched energy (in lb_f).	α_p	α_n
E2184	Split	6.5	.507	.837
E2186	Split	6.9	.561	.561
E2069	Tear	13.9	.465	.606
E2182	Hole	17.7	.504	.504

b) Effect of Angle of Notch to Extrusion Direction

Half inch slits were placed at various angles to the extrusion direction for split, tear and hole materials and the results are shown in Fig. 56. The 0° and 90° cases are the limiting values except for a slight decrease at 45° for the hole material which is not sufficient to warrant a special test. Thus the α_p and α_n values will give the range of sensitivity for the materials.

c) Effect of Position of Notch

As there is a stress variation over the film on impact the central position is not necessarily the worst case. To determine this half inch slits both parallel and normal to the extrusion direction were inserted at various distances from the point of impact. The results are shown in Figs. 57, 58 and 59. There is a slight decrease for the normal slits in the split material at an offset distance of one inch. The decrease is not below the minimum parallel value however and will be neglected. The minima for all other cases are at the impact centre (i.e. zero offset). The apparent increases above the unnotched values at about one inch offset is due to two sets of fractures forming, one at the centre and the other at the slit.

The two limiting, most severe conditions, are with the half inch slits parallel and normal to the extrusion direction at the point of impact. The values given are the means of five specimens and Fig. 60 shows the 90% confidence limit for a typical set of values with two repeated values. The confidence limits correspond to approximately $\pm$ 10% variations. The variations in the results are much less than the unnotched specimens as they are less sensitive to flaws.

The notch sensitivity factors were determined for

other types of film and are shown in Table 4.

Table 4

Name	Unnotched Value (in lb_f)	α_p	α_n
Melinex	15.6	.23	.22
M.sat.	39.5	$<.001^*$	-
Saran Wrap	70.0	.03	.03

* Two values taken; below the limit of the machine accuracy.

It is interesting to note that the higher strength films are much more notch sensitive than the polyethylenes.

A further type of flaw is a crease or fold as found along the edge of lay-flat tubing. Although less severe than razor blade slits they cover long lengths of material. A simple comparative test for the sensitivity to this effect is to test film with the fold as a diameter of the specimen. As an example polyethylene film E2183 was tested with folds parallel and normal to the extrusion direction. The results were as follows:

Unnotched value = 9.5 in lb_f.

Razor blade slit values;

$\alpha_p = .60$, $\alpha_n = .85$

Fold parallel to extrusions $\alpha = .25$

Fold normal to extrusion $\alpha = 1.00$.

The normal fold has no appreciable effect but the parallel fold can give α values much below the slit values.

9.3. Impact Fatigue Test.

In many applications film is fractured by repeated blows whose energy is below that required to cause failure in a single blow. During the interval between blows the material dissipates some of the absorbed energy and the total energy required for fracture is therefore larger than the single blow value. This total energy will depend on length of the interval(ie.frequency of blows) and for any particular value an energy per blow may be determined, similar to the normal fatigue limit, below which a very large total energy to fracture is required. If a frequency for a particular application is known this value of fatigue limit will give an indication of the safe permissible impact loading.

Ref.26 describes a machine designed for this type of testing which consists of a pendulum similar to that on the impact testing machine, mounted in a horizontal position.

It is considered that the test described here is more useful in that it can be carried out on the impact machine and that the value obtained is of immediate practical value.

The shorter the interval between blows, the lower will be the fatigue limit. In these tests a value of 1 - 2 sec. was used as it was considered to be the most severe likely to be encountered in practice. Energy absorbed to fracture versus energy per blow curves were determined for polyethylene film E2184, a split material, and E2181 a hole material by releasing the striker pendulum from appropriate heights and are shown on Figs. 61 and 62. The points are for single specimens as averages would obscure groupings at the discontinuities due to the repeated blows.

The energy increase owing to the first interval between blows is clear on both curves but increases owing to other intervals are smaller due to smaller energies per blow and are obscured by scatter. The types of fracture were identical with those obtained for a single blow except for isolated tears in the hole material. The fatigue strength factor β will be defined as the ratio of the fatigue limit to the single blow fracture energy under standard conditions. The results for these materials are given below.

Code No.	Fracture Type	Single Blow Energy	Fatigue Limit (in lb_f)	β
E2184	Split	6.5	2.5	.38
E2181	Hole	14.9	3.5	.23

The split material has a better relative fatigue strength than the hole material but the latter still has the higher absolute value.

10.0. Effect of Friction

In impact tests the film is fractured by penetration with the hemispherical striker head. The type of fracture obtained may be governed, not only by the mechanical properties of the material, but also by the friction between the film and striker head. This friction determines the deformation and stress conditions over the dome of the striker head which in turn determine the type of fracture which results. Under certain conditions polyethylene film will adhere to highly polished metal surfaces by a mechanism usually ascribed to electrostatic attraction and termed 'blocking'. This results in very high frictional forces which restrain the film from moving over the surface. The addition of

additives to the film or grease on the metal surface can eliminate this effect and allow the film to slide freely.

To determine the friction conditions in the impact test it would be desirable to analyse the dynamic loading conditions. This is a very complex problem and as a first step an analysis of the very slow or 'semi-static' case was performed. For these low speeds a basic stress-strain curve for the material may be obtained and the load deflections predicted for various frictional conditions. The general case, for any value of coefficient of friction between the surfaces, is complex and for this work it was considered sufficient to consider two limiting cases. They are zero friction and full friction. Only the material over the dome has been considered as this is of principal importance.

1) Zero Friction

Using the nomenclature defined in Fig. 63 the equilibrium of the forces across the section of contact XX gives;

$$\sigma_r t = \frac{F}{2b\pi} \cdot \frac{1}{\sin^2 \alpha} \qquad \ldots\ldots(30)$$

For this condition we shall assume σ_r to be constant over the dome and that the material over the dome originated as a circle of radius b sin α. When the principal stress ratios are constant throughout the deforma-

tion process the flow equations of plasticity may be employed:

$$\frac{\delta\varepsilon_r}{\delta\varepsilon_\theta} = \frac{\sigma_r - \frac{1}{2}(\sigma_\theta + \sigma_t)}{\sigma_\theta - \frac{1}{2}(\sigma_t + \sigma_r)}$$

where $\delta\varepsilon_r$ and $\delta\varepsilon_\theta$ are the increments of radial and hoop strains. Strain is defined as

$$\varepsilon = \ln.\lambda \text{ and } \delta\varepsilon = \frac{\delta\lambda}{\lambda}$$

where λ = extension ratio, the ratio of the strained to the original length.

For σ_r = const; $\sigma_r = \sigma_\theta$ and $\sigma_t = 0$ for thin films.

$\therefore \quad \delta\varepsilon_r = \delta\varepsilon_\theta$ and $\lambda_r = \lambda_\theta$.

Thus using the second assumption;

$$\lambda_\theta^2 = \frac{2}{1 + \cos\alpha} \qquad \text{.....(31)}$$

The equivalent strain increment is defined as follows:

$$\delta\bar{\varepsilon} = \frac{\sqrt{2}}{3}\left[(\delta\varepsilon_1-\delta\varepsilon_2)^2 + (\delta\varepsilon_2-\delta\varepsilon_3)^2 + (\delta\varepsilon_3-\delta\varepsilon_1)^2\right]^{1/2} \qquad \text{..(32)}$$

For polyethylene we may assume a constant volume deformation and thus:

$$\lambda_r\lambda_\theta\lambda_t = 1 \qquad \text{.....(33)}$$

where λ_t = through thickness extension ratio.

Thus $\delta\varepsilon_r + \delta\varepsilon_\theta + \delta\varepsilon_t = 0$ and $\delta\varepsilon_r = \delta\varepsilon_\theta$

$$\therefore \quad \delta\varepsilon_t = -2\delta\varepsilon_\theta$$

Substituting into equation 32:

$$\delta\bar{\varepsilon} = 2\delta\varepsilon_\theta \quad \text{i.e.} \quad \bar{\varepsilon} = 2\varepsilon_\theta$$

$$\text{But } 2\varepsilon_\theta = \ln \lambda_\theta^2$$

and
$$\bar{\varepsilon} = \ln \frac{2}{1 + \cos \alpha} \qquad \text{.....(34)}$$

The equivalent stress is defined as follows:

$$\bar{\sigma} = \frac{1}{\sqrt{2}}\left[(\sigma_1-\sigma_2)^2 + (\sigma_2-\sigma_3)^2 + (\sigma_3-\sigma_1)^3\right]^{1/2} \qquad \text{.....(35)}$$

For thin film we may assume $\sigma_t = 0$ where σ_t is the through thickness stress and hence:

$$\bar{\sigma} = \sigma_t$$

From equation (4) we have:

$$t = t_o \frac{(1 + \cos \alpha)}{2} .$$

Substitution in equation (1) gives:

$$\left(\frac{F}{\pi b t_o}\right) = \bar{\sigma}.\sin^2\alpha(1 + \cos \alpha) \qquad \text{.....(36)}$$

Thus for any value of α the corresponding value of $\bar{\varepsilon}$ may be calculated from equation (34). Reference to the equivalent stress-strain curve for the material will give the appropriate value of $\bar{\sigma}$. This may then be substituted in equation (36) to give the value of F corresponding to the value of α. By choosing a number of values of α the curve of F versus α may be constructed.

2) Full Friction

For this case there is no movement of the material over the dome and hence all the material distortion is in the radial direction and $\lambda_\theta = 1$ i.e. zero straining in the hoop direction. Assuming as before that the material over the dome comes from a circle of radius b sin α, λ_r at the point of contact is given by:

$$\lambda_r = \frac{bd\alpha}{d(b \sin \alpha)} = \frac{1}{\cos \alpha} \qquad \ldots\ldots(37)$$

When the principal stress ratios are constant the flow equations of plasticity are applicable:

$$\frac{\delta\varepsilon_r}{\delta\varepsilon_\varepsilon} = \frac{\sigma_r - \frac{1}{2}(\sigma_\theta + \sigma_t)}{\sigma_t - \frac{1}{2}(\sigma_r + \sigma_\theta)} \qquad \ldots\ldots(38)$$

As $\lambda_\theta = 1$, $\delta\varepsilon_\theta = 0$ and from constant volume we have:

$$\delta\varepsilon_r = -\delta\varepsilon_t.$$

Also $\sigma_t = 0$ and therefore, from equation (38):

$$\sigma_\theta = \frac{\sigma_r}{2} \qquad \ldots\ldots(39)$$

Substituting in equations (32) and (35) we have

$$\bar{\varepsilon} = \frac{2}{\sqrt{3}} \ln \frac{1}{\cos \alpha} \qquad \ldots\ldots(40)$$

and $$\bar{\sigma} = \frac{\sqrt{3}}{2} \sigma_r$$

From constant volume, $t = t_o \cos \alpha$ and substituting

in the equilibrium equation (30) gives:

$$\left(\frac{F}{\pi b t_o}\right) = \bar{\sigma}.\frac{4}{\sqrt{3}} \sin^2\alpha \cos\alpha \qquad \ldots\ldots(41)$$

Thus by the use of the equivalent stress-strain curves and equations (40) and (41) the curve of F versus α may be determined.

To obtain the experimental load versus angle of overlap α curve a piece of cord was attached to the striker pendulum and passed over a pulley. Weights were then hung on the chord and α was determined by measuring the diameter of the circle of contact. The polyethylene film used was E2066 and two curves were obtained, one with the polished aluminium head dry and the other with it covered with grease. These curves are shown in Fig. 64 together with the theoretical curves for full and zero friction derived using an appropriate basic stress-strain curve obtained from a plane strain compression test.

The lubricated head gives a close approximation to zero friction and this is borne out by observing the types of fracture produced. For all three types of fracture in polythene film there was evidence of even stretching over the dome with the multiple fractures forming in many cases.

The polished head condition approximates to full

friction and the conclusion that the radial extension increases with α, ($\lambda_r = \frac{1}{\cos \alpha}$), is borne out, by highly deformed annuli at high angles of overlap prior to fracture.

Comparison of these static fracture types with those obtained under the standard dynamic conditions indicated that the lubricated head did give the uniform stress system for the split materials where low overall deformations were involved. For tears and holes however the effect was not so marked. The polished head gives split and tear fractures from the pole of the dome under dynamic conditions while holes are formed by fracture in the annular region around the head. The most reasonable explanation for this is that for small penetrations sliding does occur resulting in low deformation fractures at the pole. For large penetrations friction becomes more effective and the annular failure corresponding high friction takes place. The presence of a lubricant increases the amount of penetration which takes place under low friction conditions and thus increases the likelihood of failures at the pole. The material properties are therefore the governing factor in determining the type of fracture formed. Splits form at low deformations which correspond to low friction and tears form with higher deformations but when the friction is not sufficiently pronounced to produce an

annular stress concentration. Holes arise when fracture takes place at such high deformations that the frictional effect produces the stress concentration around the head.

The frictional conditions on the striker head are not then of any fundamental importance in this type of test. If however it is required to test a material under conditions of 1:1 tension for a particular application then the lubricated head will give a more accurate assessment of the energy absorbed.

11.0. Comparison with other Tests

There is no well defined direct correlation between the tensile or Elmendorf Tear test results and the Impact test results shown in Table 2. There is however some correlation with the Dart Drop test as is shown in Fig. 65. Such a correlation would be expected considering the similarities of the tests. The correlation of the Dart Drop test with other parameters such as thickness is very poor and the variations in Fig. 65 are due mainly to scatter in the Dart Drop values. An approximate conversion factor could be taken as:

Impact Energy = .14 x Dart Drop value.

Future work includes a large scale comparison of the two tests.

The sand bag drop test is frequently employed as it is very close to practical conditions. Unfortunately, results are subject to wide scatter depending on how the bag is made, tied and dropped. As a comparison bags were made from polyethylene film E2183 by heat sealing the lay-flat tubing. The bags were filled with 13 lbs. of dry sand and tied at the neck. They were then dropped and a bursting height of approximately 30 ins. was determined. Examination revealed that all the bags fractured along the edge folds and that there was approximately 100 in^2 of effective area absorbing the shock determined by a circle of stressed material 12 ins diameter. This corresponds to an energy per unit volume of material to fracture of 3,250 in lb_f/in^3.

The stress system of the bag is approximately 1:1 tension and accordingly a lubricated impact test was performed on both plain and creased specimens. The effective area of the material was assumed to be a circle of equal diameter to the striker head. The energies per unit volume were 5,700 in lb_f/in^3 for the plain film and 3,630 in lb_f/in^3 for the folded specimens. The agreement of the second value with the 3.250 in lb_f/in^3 of the bag test is good and illustrates the practical value of the impact test.

12.0. Impact Fracture of Polyethylene Film

12..1. General Introduction

In general when a material is subjected to a stress system it deforms first elastically, then plastically and finally ruptures. The amount of plastic deformation or flow that a material undergoes largely governs the energy required to cause fracture and is determined by the material ductility or ability to undergo plastic deformation. The fracture criteria (i.e. stress or strain conditions at which fracture occurs) are not usually greatly affected by such parameters as strain rate or temperature. The onset of flow is sensitive to them however and usually this criterion is increased by increasing the strain rate and decreasing the temperature and under such conditions fracture may occur before plastic flow. Fractures produced before plastic flow therefore are at much lower energies than those preceded by flow and the terms brittle and ductile are applied respectively. The terms do not however refer to any particular type of fracture but refer to the relative values of energy absorbed in the two types.

In certain cases low energy fractures may result even when flow precedes the fracture. If a flaw or material discontinuity is present an elastic stress concentration and very localised plastic flow will result. For

highly ductile materials the plastic flow may completely relieve the concentration but often it will not and fracture will occur. Material anisotropy which restricts the flow to one direction in effect concentrates the deformation still further and increases the likelihood of localised failure.

The formation of the fracture releases elastic energy from the rest of the material and if the plastic flow is very localised this energy may be sufficient to propagate the fracture through the material. Fractures taking place before plastic flow has occurred may also be of this type and it is usually referred to as unstable cracking. In other cases an external supply of energy is required to propagate the fracture and this is termed stable cracking. Initiation energies are usually associated with unstable fractures and may be accounted for as follows. The released elastic energy is generally in excess of that required to propagate the fracture. If a very sharp notch is present the elastic energy has only to reach the propagation value for the crack to form. The difference between the two values is therefore an apparent energy necessary to initiate the crack.

Two types of unstable fracture are therefore possible.

1) When the material ruptures before plastic flow takes place. This can be brought about by measuring the strain rate or decreasing the temperature which give a flow initiation at a higher stress level than the fracture criterion. Certain triaxial stress systems can also produce the same effect by lowering the fracture criterion.

2) Very localised plastic deformation can be produced by stress concentrations owing to specimen or load geometrys and by material anisotropy. These conditions are aggravated by any increase in the flow criterion as described in 1) as the amount of flow prior to fracture is decreased.

For the discussion of the impact failure of polyethylene film which follows the second type is of principal interest.

12.2. Film Manufacture

Most of the polyethylene film is manufactured by extruding a melt through an annular die. The tube produced is then drawn off to give a considerable reduction in thickness and then cooled rapidly at some distance from the die generally termed the "freeze line distance". For blown film the drawn tube is inflated to form a bubble prior to freezing. The effect of the manufacturing conditions on the impact properties of the film has been discussed in

ref.27 and the conclusion reached is that the relationships are extremely complex. This discussion will however consider the possibility of relating the impact properties to the principal mechanical properties determined by the manufacturing conditions.

The melt index of polyethylene is a very approximate measure of the mean molecular weight. It is approximately inversely proportional to the molecular weight and may be considered as a measure of the mean length of the long chain molecules. The manufacturing conditions have very little effect on its value.

The density may be regarded as a measure of the degree of order within the material. The higher the density the more closely packed are the molecules. The packing is in the form of crystallites and the formation of these is largely determined by the manufacturing conditions. The ductility of the material is greatly reduced by the presence of the crystallites and hence the higher the density the lower the ductility.

The orientation in the film is almost totally dependent on the amounts of drawing and blowing used in manufacture. The amount present will however be affected by the cooling conditions as slow cooling gives the material time to readjust to lower orientation conditions. Thus, for

example, under a fixed set of conditions thick film will tend to be less orientated than thin as it cools less rapidly. Low density film will in general tend to have low anisotropy as the molecular movement is less restricted than for high densities. High anisotropy can be produced in low density film however by suitably rapid cooling.

The two principal mechanical characteristics influenced by the manufacturing process are therefore ductility and anisotropy and these will be considered as the main criteria for fracture.

12.3. Measurement of Ductility and Anisotropy

The ductility of a polyethylene will be determined by its density and to a lesser extent by the melt index as the larger molecules tend to restrict flow more than the smaller ones. To determine a single value combining these two effects a modification of the plane strain compression test(Part I) was employed. In this test a plate of the material is indented from both sides by two lubricated, highly polished, dies. It is usual to determine a full stress-strain curve for the material but in this case a single value test was devised. Dies of 0.25 ins breadth were used and a stress of 3,000 psi was applied to the material for a 'dwell' time' of 10 minutes at 20°C and the resulting deformation was

measured 24 hours after unloading. The ductility was characterized by the ratio λ defined as:

$$\lambda = h/h_o$$

where h_o = original thickness of the plate

h = final thickness of deformed section after 24 hours recovery.

A number of isotropic plates were used of various densities and melt indices and of thickness .075 ins and width 2 ins. The Polymer Services code number together with density, melt index and λ are shown in Table 5 and λ plotted against the density is shown in Fig. 66. The expected trends with density and melt index are evident although parts of the

Table 5

U.S.I. Ref. No.	Density	Melt Index	λ at 3000 psi
E2065	.918	3.0	0.589
E2073	.920	3.0	0.685
E2179	.923	3.0	0.802
E2176	.933	3.0	0.945
E2078	.922	5.0	0.715
E2074	.923	5.0	0.716
E2167	.929	5.0	0.856
E2077	.918	8.0	0.514
E2072	.923	8.0	0.674

curves are necessarily speculative due to the small number of points. The values of λ corresponding to each film were determined from Fig. 66 and are shown in column 13 in Table 2.

The anisotropy of the films is determined from the tensile data shown in columns 5, 6 and 7 of Table 2. The yield stress is not easy to define and any measure of anisotropy involving it would be unreliable. The elongation to failure is the most meaningful measure of anisotropy but this is also subject to wide variations. The stress at tensile break is related to the elongation in that an increase in fracture stress results in a decrease in elongation. The values are generally repeatable and thus the ratio of the fracture stress along the tube direction to that transverse to it is taken as the measure of anisotropy. The values for the films used are shown in column 14 of Table 2.

12.4. Fracture Types.

Splits: Fig. 67 shows the anisotropy of each film plotted against its ductility. The splits are seen to form when the material is highly anisotropic and of low ductility. The mechanism of its formation may be described as follows. When the film is stressed a flow or thin spot will initiate very localised plastic deformation. The anisotropy will restrict this deformation to the extrusion direction and a very localised neck will be produced. The lack of ductility of the material prevents the orientated material from flowing into the neck at the high strain rates involved in impact

tests. High ductility or low speeds result in the material being able to flow and the localised neck does not occur.

It is now necessary to consider the question of adiabatic heating in the neck as described in ref. 22. When polythene necks at slow rates the material in the neck work hardens due to orientation until eventually it becomes stronger than that in the shoulder i.e. transition from neck to gauge section zone. The neck then becomes stable and the shoulders flow into the neck. This process is referred to as cold drawing. If the necking process takes place rapidly however the heat produced by the plastic deformation in the neck cannot be dissipated and the neck heats up and softens. This prevents the stabilisation of the neck and the resulting fracture is not preceded by cold drawing in the neck. Thus the effect of this heating is a lack of cold drawing in the fractured section.

If the two materials E2064 and E2185 are considered the anisotropy value are both high and similar, i.e. 1.32 and 1.34 respectively. The former has a density of 0.918 and the latter .933 corresponding to temperature rises in the neck as determined by ref. 22, of $16^{\circ}C$ and $21^{\circ}C$ respectively. E2064 gave hole fracture while E2185 gave splits. The difference in temperature rises would not appear adequate to explain the difference and the wide variation in ductility

is considered a more likely factor. The adiabatic heating may reduce the amount of cold drawing but will not substantial ly alter the form of the fracture. The lower ductility of the split materials would also reduce the amount of cold drawing produced and it is considered that the adiabatic heating i a secondary effect in determining the fracture type.

The extreme localisation of the fracture results in a very small energy being necessary for fracture and the fractures are self propagating as is witnessed by their length being greater than the striker head.

Tears: Tears are formed with lower levels of anisotropy and higher ductilities than those which produced splits. The fractures are shorter than the striker head diameter indicating that they were formed by the head forcing the material apart. This is a stable fracture and is formed when there is sufficient anisotropy to produce a line fracture but not sufficient to give instability.

Holes: Holes form when the ductility is sufficiently high ($\lambda < .625$) to counteract any anisotropy concentration effects and the material deforms until a ring fracture forms.

The dividing lines between the types of fracture are approximate but give a good indication of the type of failure

to be expected. As shown in Table 2 there are often two types of failure in one film. In the case of tear and hole materials this is to be expected as local variations in anisotropy could produce the two types. Materials E2070, 2069 and 2068 of the same melt index and density show clearly the effect of thickness and anisotropy. E2070 had a thickness of 0.9×10^{-3} ins and an anisotropy of 1.11 and gave two splits and eight tears. E2069 was 1.2×10^{-3} ins thick and had an anisotropy of 1.10 and gave ten tears while E2068 of 1.6×10^{-3} ins and 1.07 gave nine tears and one hole. The three films E2180, 2181, 2182 indicate a similar trend. The tendency to increased ductility with increasing thickness has been explained under manufacture but the properties of each type of fracture show that the zones in Fig. 67 only indicate the most likely type of failure and much depends on local variations in the material.

The results show that the ductility and anisotropy govern the type of fracture obtained but that once the type is determined variations in energy absorbed within that type due to material properties are small and hence the graph of energy versus thickness (Fig. 51) for each type results in a single line.

13.0. Conclusions

The impact machine is extremely accurate and the large scatter in values obtained is due solely to variations in the film. It is now possible to accurately assess the quality of a film by means of its impact properties. The notch sensitivity and fatigue tests are useful for determining general properties but more information is needed for a precise interpretation of their significance. Future work will include the examination of these tests considering such items as frequency in the fatigue test. Tests will also be carried out to extend the range of the machine to cope with the higher strength materials.

The mechanism of failure in polyethylene film appears to be fairly well understood but is based on a limited amount of evidence and many further results are required to test the conclusions. The relation of these findings to other types of film and to fracture mechanics in general will be attempted in future work.

REFERENCES

1. Vincent, P.I. Strength of Plastics. Plastics. Vol. 26, Pts. VII and VIII. June, July, 1961.

2.a. Ford, H. Researches into the deformation of metals by cold rolling. Proc. I. Mech. Eng. 1948, 159, p. 115.

b. Watts, A.B. and Ford, H. An experimental investigation of the yielding of strip between smooth dies. Proc. Inst. Mech. Eng. Proc.(B), 1952-53. Vol. 1B, No. 10.

c. Watts, A.B. and Ford, H.Yield Stress Curve for a Metal. Proc. Inst. Mech. Eng. 1955, Vol. 169, p. 1141.

3. Takahashi, H. and Alexander, J.M. Friction in the Plane Strain Compression Test. Jour. Inst. Metals. Vol. 90, 1961-62.

4. Gummski, R.D. and Willis, J. Development of Cold Rolling Lubricants for Aluminium Alloys. Jour. Inst. Metals. Vol. 88, Aug. 1960.

5. Green, A.P. Theoretical Investigation of the Compression of a Ductile Material between Smooth Flat Dies. Phil. Mag. Ser. 7, Vol. 42, p. 951, p. 911.

6. Love, A.E.H. The Mathematical Theory of Elasticity. Cambridge University Press. 1926.

7. Bland, D.R. The Theory of Linear Viscoelasticity. Pergamon Press. 1960.

8. Tobolsky, A.V. Properties and Structures of Polymers. John Wiley and Sons, Inc. 1960.

9. Sandiford, D.J. Non-linear Viscoelastic Effects in Ethylene Polymers. Sym. on the Phys. Props. of Polymers. Soc. Chem. Ind. April 1958.

10. Rivlin, R.S. Large elastic deformations of isotropic materials. Phil. Trans. Vol. 240. 1940.

11. Green, A.E., Adkins, J.E. Large Elastic Deformations and Non-linear Continuum Mechanics. Oxford, 1960.

12. Treloar, L.R.G. The Physics of Rubber Elasticity. Oxford, 1949.

13. Carmichael, R.J. and Holdaway, H.W. Phenomenological Behaviour of Rubbers over a Wide Range of Strains. Jour. App. Phys. Vol. 32, No. 2, Feb. 61.

14. Oldroyd, J.G. On the Theory of Creep in a Solid in which the Elastic Strain is Large. Paris, 1960.

15. Hill, R. The Mathematical Theory of Plasticity. Oxford, 1960.

16. Perzyna, P. The Constitutive Equations for Rate Sensitive Plastic Materials. Report, Div. of App. Maths., Brown Univ. April 62.

17. Hill, R. A Theory of the Plastic Bulging of a Metal Diaphragm by Lateral Pressure. Phil. Mag. Ser.7. Vol. 41, No. 332. Nov. 1950.

18. Ford, H. Advanced Mechanics of Materials. Chap. 29. P. 460 et seq. Longmans Green and Co.

19. Supurk, R.H. and Adams, C.M. A Ball-drop Technique for Estimating Polythene-film Toughness. Plastics Tech. Sept. 1957.

20. The Dart Drop Test. A.S.T.M. D-1709-59T.

21. Carey, R.H., Natkis, M.S. Tensile Impact Tests on Films. Mod. Packaging. Sept. 1958.

22. Clegg, C.L., Turner, S., Vincent, P.I. Polythene-Mechanism of Failure. Plastics, Jan. 1959.

23. Ninnemann, K.W. New Pendulum Impact-Tester. Mod. Packaging. Nov. 1956.

24. Collingwood, R.S. Plastic Film Impact Testing Machine. D.I.C. Dissertation, Imperial College, London. 1963,

25. Thwing-Albert Instrument Co. Spencer Impact Attachment.

26. Glyde, B.S., Holmes-Walker, W.A., Jeffs, K.D. An Impact Fatigue Test for Polyethylene Film. British Plastics. Aug. 1961.

27. Huck, N.D., Clegg, P.L. The Effect of Extrusion Variables on the Fundamental Properties of Tubular Polythene Film. S.P.E. Trans. July 1961.

28. Anderson, A.A., Morfitt, G.L. Mechanical Properties of Thin Polyethylene Film. Mod. Plastics. Vol. 35, 1958.

29. Robertson, R.E. On the Cold-drawing of Plastics. General Electric Research Lab. Report No. 61-RL-(28466). October 1961.

30. Reed, D.R., Horsley, R.A. Impact Testing of Thermoplastics. Brit. Plastics. April 1959.

31. Kucher, C.G. Effect of Blow-up Ratio on the Properties of Polyethylene. Plastics Tech. Sept. 1957.

32. McTedrie, R.Jr., Brown, W.E., McGasny, F.J. Evaluation of Brittle Failure of Polyethylene by Subjection to Biaxial Stress. S.P.E. Trans. April 1962.

33. Thor, C.J.B. Polyethylene Films. S.P.E. Journal. Feb. 1962.

34. Amborski, C.E., Mecca, T.D. A Study of Polymer Film Brittleness. J. App. Pol. Sci. Vol. 4, 1960.

35. Mannheim, M.C., Nielson, A.I., Sleaberg, M.P. Testing Film Packaging Strengths. Mod. Packaging. Nov. 1956.

36. Auerbach, B.L., Fielbeck, D.K., Hahn, G.T. Thomas, D.A. Editors. Fracture. John Wiley and Sons. Inc. 1959.

37. Alfrey, J. Mechanical Behaviour of High Polymers. Interscience Pub. 1948.

38. Renfrew Morgan. Polyethylene. Iliffe Press. 1957

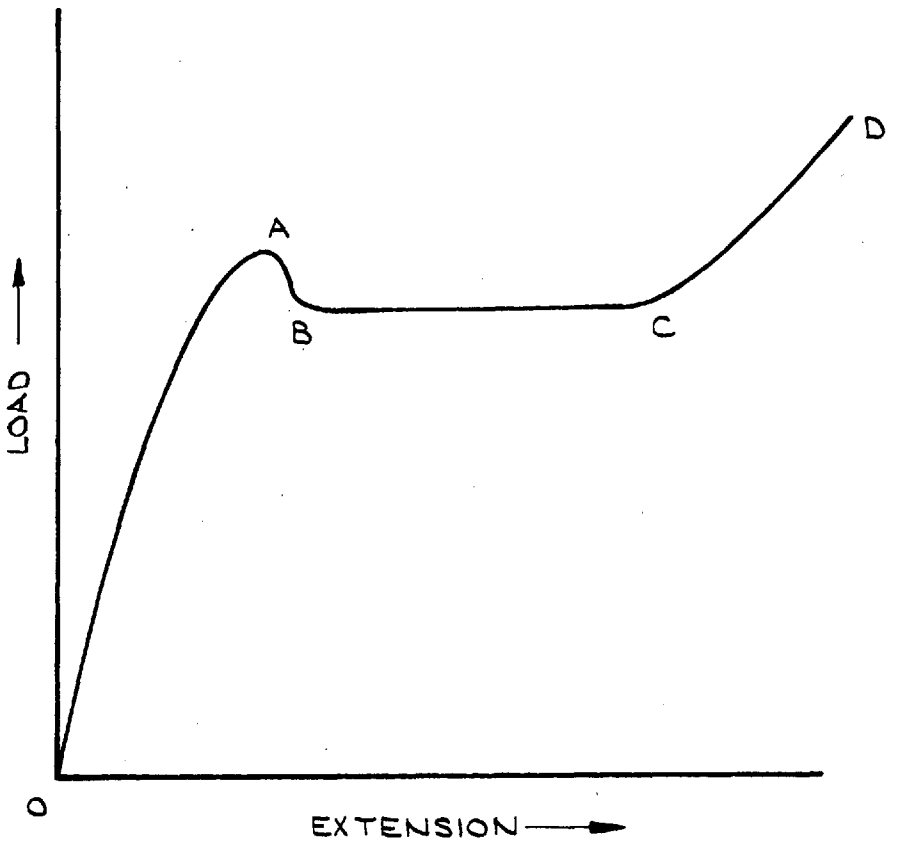

FIG.1

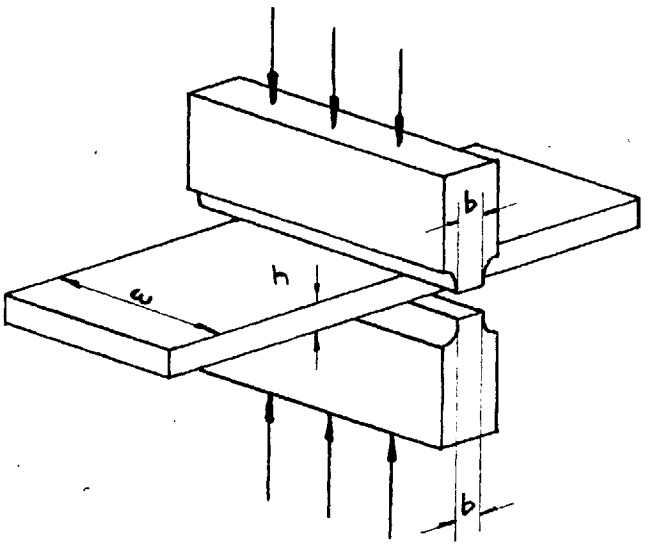

FIG. 2.

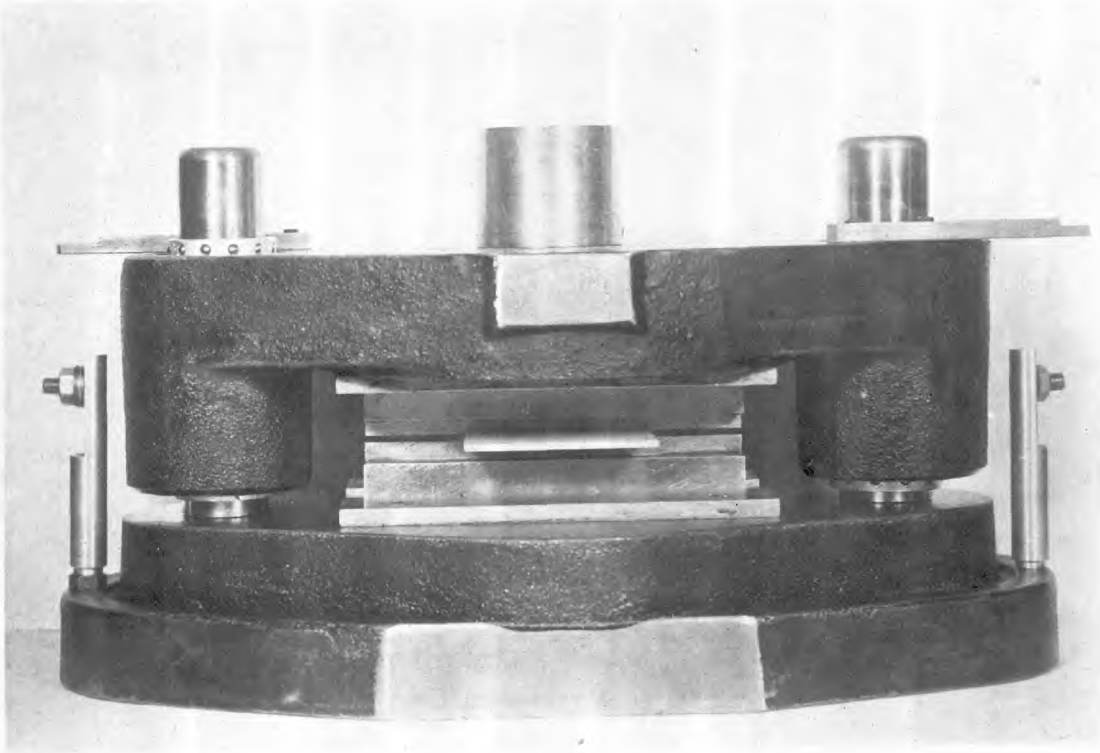

FIG. 3. SUB-PRESS

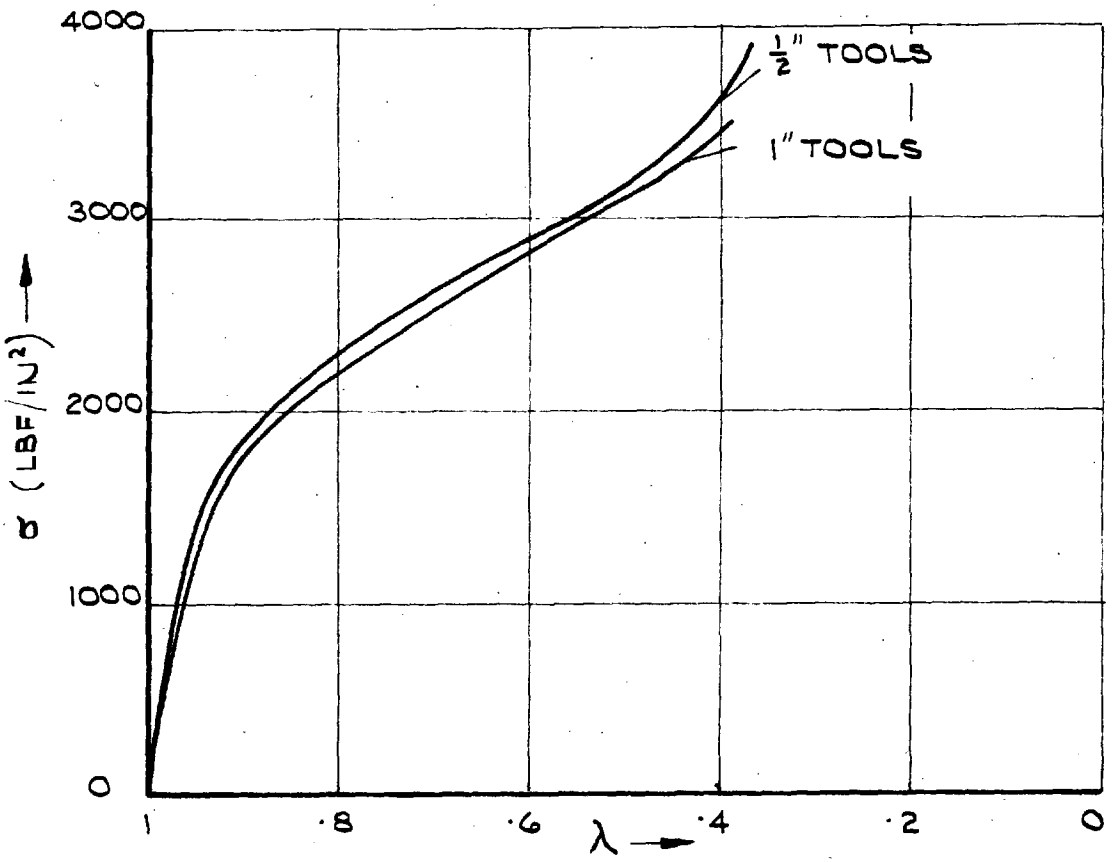

FIG. 4. STRESS/STRAIN CURVES FOR POLYETHYLENE WITH TWO TOOL WIDTHS.

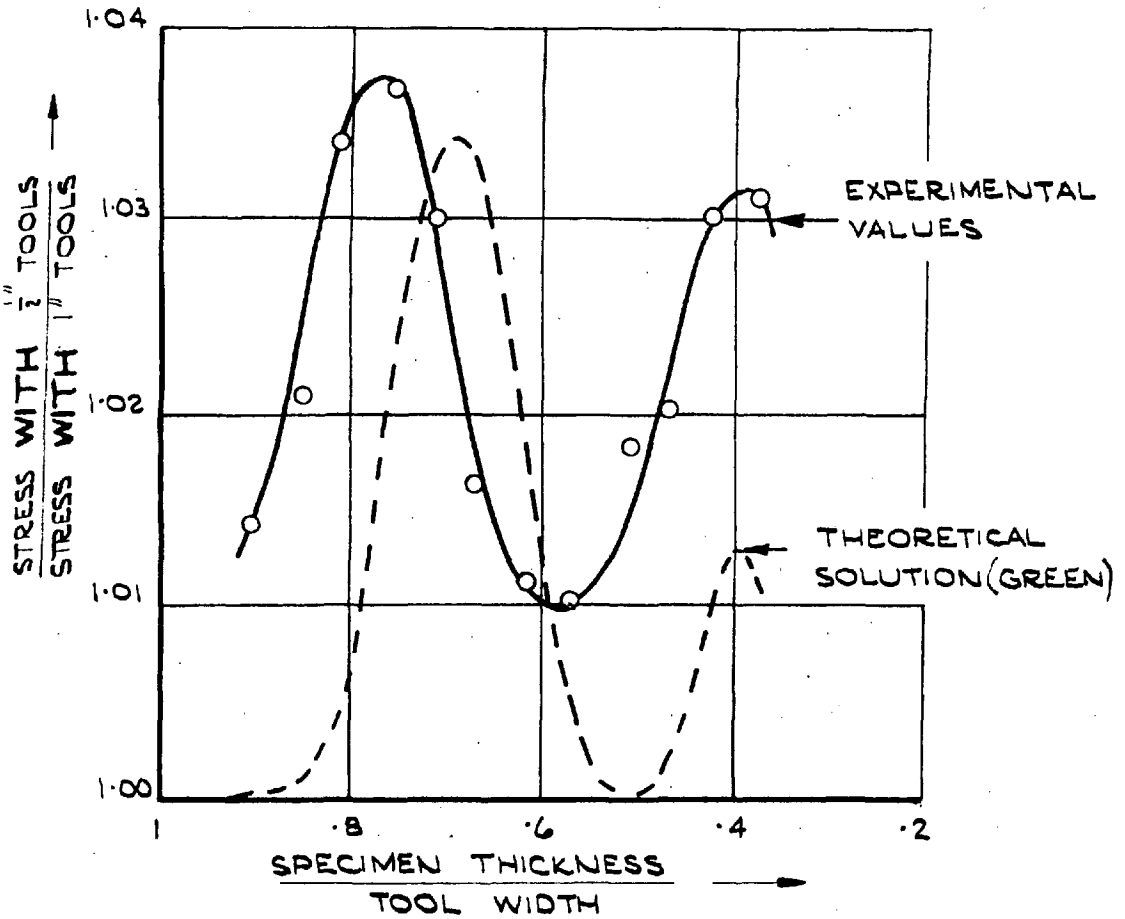

FIG. 5. EFFECT OF TOOL GEOMETRY ON STRESS / STRAIN CURVES OF POLYETHYLENE

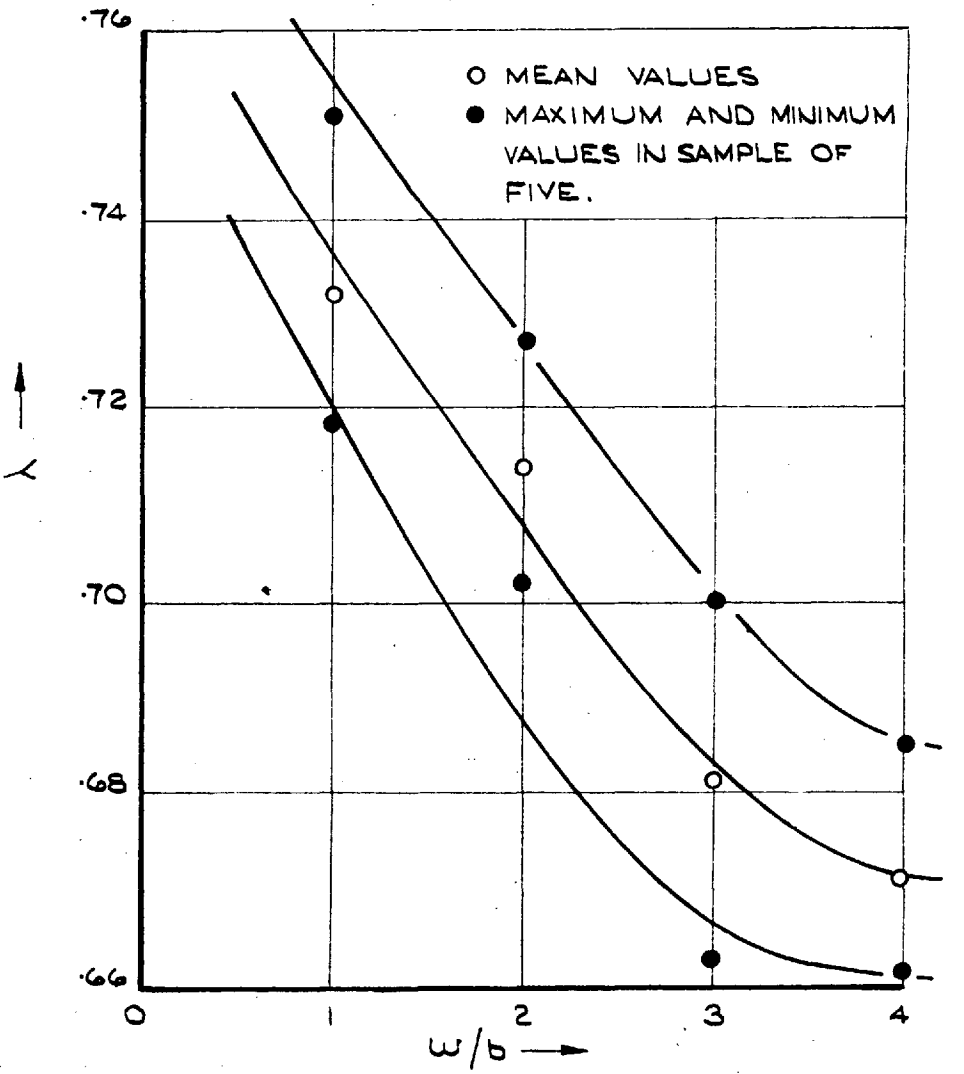

FIG.6. VARIATION OF λ WITH SPECIMEN WIDTH FOR POLYETHYLENE $b = 3000$ LBF/IN^2 1" TOOLS.

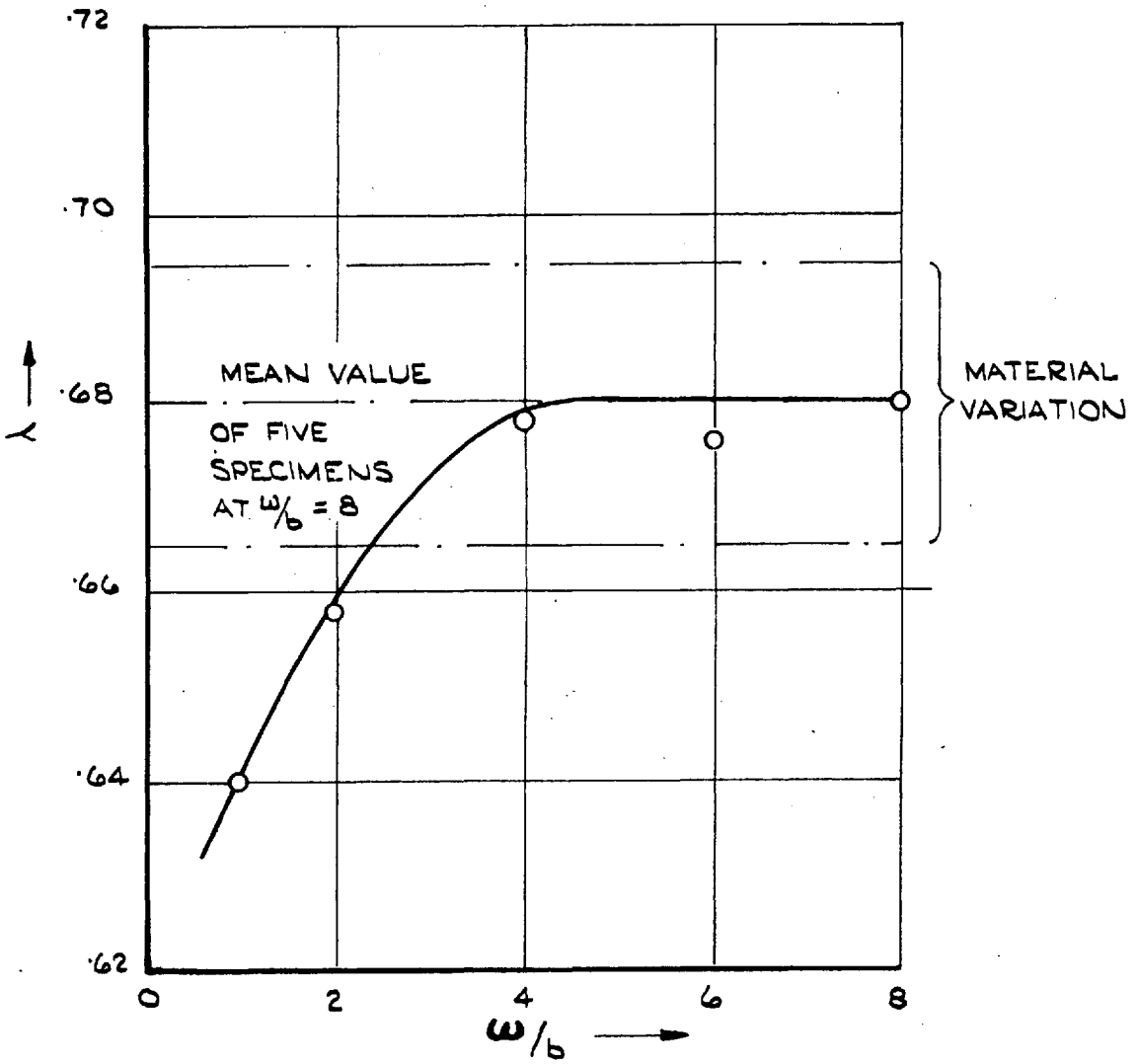

FIG. 7. VARIATION OF λ WITH SPECIMEN WIDTH FOR P.V.C. σ = 14,000 LBF/IN^2, $\frac{1}{2}$" TOOLS.

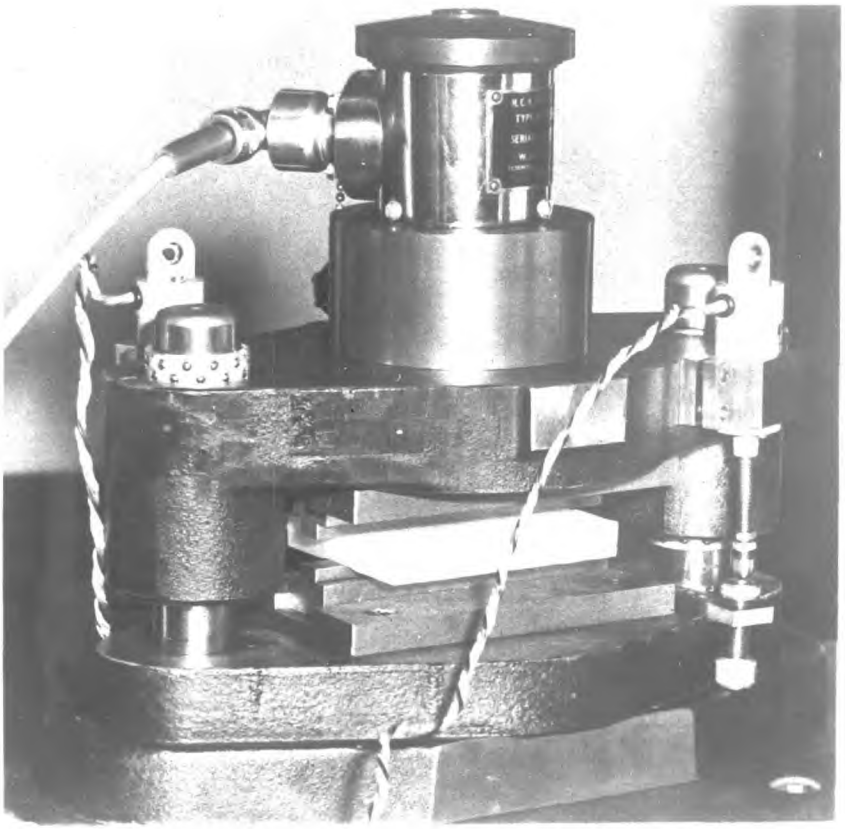

FIG. 8 a) INSTRUMENTED SUB-PRESS

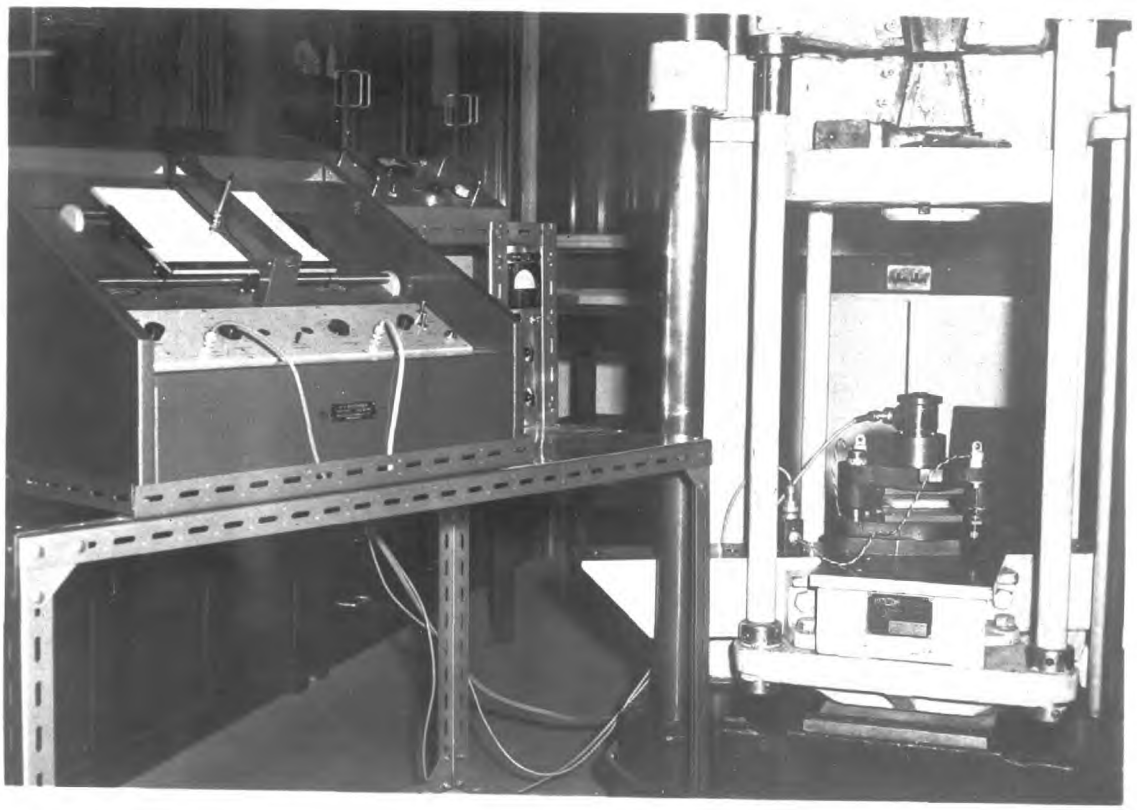

FIG 8 b) INSTRUMENTED SUB-PRESS; TESTING MACHINE AND X-Y PLOTTER

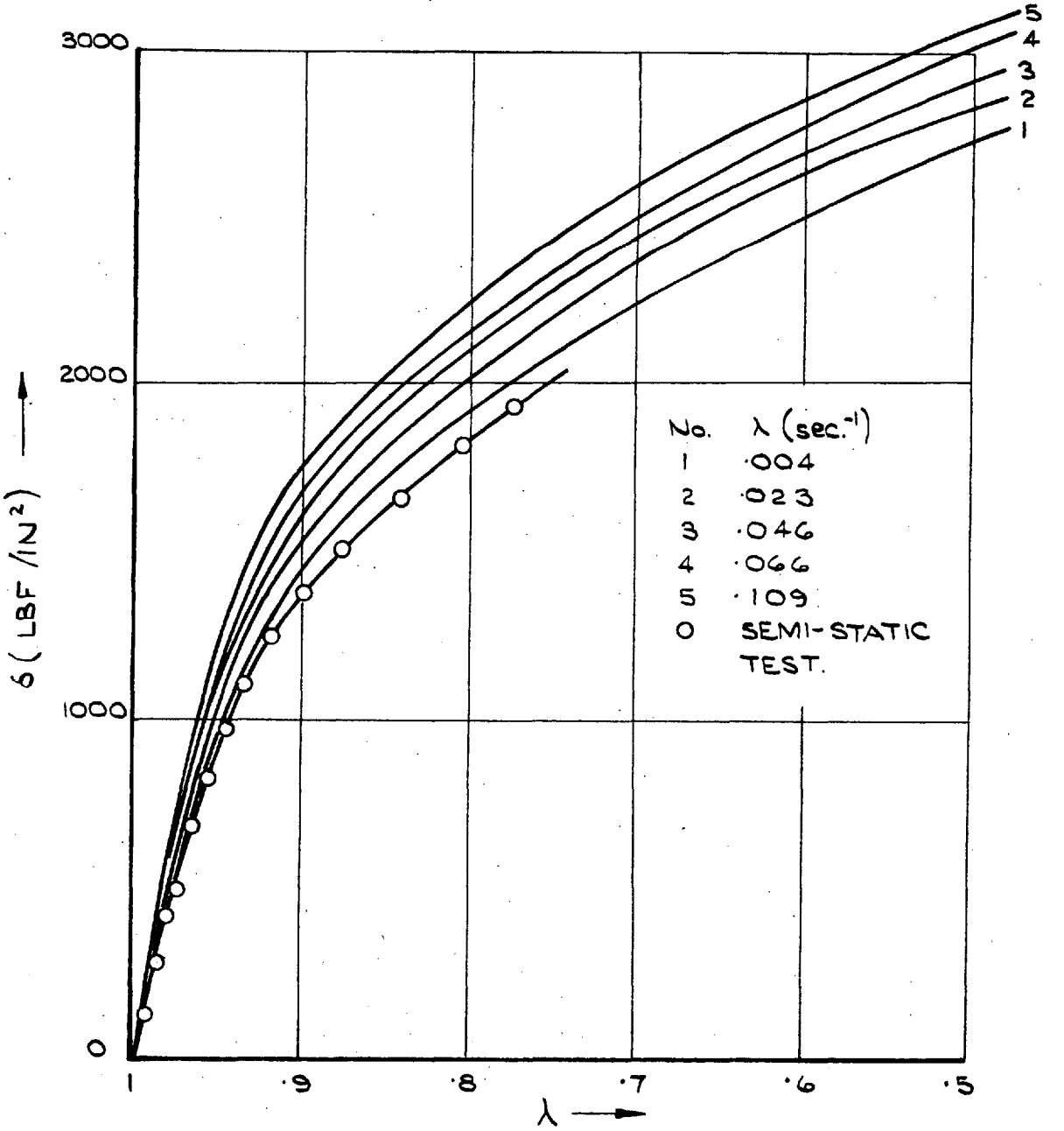

FIG. 9. EFFECT OF STRAIN RATE ON THE TOTAL DEFORMATION CURVES FOR POLYETHYLENE.

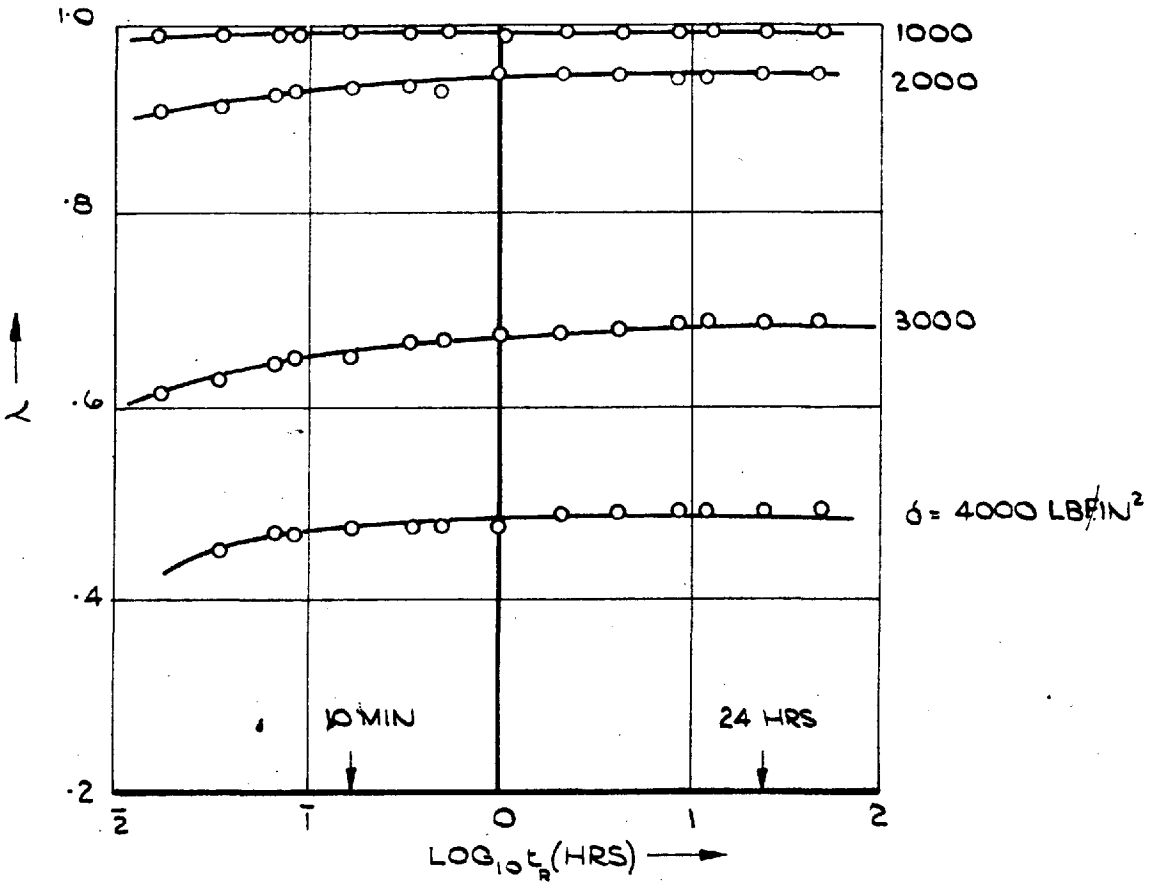

FIG. 10 RECOVERY CURVES FOR POLYETHYLENE WITH DWELL TIME t_D = 10 MINS

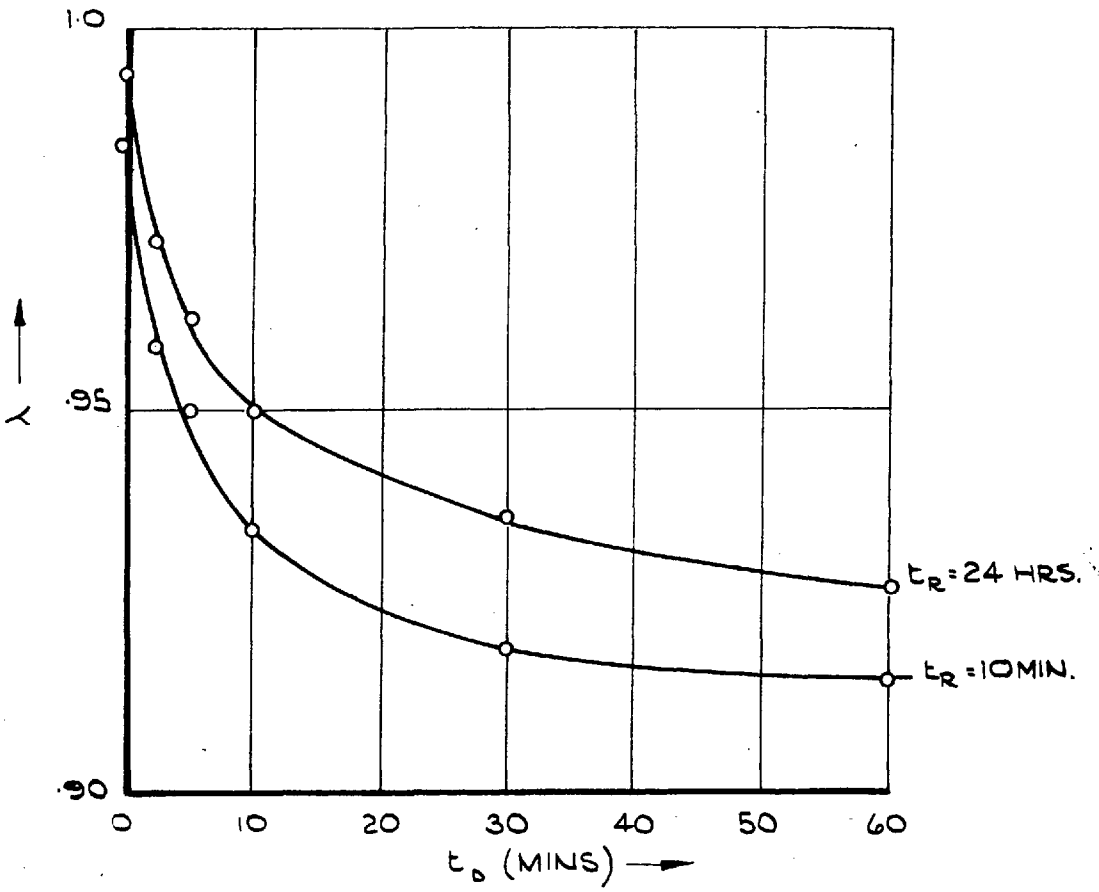

FIG. 11. EFFECT OF DWELL TIME FOR POLYETHYLENE. STRESS 2000 LBF/IN^2

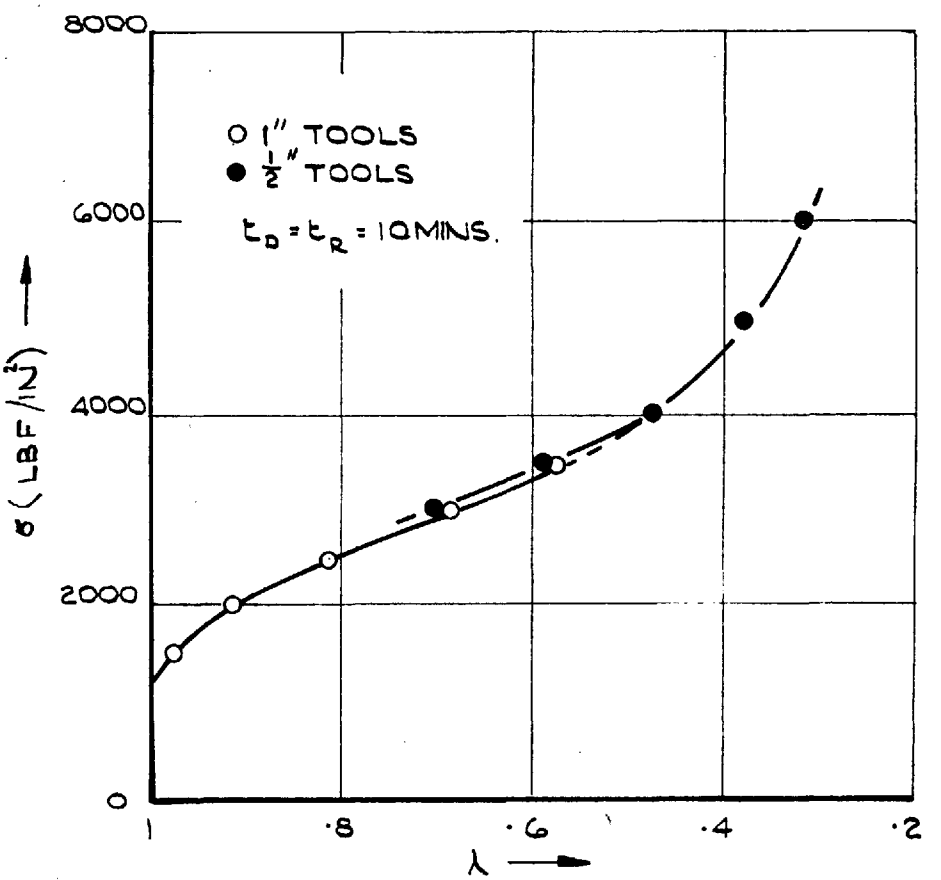

FIG. 12. PERMANENT DEFORMATION TEST ON POLYETHYLENE. EFFECT OF TOOL WIDTH ON SEPERATE SPECIMENS.

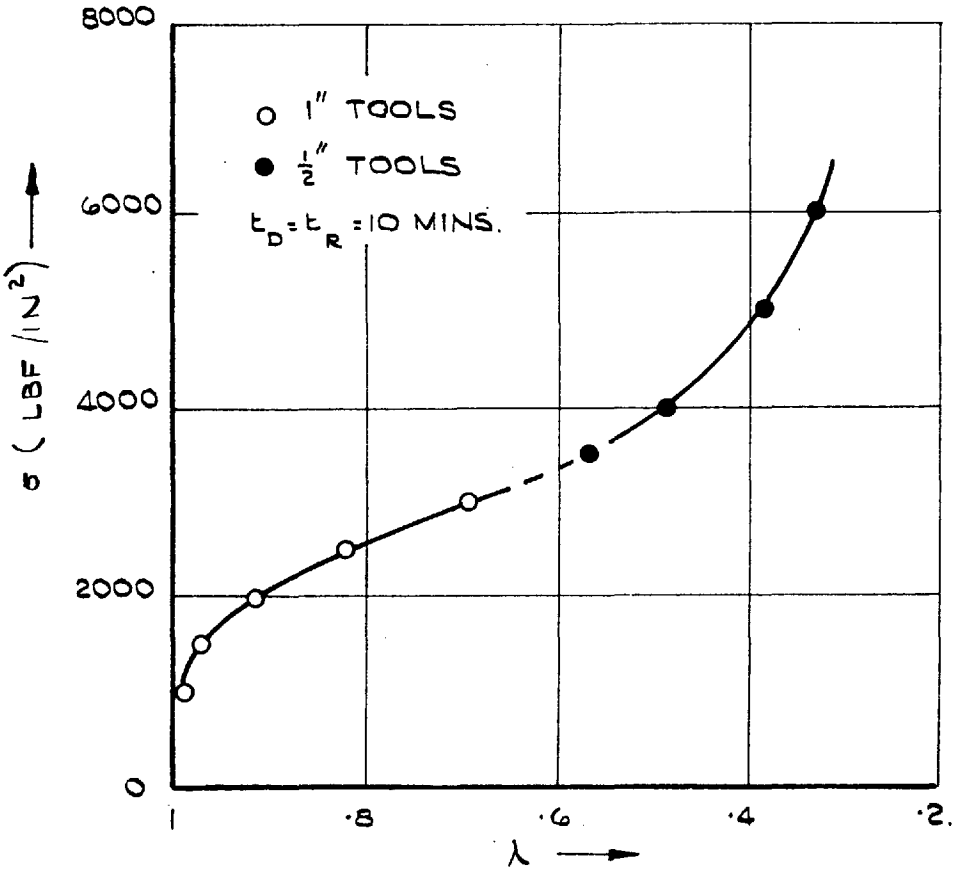

FIG. 13. PERMANENT DEFORMATION TEST ON POLYETHYLENE. EFFECT OF TOOL SIZES ON A SINGLE SPECIMEN.

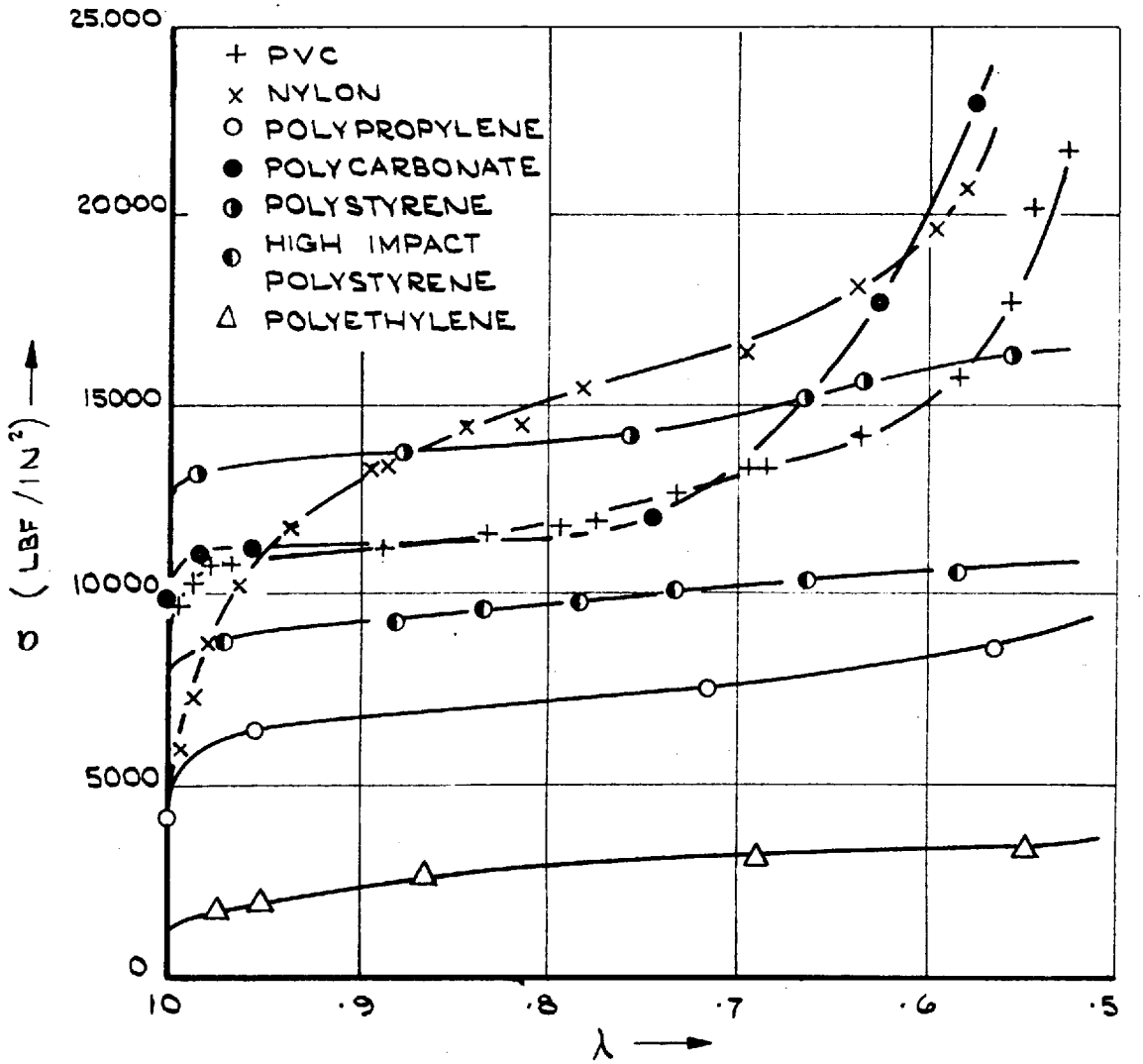

FIG. 14. PERMANENT DEFORMATION CURVES FOR VARIOUS PLASTICS t_D = 10 MIN. t_R = 24 HRS

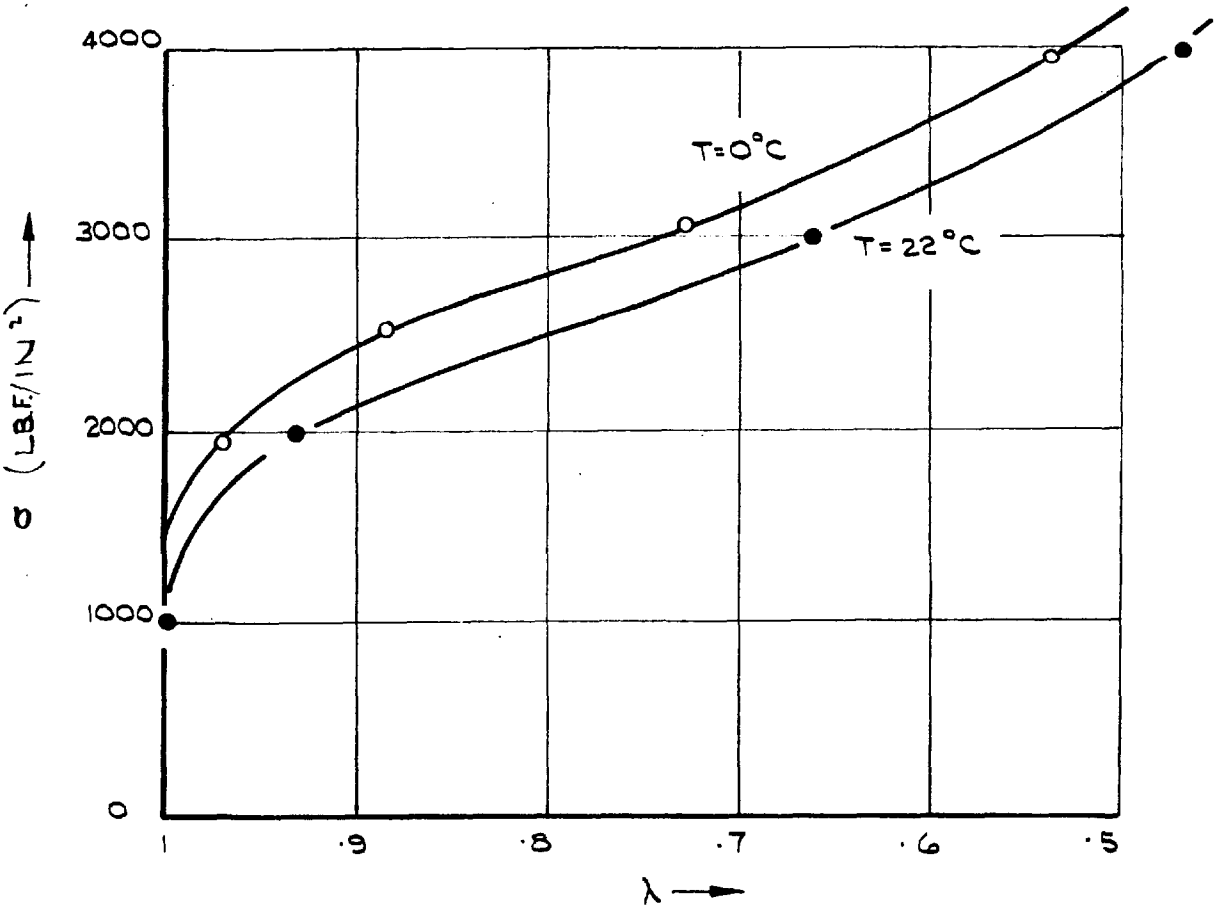

FIG. 15. PERMANENT DEFORMATION CURVES AT TWO TEMPERATURES FOR POLYETHYLENE

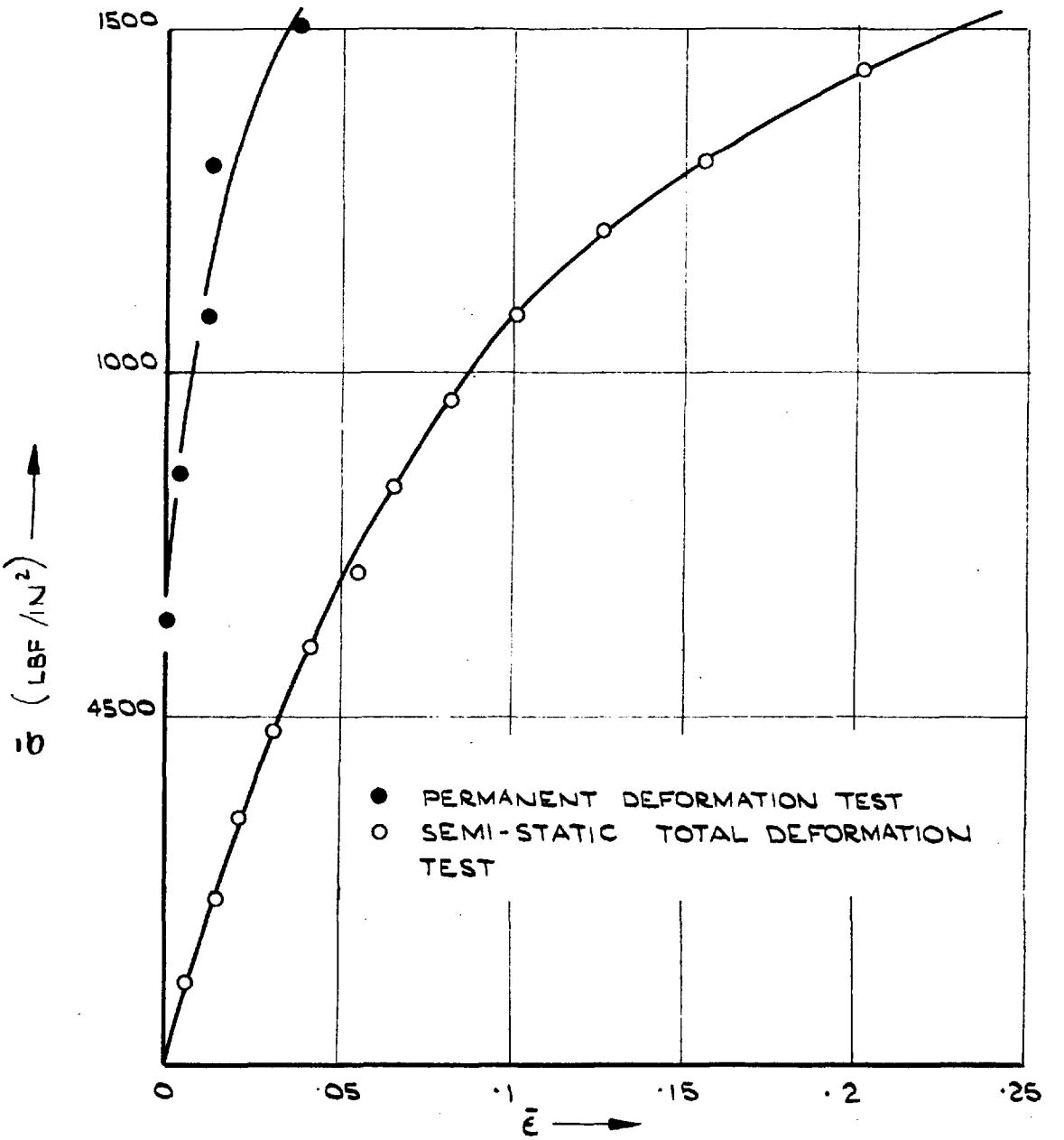

FIG. 16. EQUIVALENT STRESS/STRAIN CURVES FOR POLYETHYLENE.

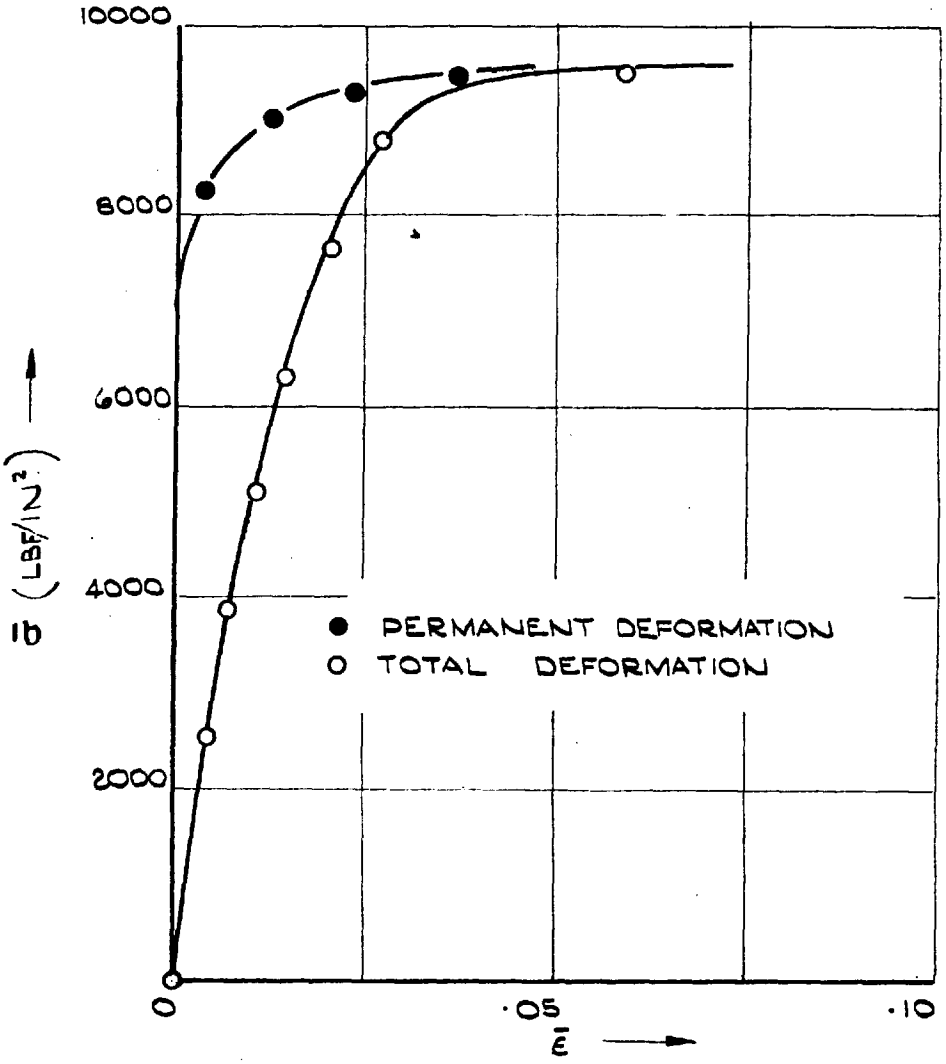

FIG. 17. EQUIVALENT STRESS/STRAIN CURVE FOR PVC.

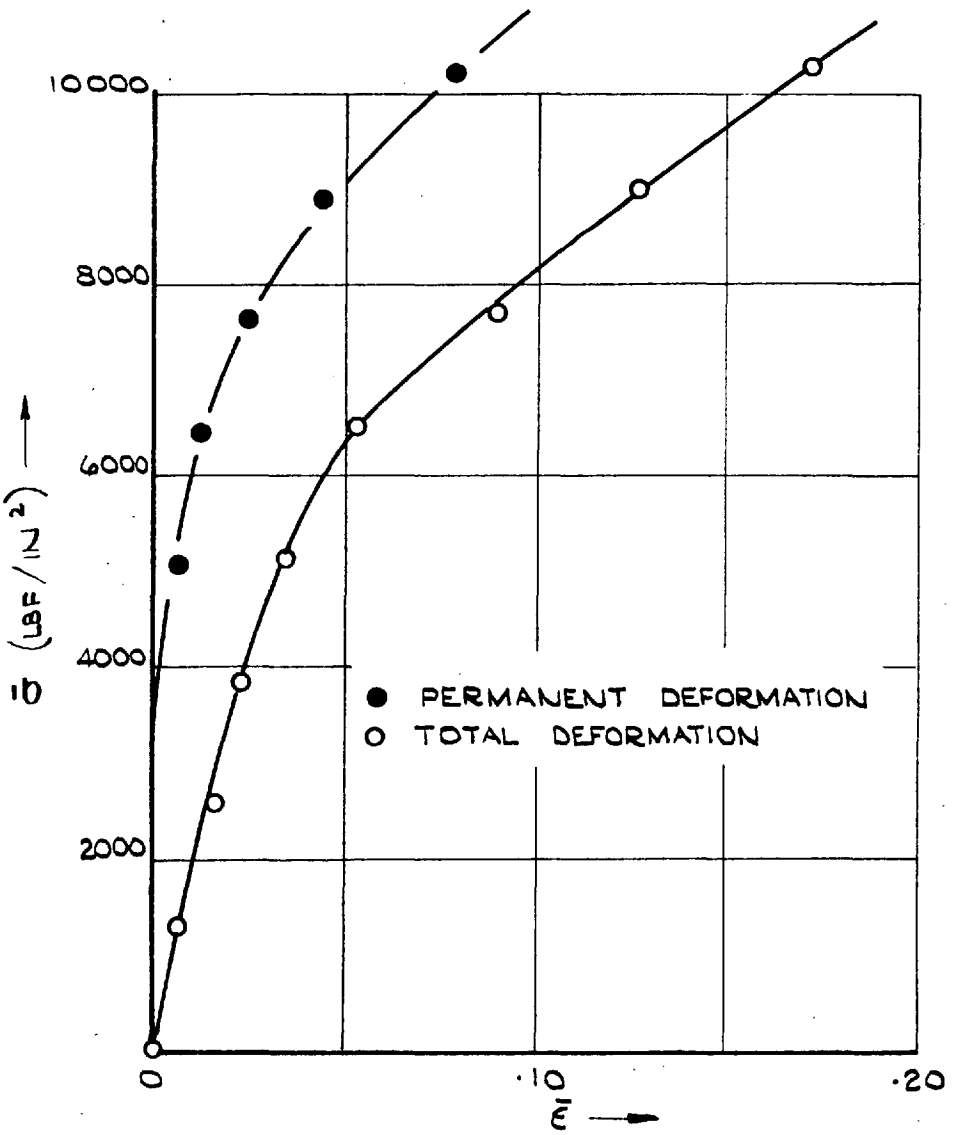

FIG. 18. EQUIVALENT STRESS / STRAIN CURVES FOR NYLON.

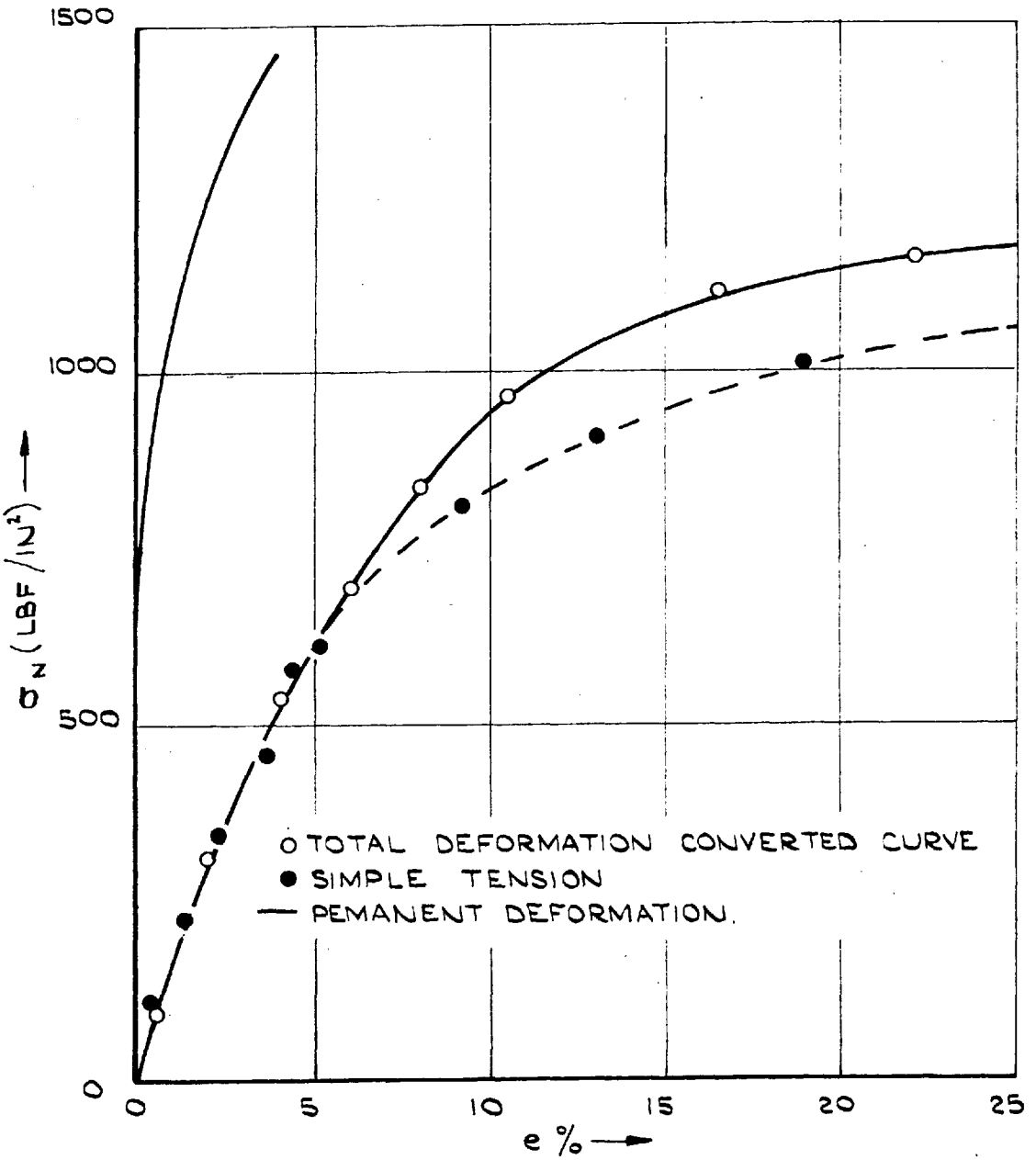

FIG. 19. SIMPLE TENSION CURVES FOR POLYETHYLENE.

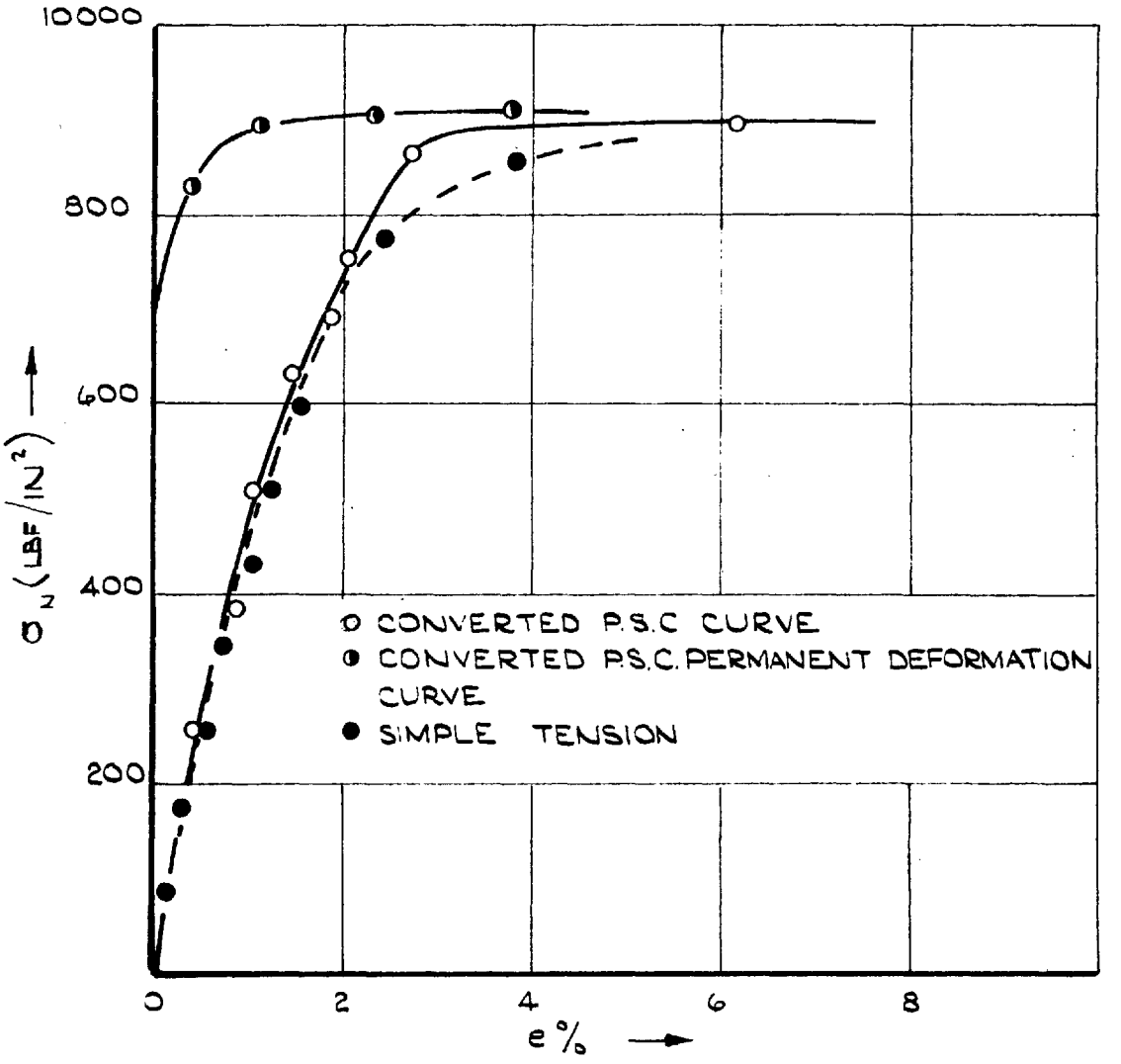

FIG. 20. SIMPLE TENSION CURVES FOR P.V.C.

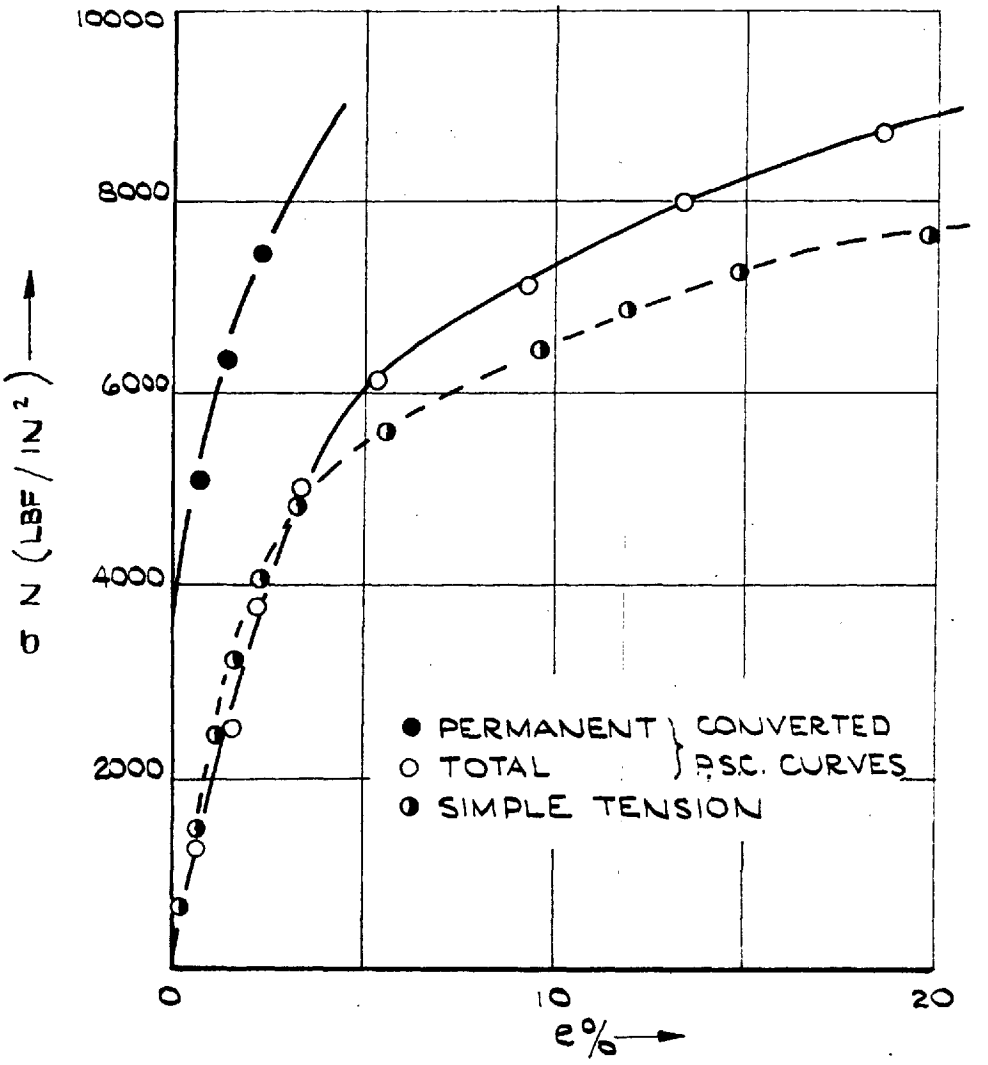

FIG. 21 SIMPLE TENSION CURVES FOR NYLON.

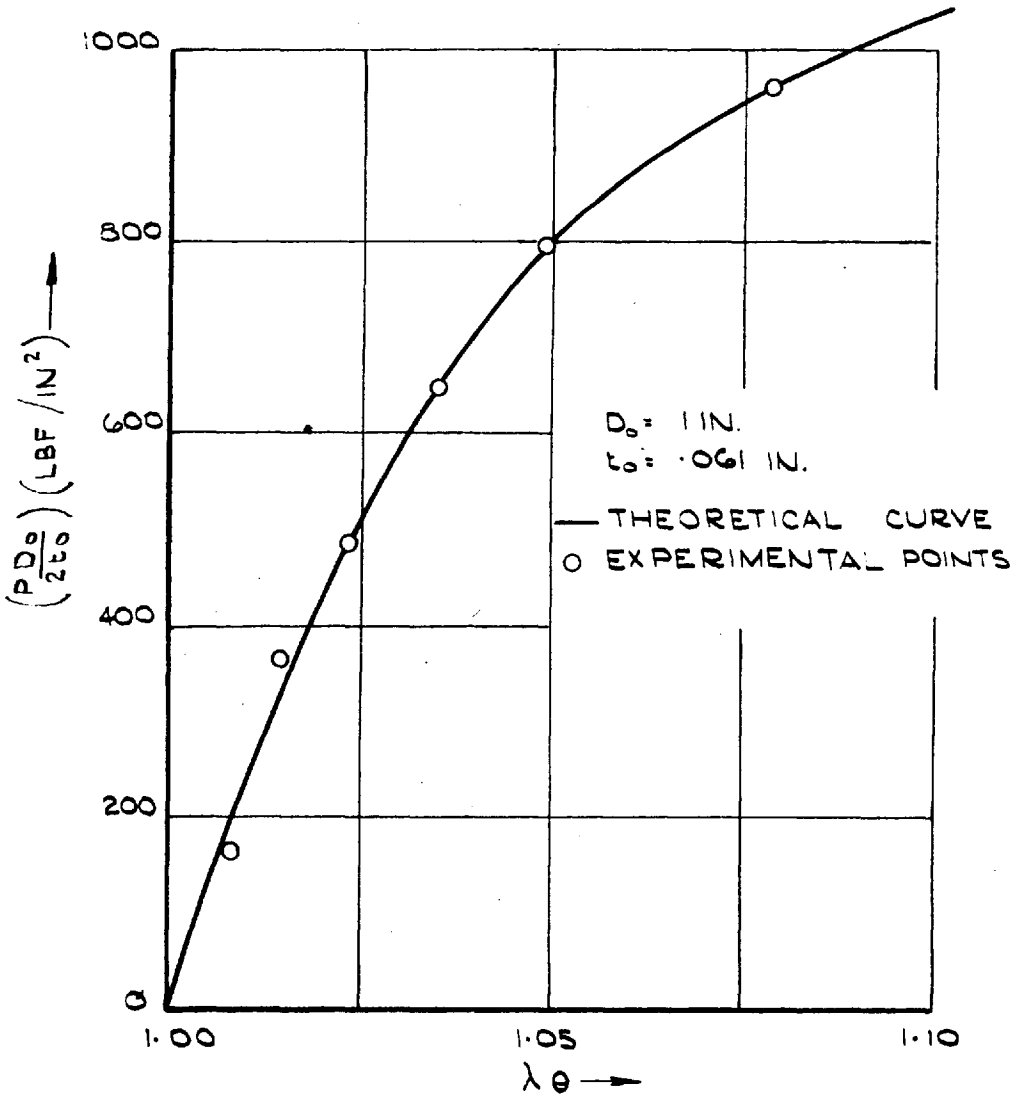

FIG 22. THIN WALLED CYLINDER UNDER INTERNAL PRESSURE

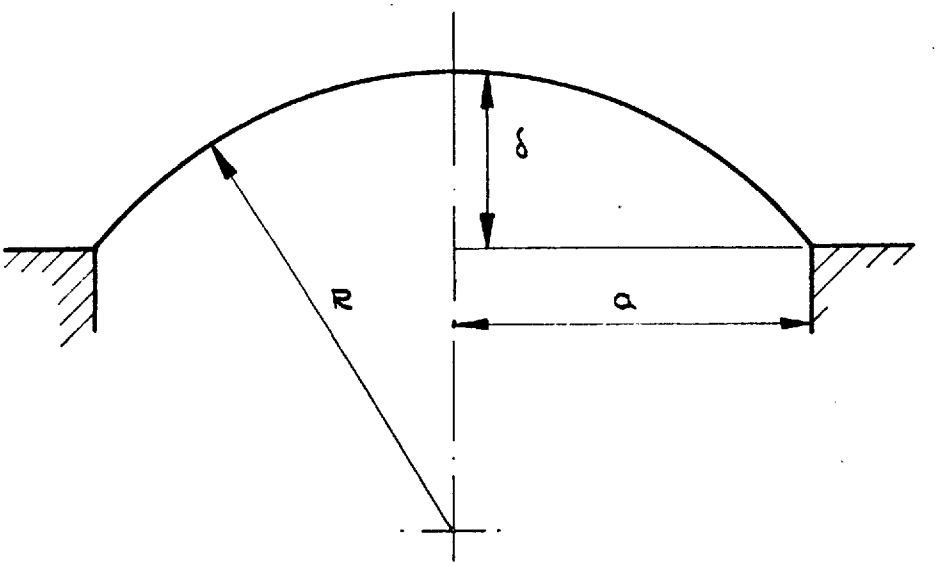

FIG. 23.

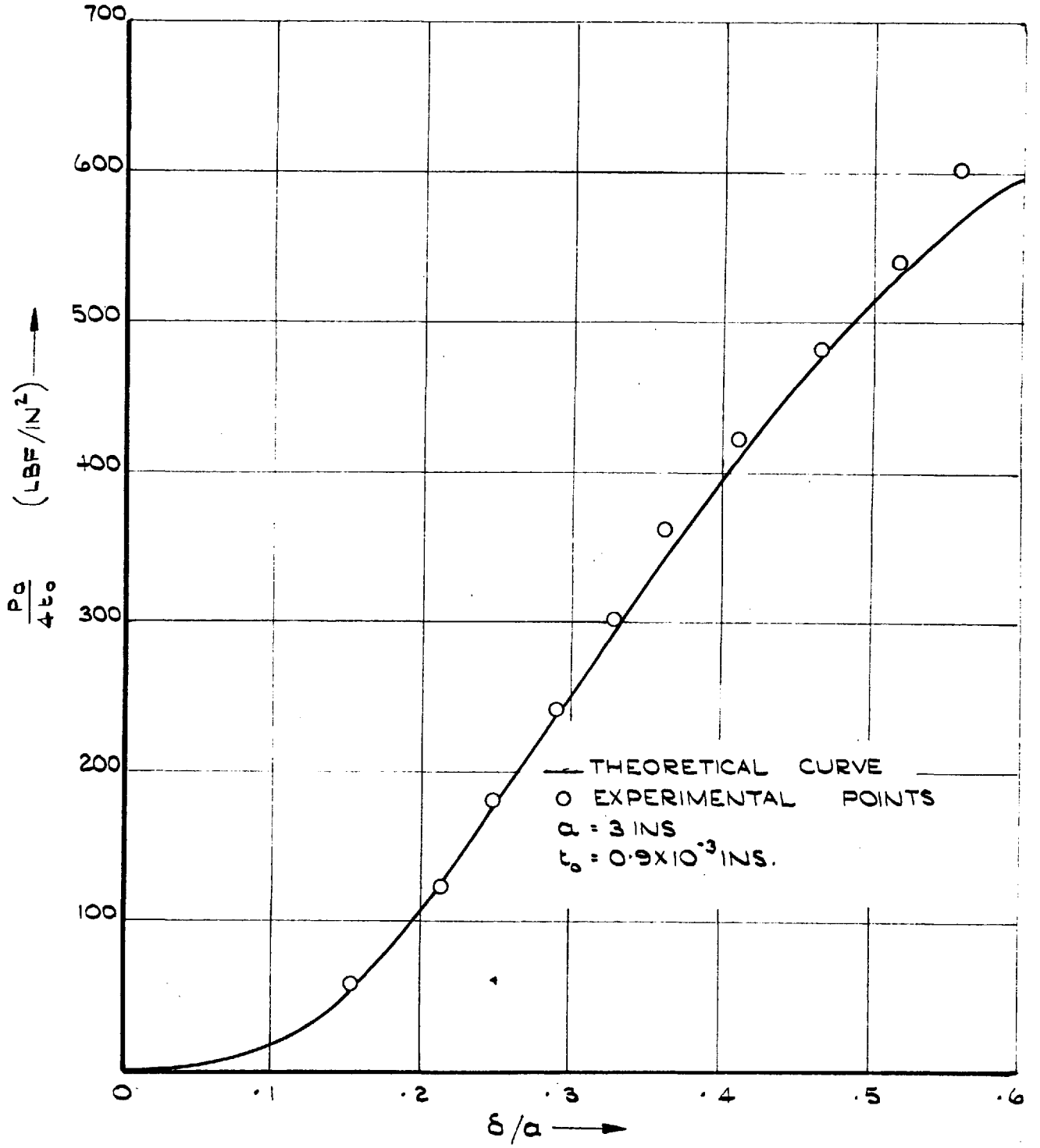

FIG. 24. PRESSURE DEFLECTION CURVE FOR CIRCULAR MEMBRANE SUBJECTED TO LATERAL PRESSURE

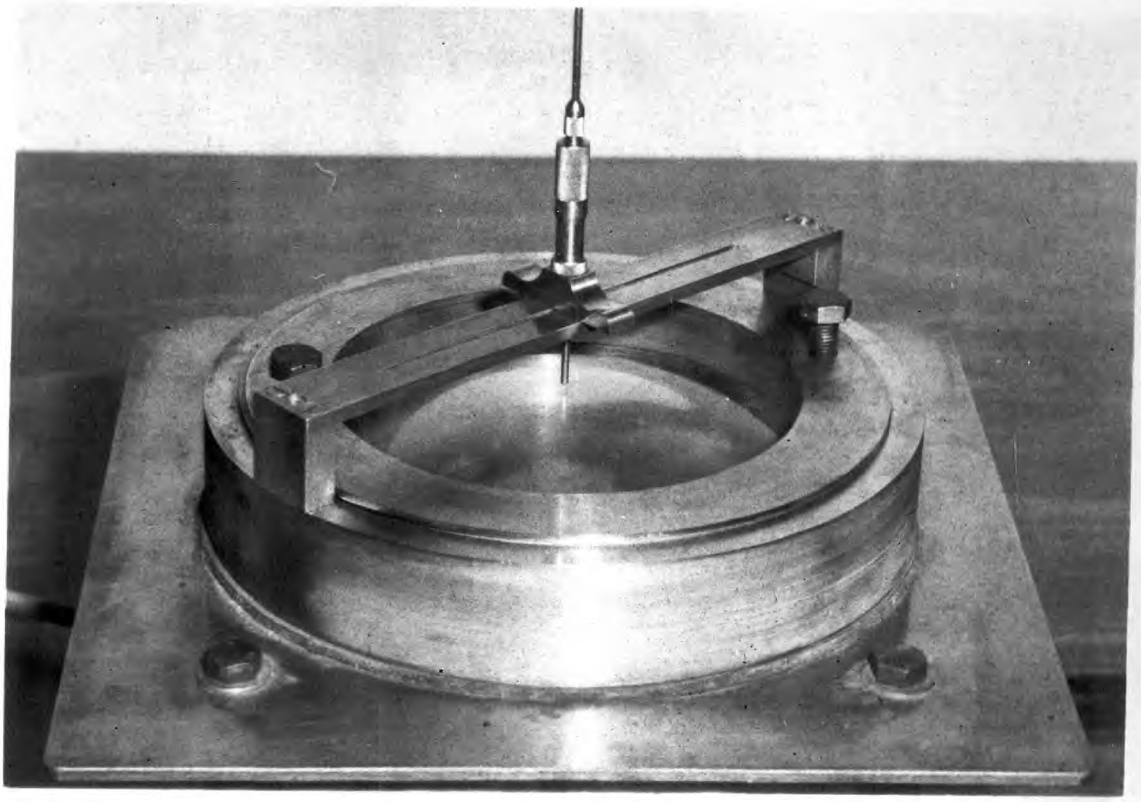

FIG 25 APPARATUS FOR THE INFLATION OF CIRCULAR MEMBRANE BY LATERAL PRESSURE

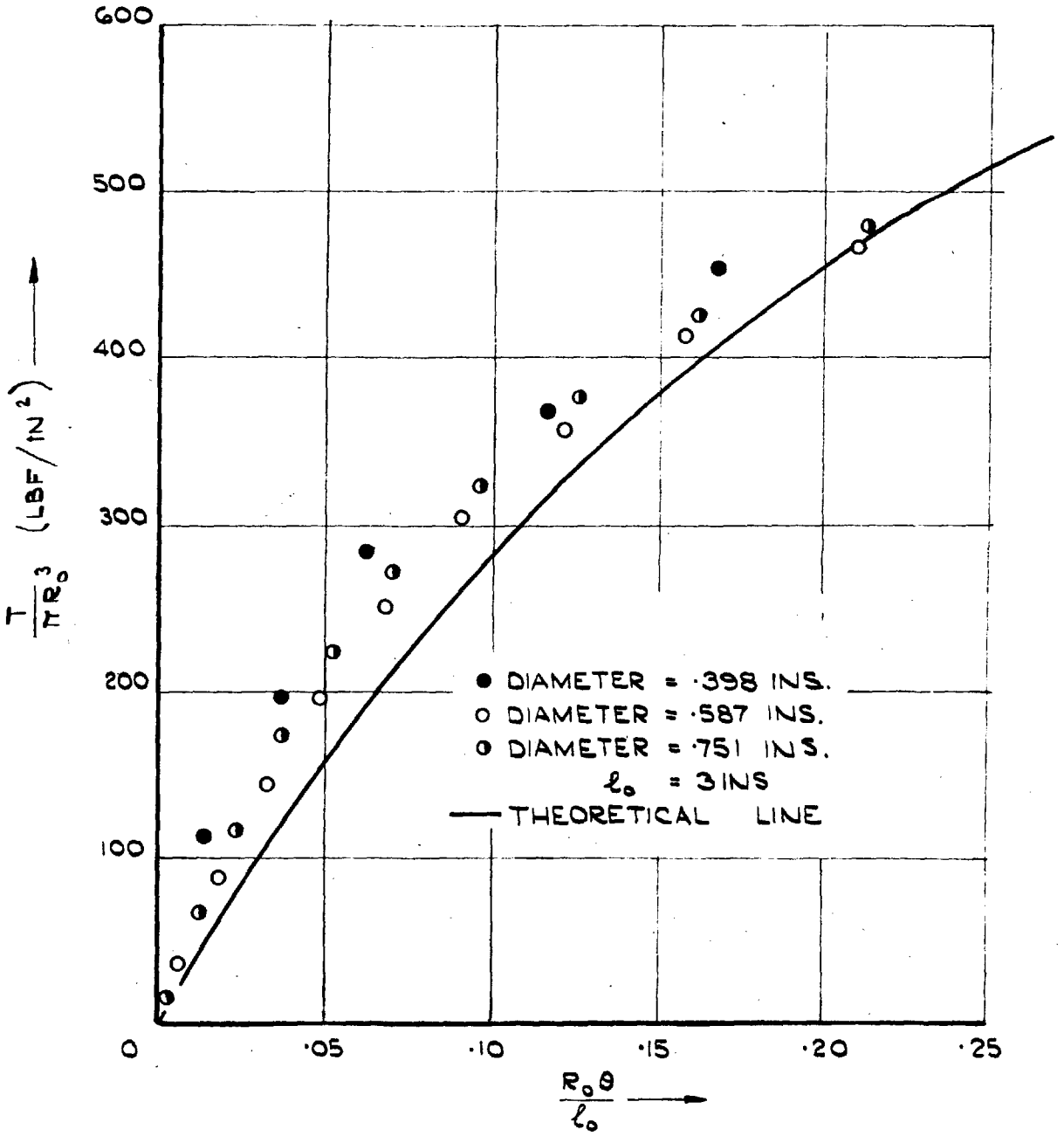

FIG. 26. TORSION OF POLYTHYLENE CIRCULAR RODS.

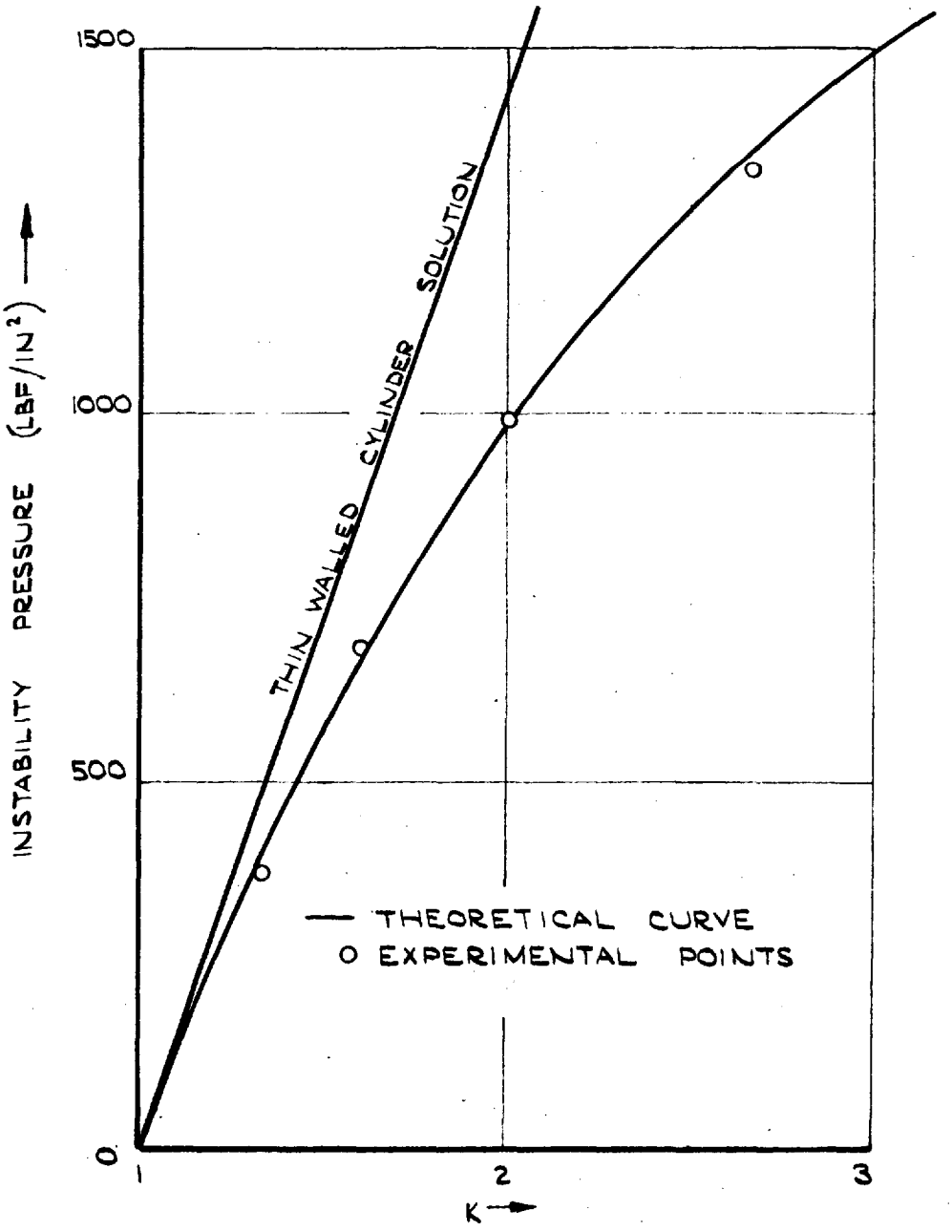

FIG. 27. INSTABILITY OF THICK WALLED POLYETHYLENE CYLINDER

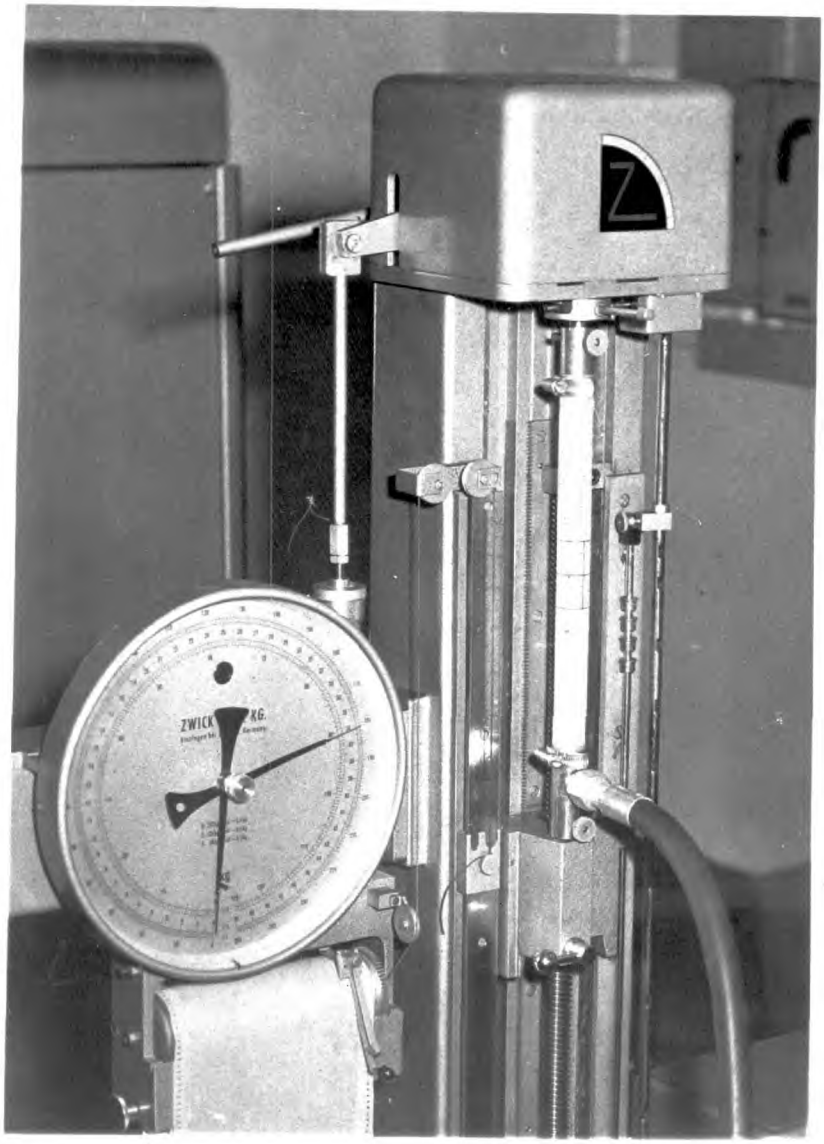

FIG 2 8 APPARATUS FOR SUBJECTING THIN WALLED POLYETHYLENE CYLINDERS TO INTERNAL PRESSURE AND AXIAL LOAD

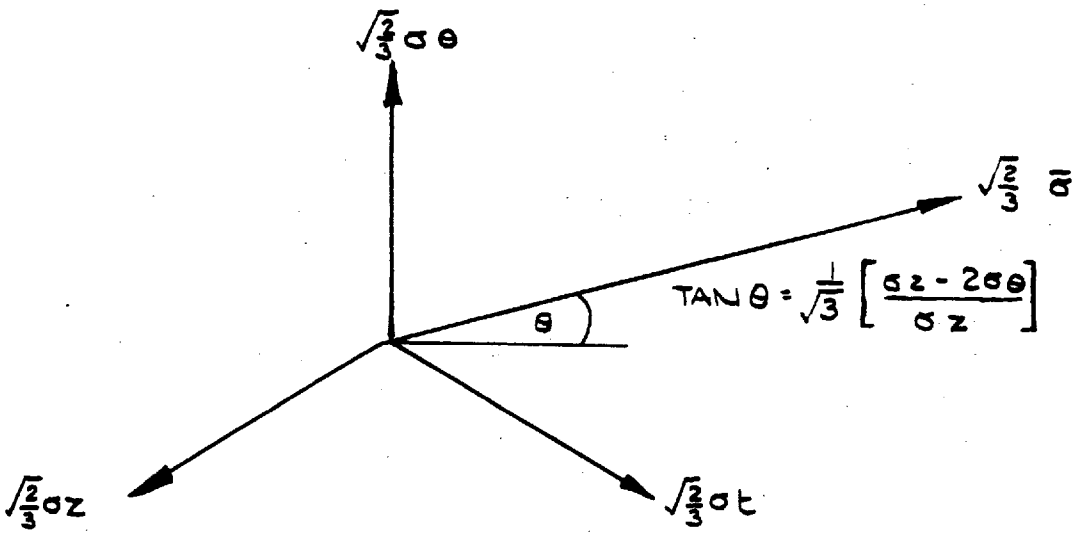

FIG. 29 PROJECTIONS ON THE DEVIATORIC PLANE

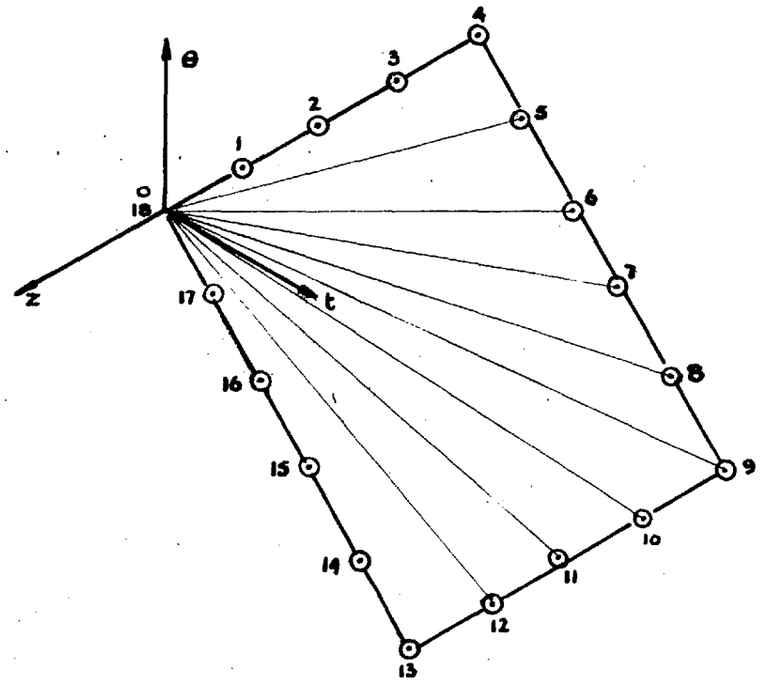

STRESS PATH

$\bar{\sigma}$, 1cm. = $100\sqrt{\frac{2}{3}}$ lb.f./in².

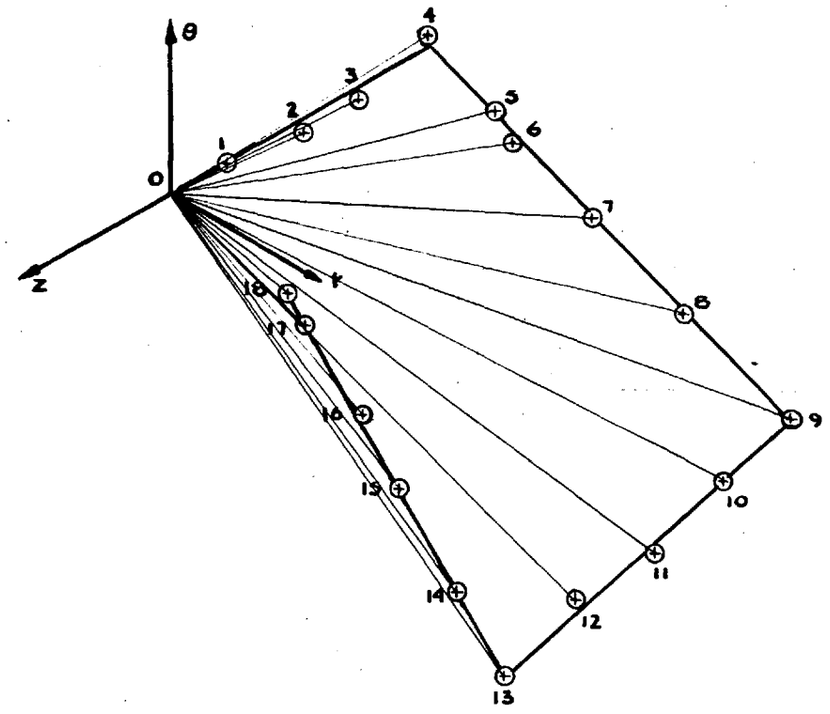

STRAIN PATH

$\bar{\epsilon}$, 1cm. = $\frac{2}{3}\sqrt{\frac{1}{3}} \times 10^{-2}$

FIG. 30 SYSTEM 3) AXIAL LOAD INCREASED TO 4, LOAD HELD CONSTANT AND PRESSURE APPLIED TO 9, PRESSURE CONSTANT AND LOAD DECREASED TO 13, PRESSURE DECREASED TO 18.

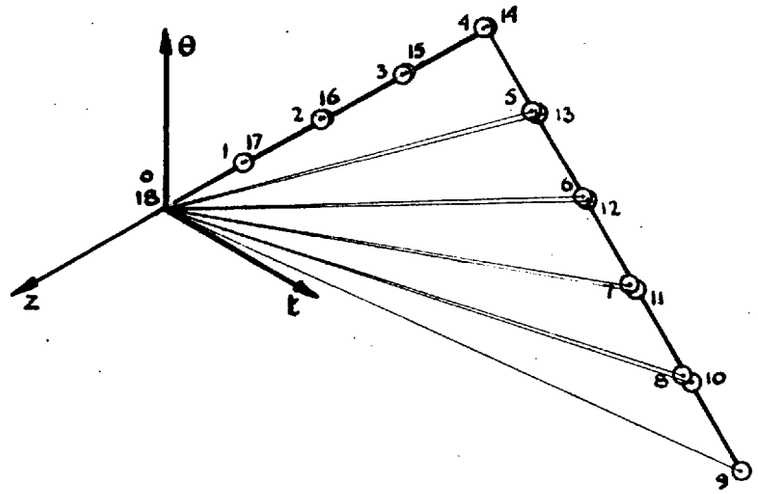

STRESS PATH

$\bar{\sigma}$, 1cm. = $100\sqrt{\frac{7}{5}}$ lbf/in².

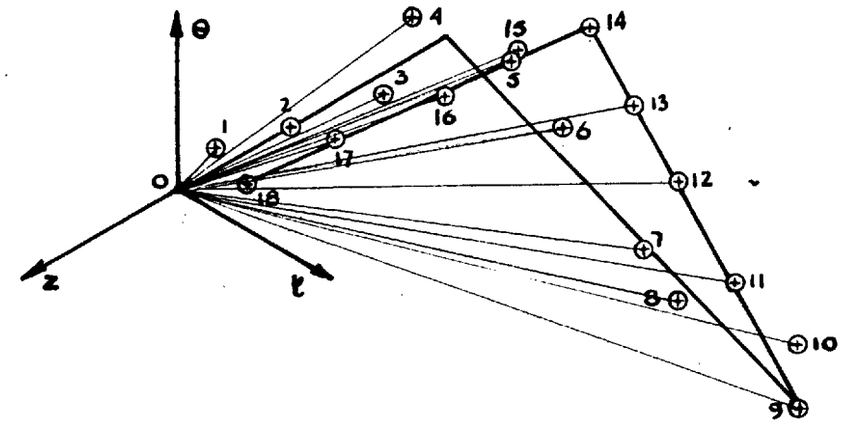

STRAIN PATH

$\bar{\epsilon}$, 1cm. = $\frac{2}{3}\sqrt{\frac{2}{3}} \times 10^{-2}$.

FIG. 31. SYSTEM 4) LOAD INCREASED TO 4, LOAD CONSTANT AND PRESSURE INCREASED TO 9, LOAD CONSTANT AND PRESSURE DECREASED TO 14, LOAD DECREASED TO 18.

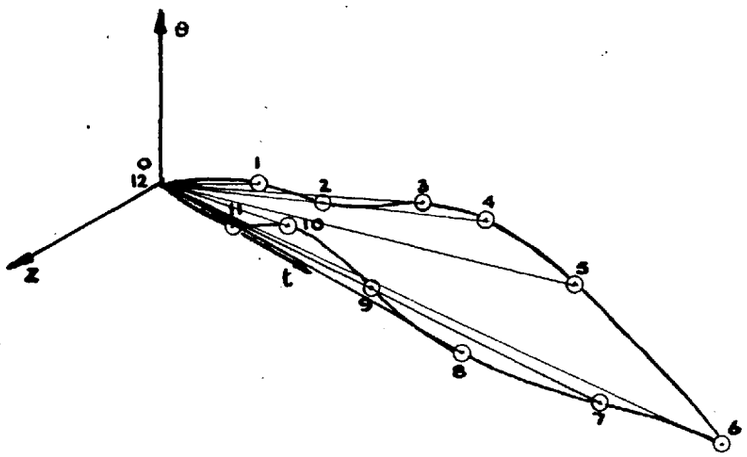

STRESS PATH

$\bar{\sigma}$, 1cm. = $100\sqrt{\frac{2}{3}}$ lb.f./in².

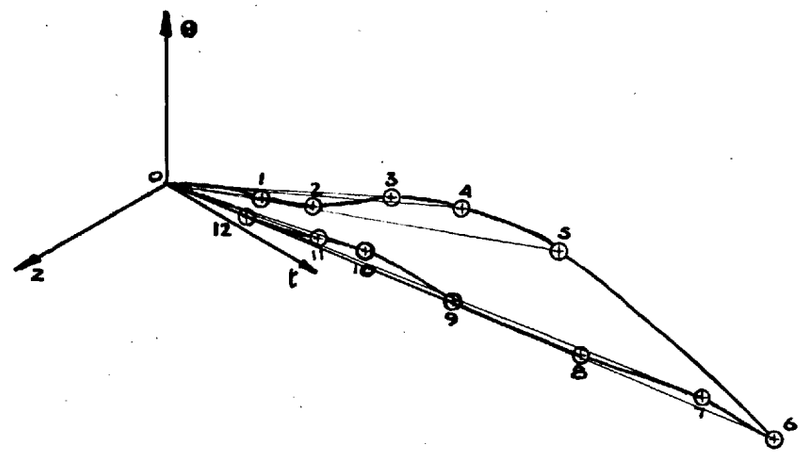

STRAIN PATH

$\bar{\epsilon}$, 1cm. = $\frac{2}{3}\sqrt{\frac{2}{3}} \times 10^{-2}$.

FIG. 32. SYSTEM 5) RANDOM INCREMENTS OF LOAD AND PRESSURE

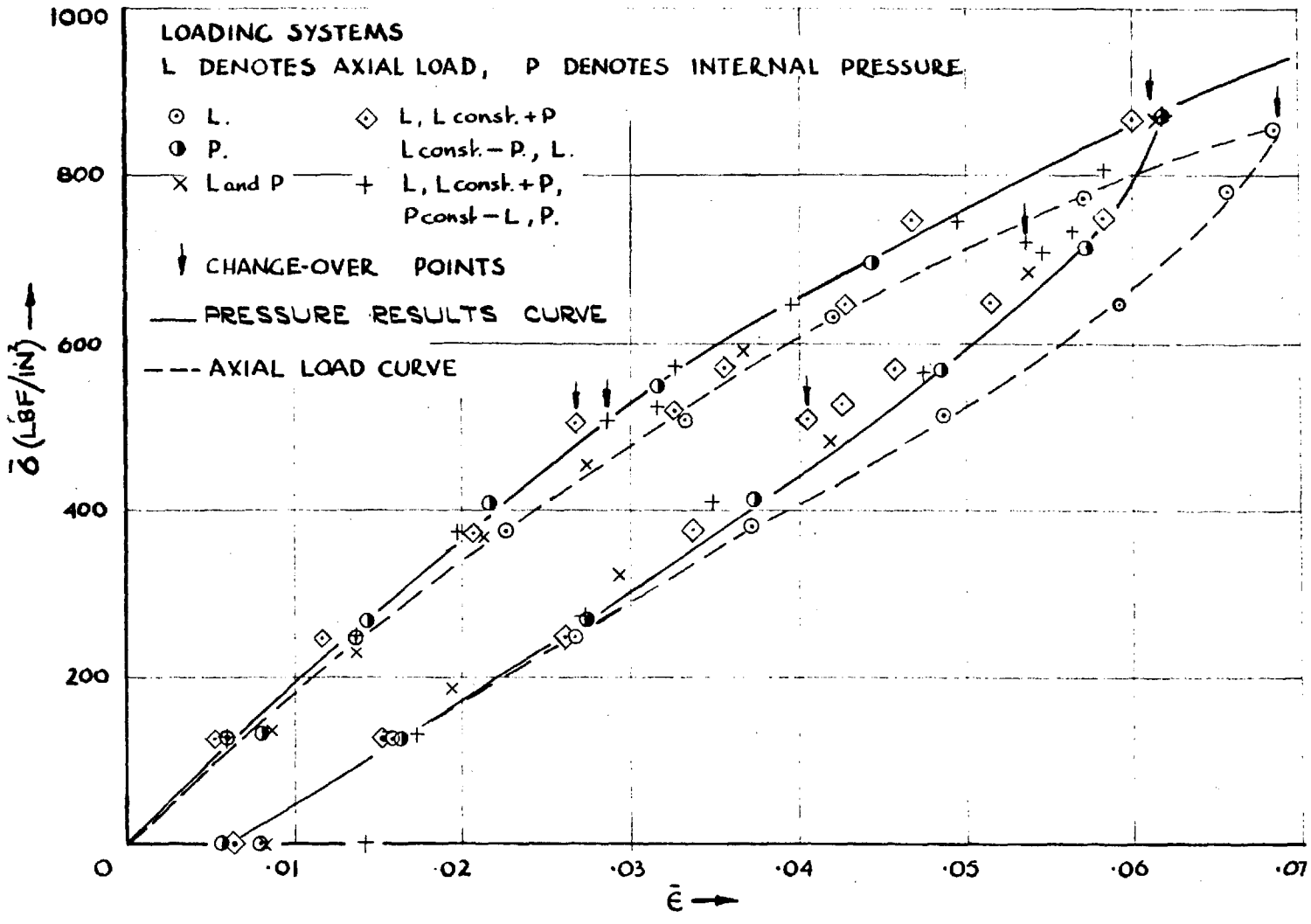

FIG.33. EQUIVALENT STRESS/STRAIN CURVES FOR A THIN WALLED POLYETHYLENE CYLINDER UNDER INTERNAL PRESSURE AND AXIAL LOAD.

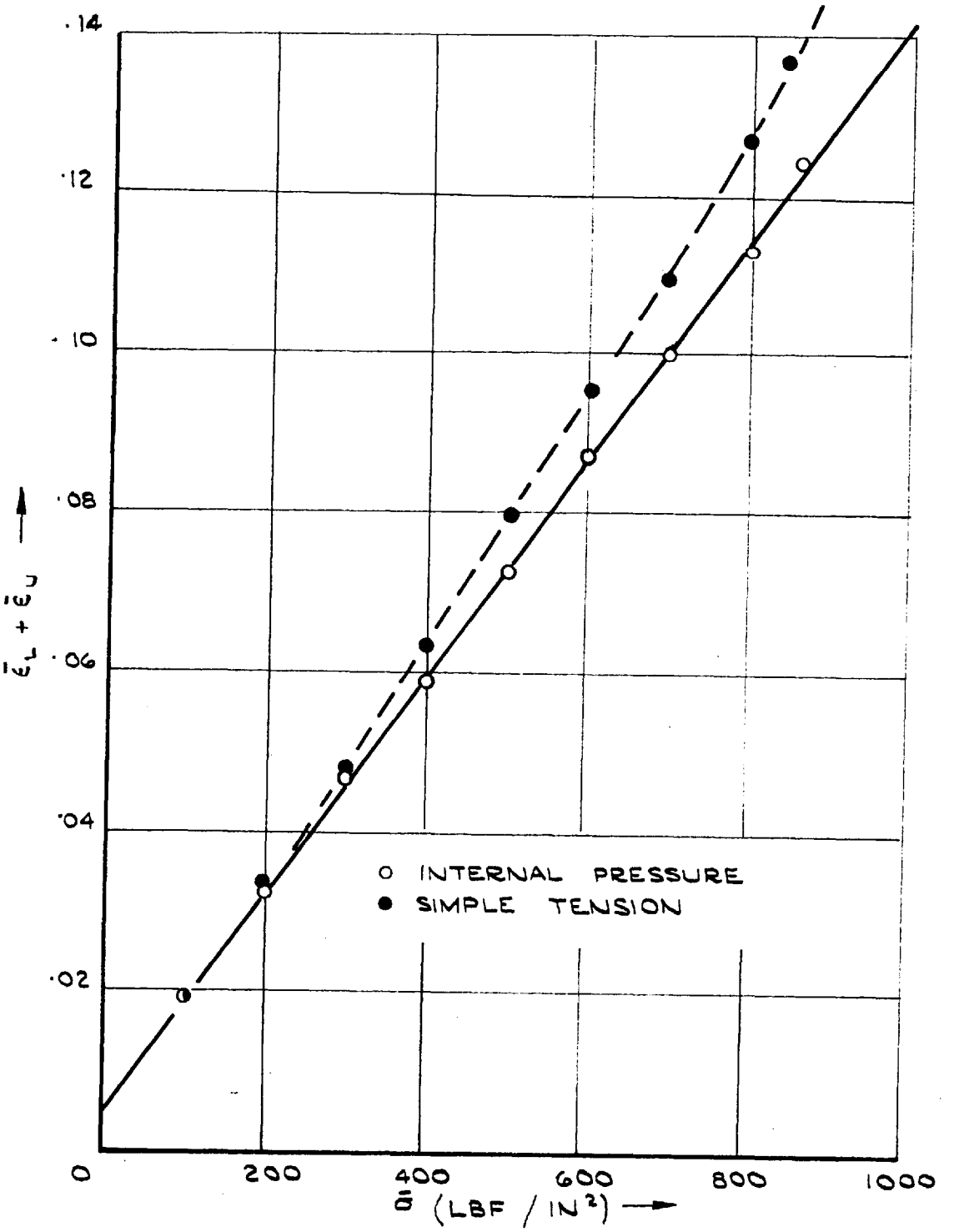
.14
.12
.10
.08
.06
.04
.02
0
200
400
600
800
1000
$\bar{\varepsilon}_L + \bar{\varepsilon}_U$
$\bar{\sigma}$ (LBF / IN^2)
INTERNAL PRESSURE
SIMPLE TENSION

FIG. 34

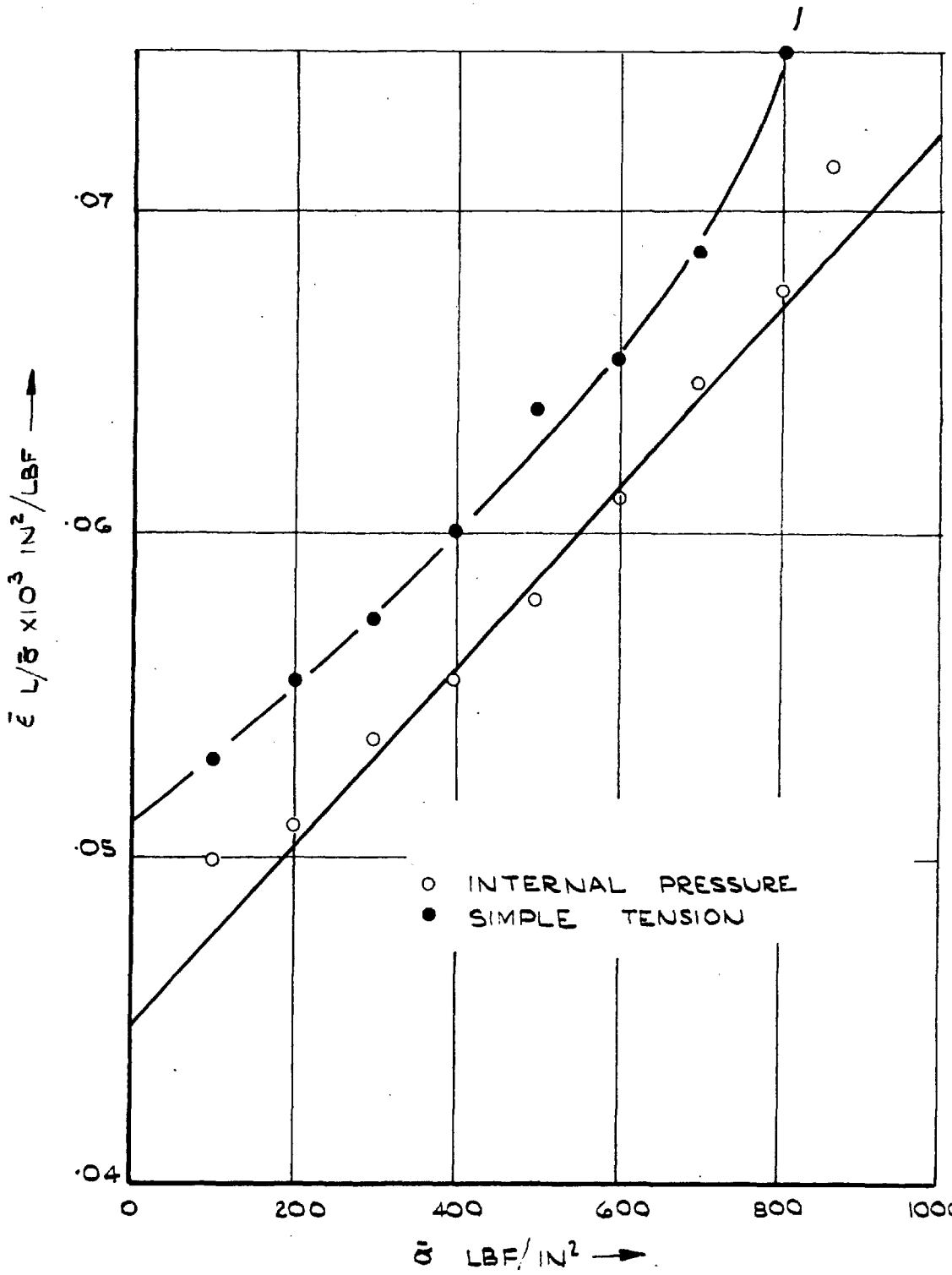
1
·07
·06
·05
·04
0
200
400
600
800
1000
$\bar{\epsilon}$ L/$\bar{\sigma}$ x10^3 IN^2/LBF
$\bar{\sigma}$ LBF/IN^2
INTERNAL PRESSURE
SIMPLE TENSION

FIG. 35

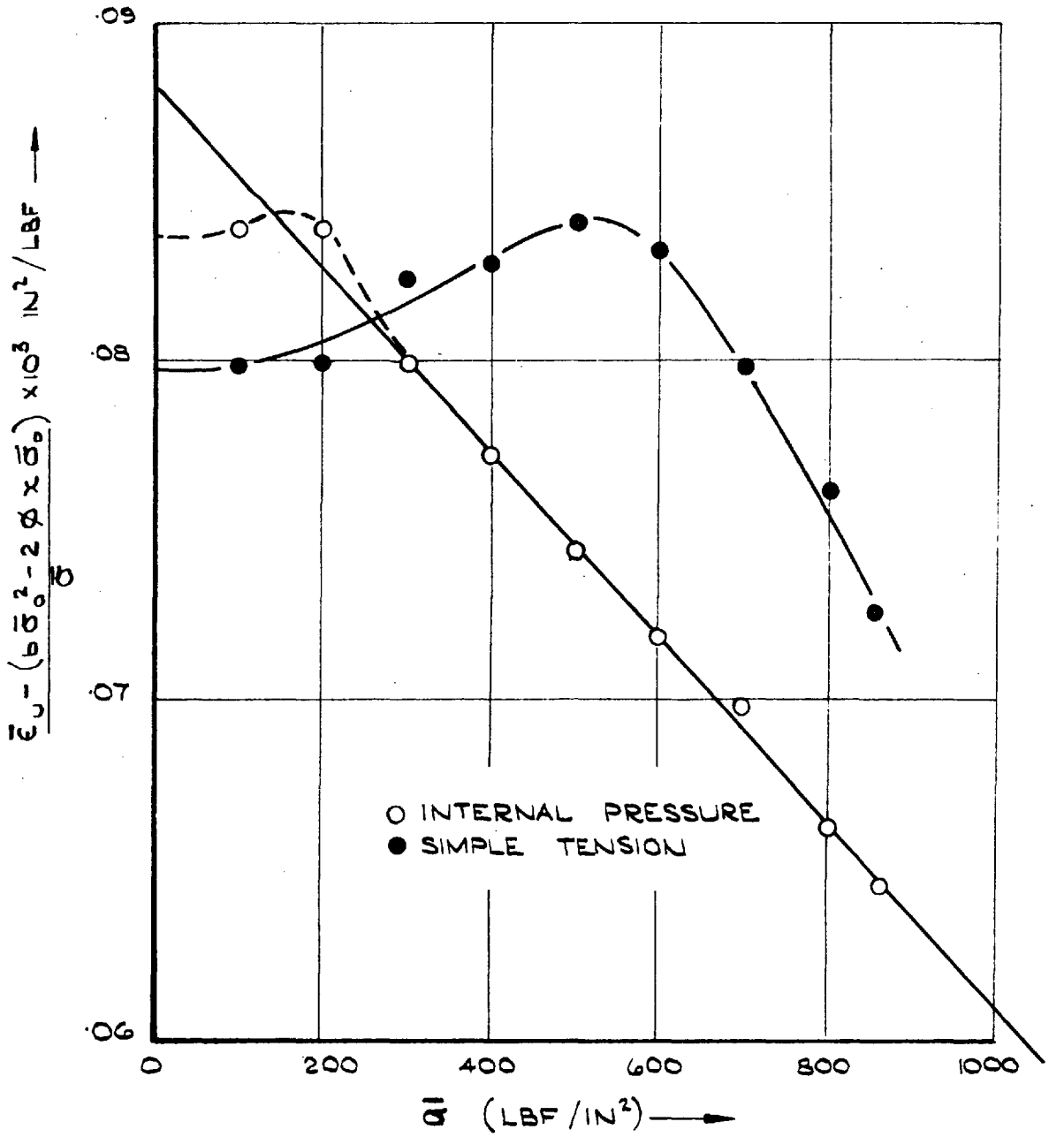
·09
·08
·07
·06
0
200
400
600
800
1000
$\bar{\epsilon}_v - (b\bar{\sigma}_0^2 - 2\phi \times \bar{\sigma}_0) \times 10^3$ IN²/LBF
$\bar{\sigma}$ (LBF/IN²)
O INTERNAL PRESSURE
● SIMPLE TENSION

FIG. 36.

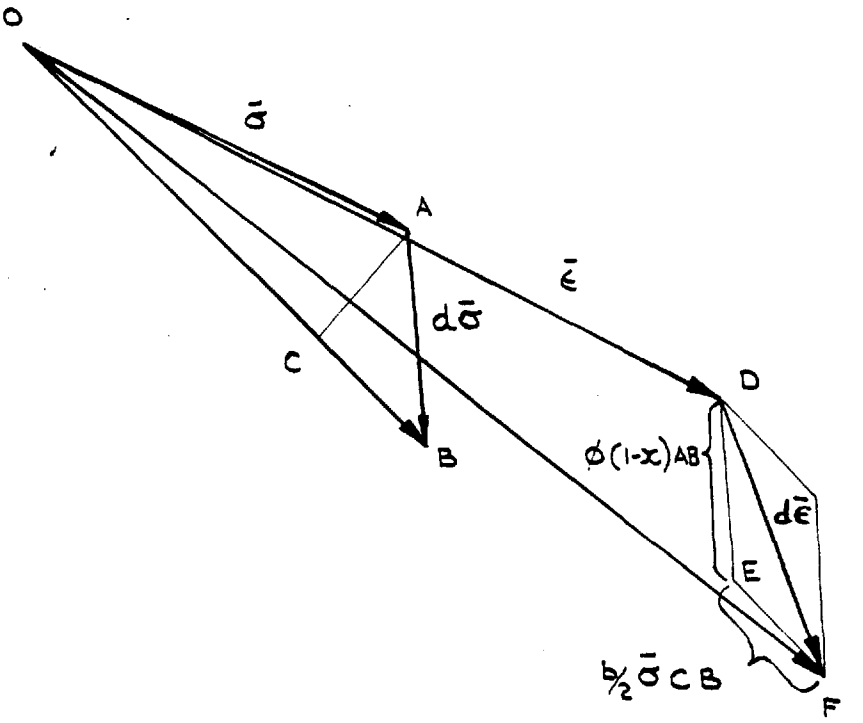

FIG. 37. STRAIN PATH CONSTRUCTION FOR COMPLEX LOADING.

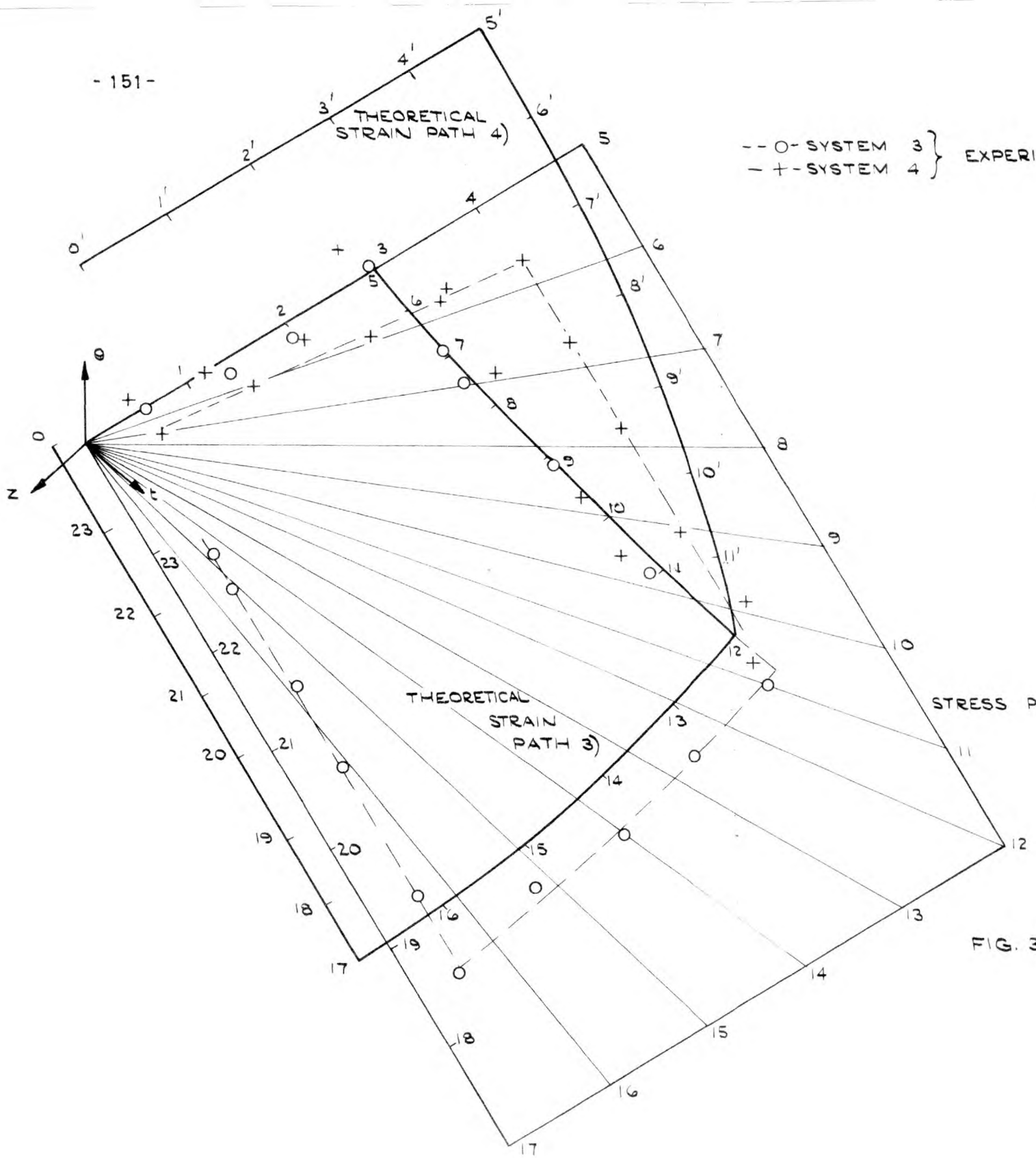

-- O- SYSTEM 3
— + - SYSTEM 4
} EXPERIMENTAL POINTS

SCALES

STRESS 1 INCH = $\sqrt{\frac{2}{3}}$. 100 LBF / IN^2

STRAIN 1 INCH = $\sqrt{\frac{2}{3}}$. 0·01

FIG. 38 THEORETICAL STRAIN PATHS FOR LOADING SYSTEMS. 3 AND 4

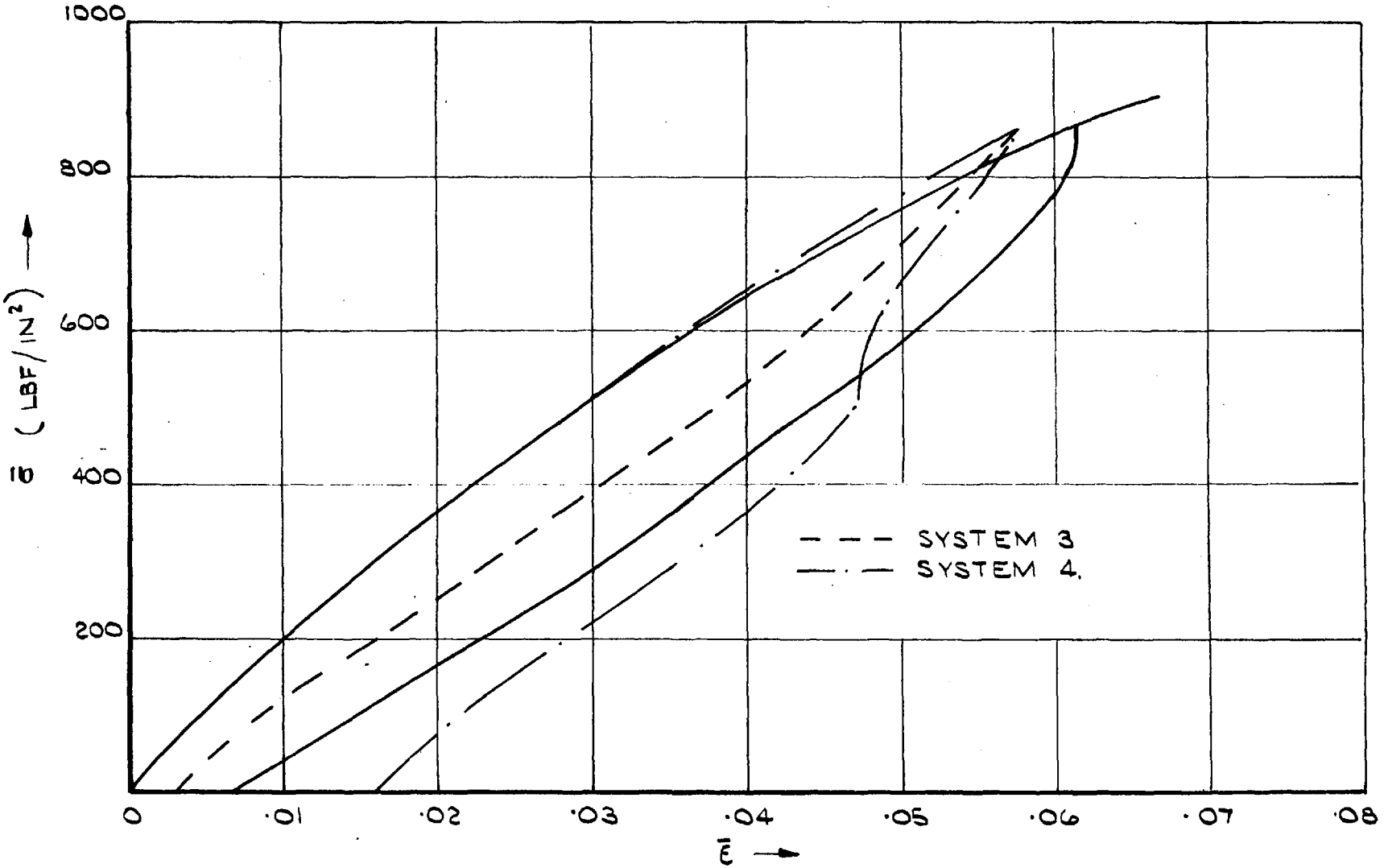

FIG. 39. THEORETICAL EQUIVALENT STRESS STRAIN RELATIONS FOR SYSTEMS 3 AND 4

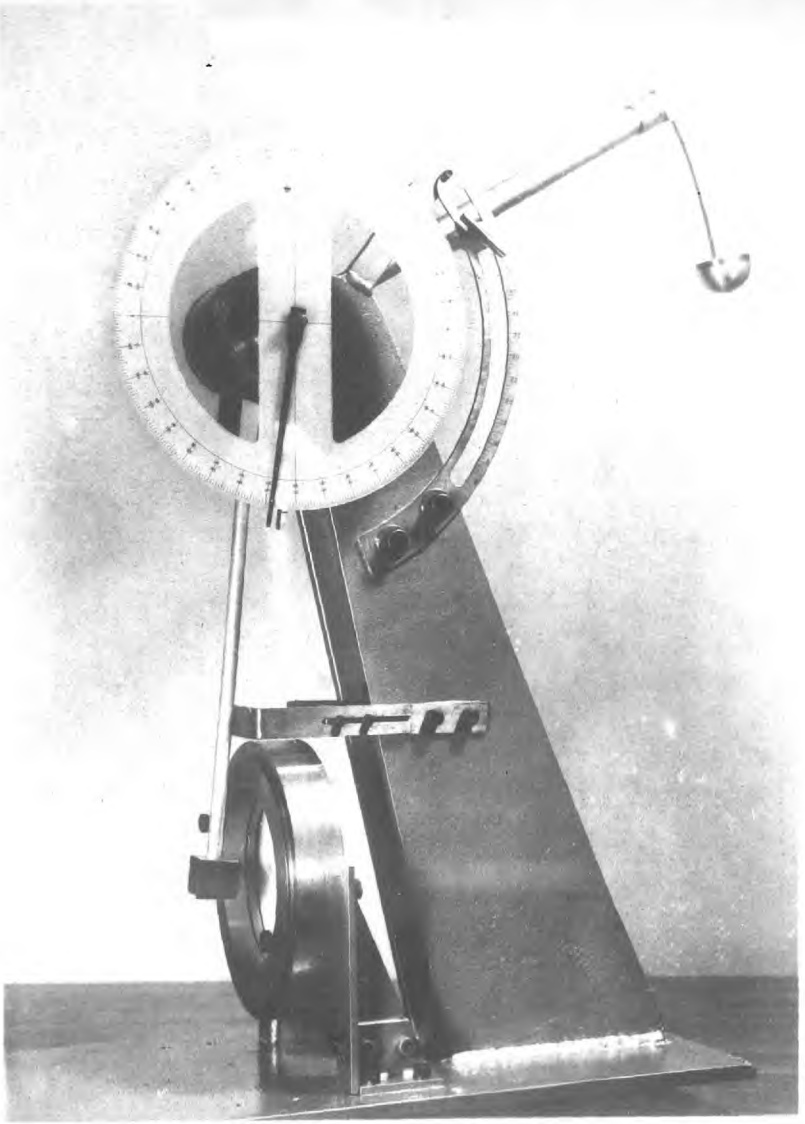

FIG 40 FILM IMPACT TESTING MACHINE

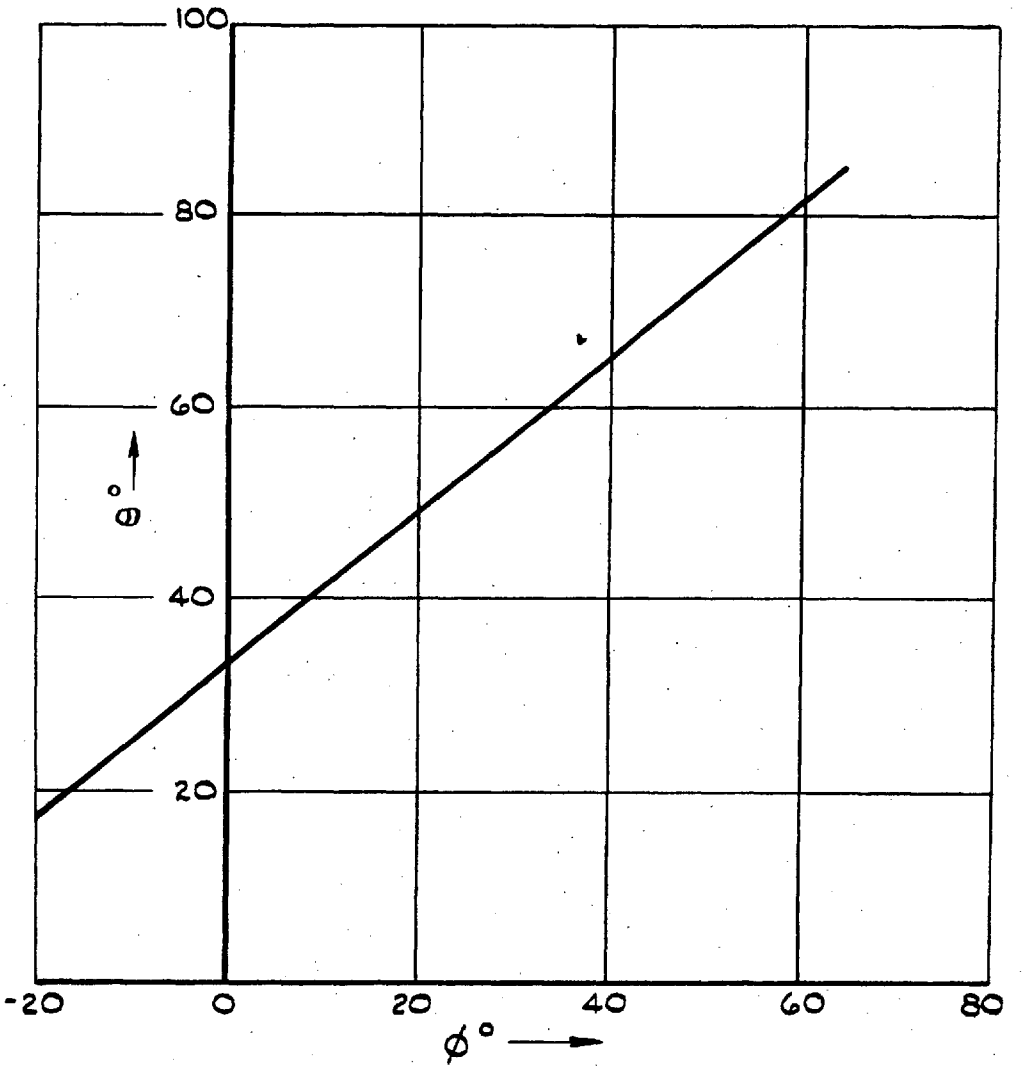

FIG. 41 ABSORBER PENDULUM ANGLE θ VERSUS STRIKER PENDULUM ANGLE φ.

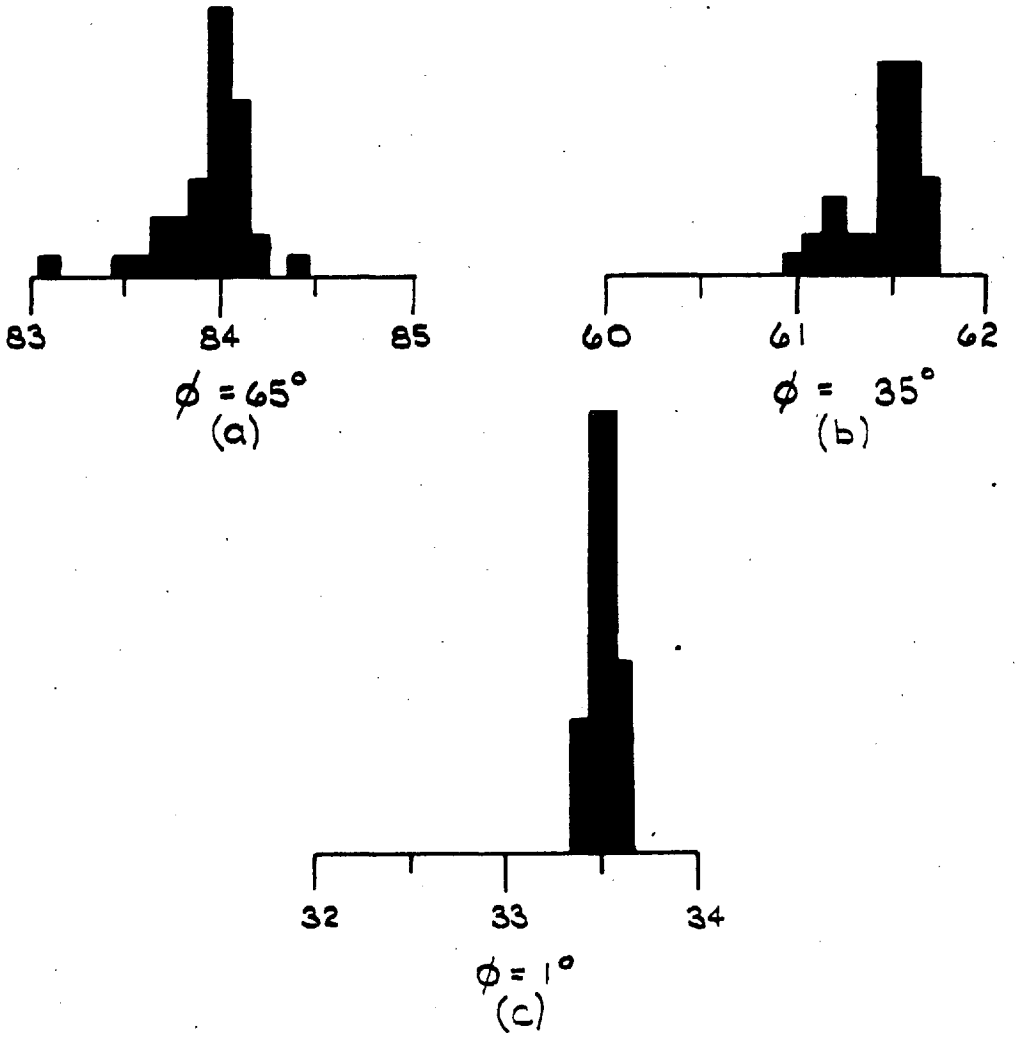

FIG. 42 DISTRIBUTIONS OF FORTY READINGS OF θ FOR THREE VALUES OF φ

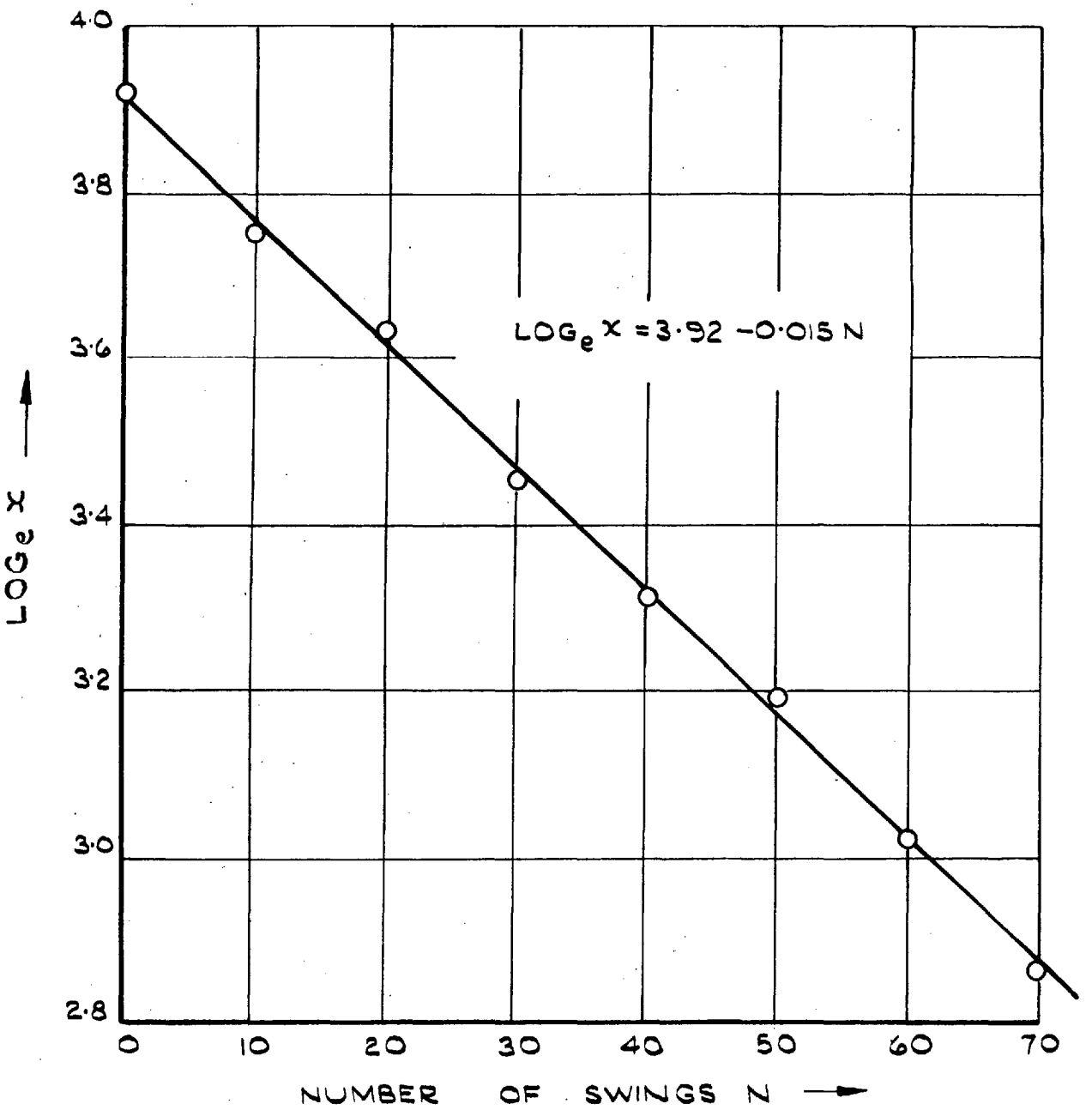

FIG. 43. WINDAGE LOSS LINE FOR STRIKER PENDULUM.

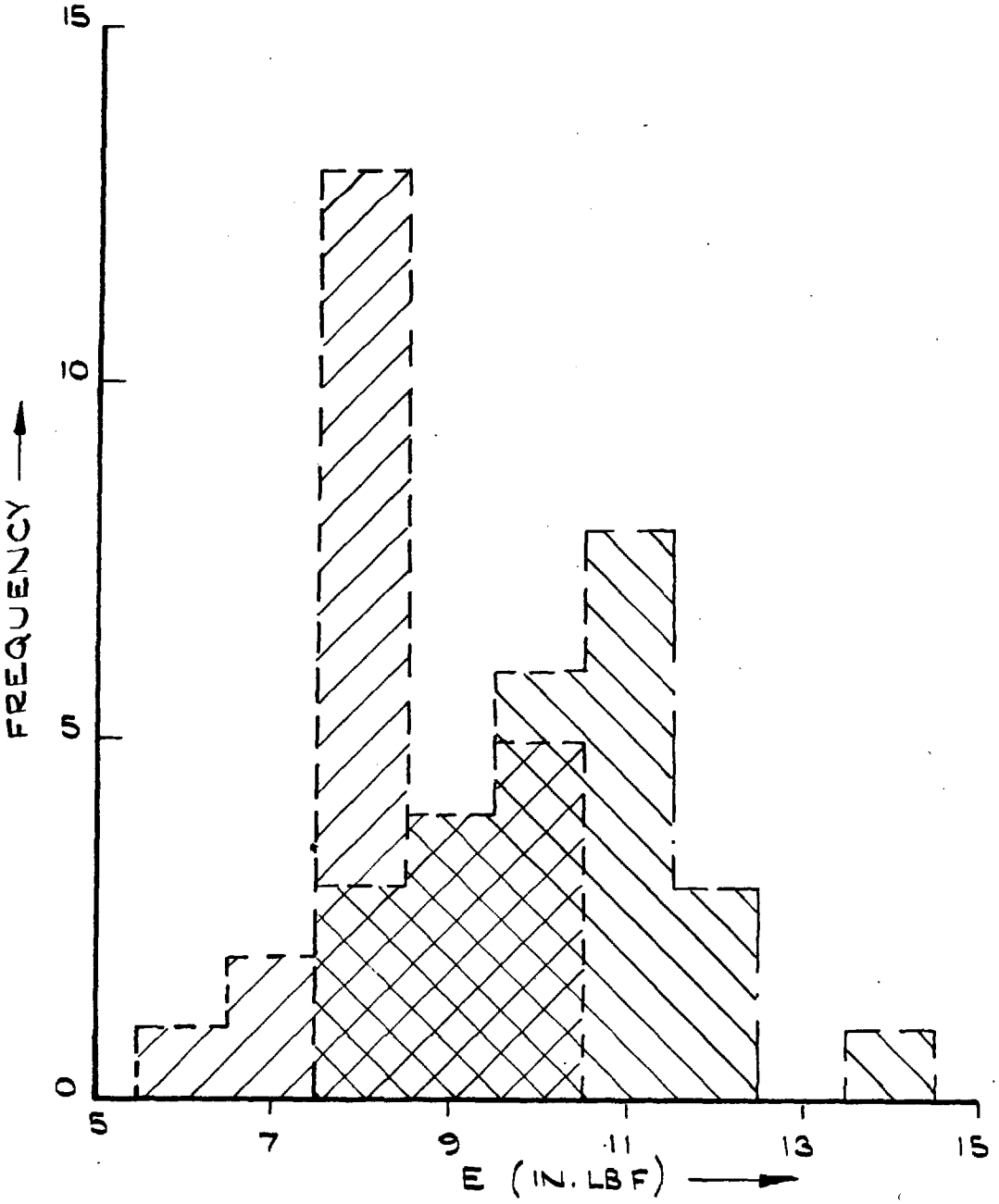

FIG. 44 DISTRIBUTION OF ENERGY VALUES FOR EACH SIDE OF THE TUBE.

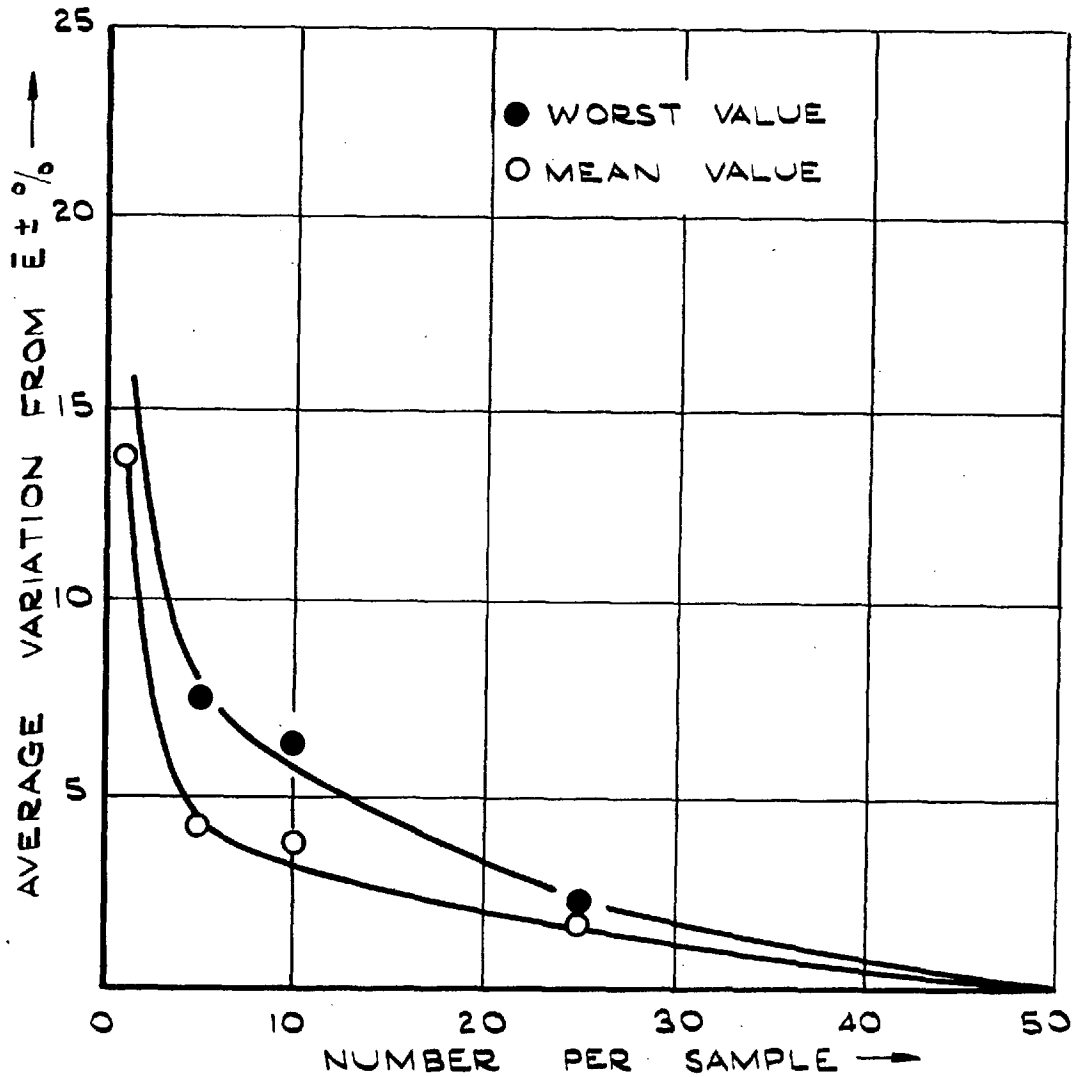

FIG. 45 SAMPLE VARIATIONS FOR FIFTY SPECIMENS OF E2029.

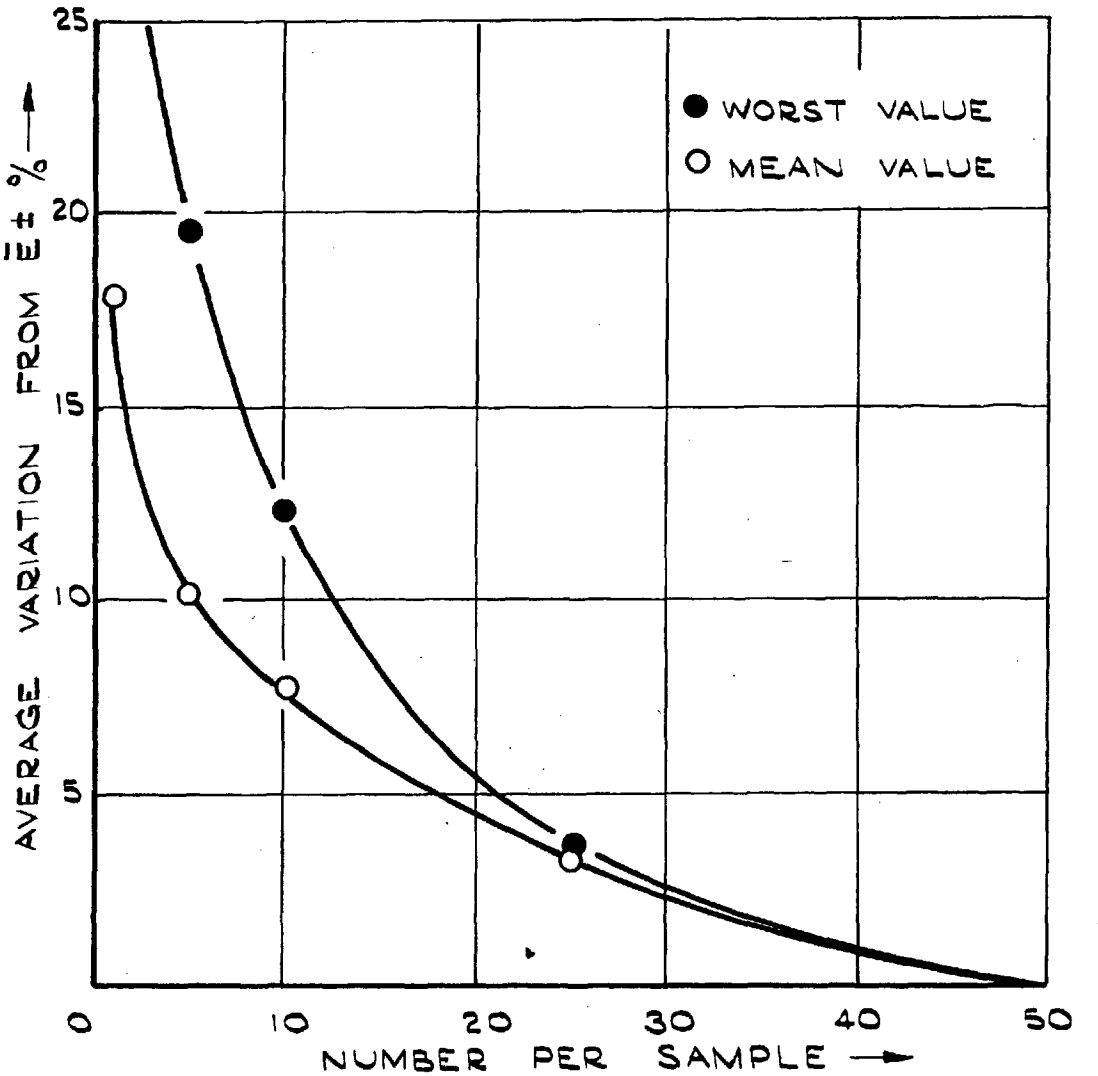

FIG. 46 SAMPLE VARIATIONS FOR FIFTY SPECIMENS OF E2066.

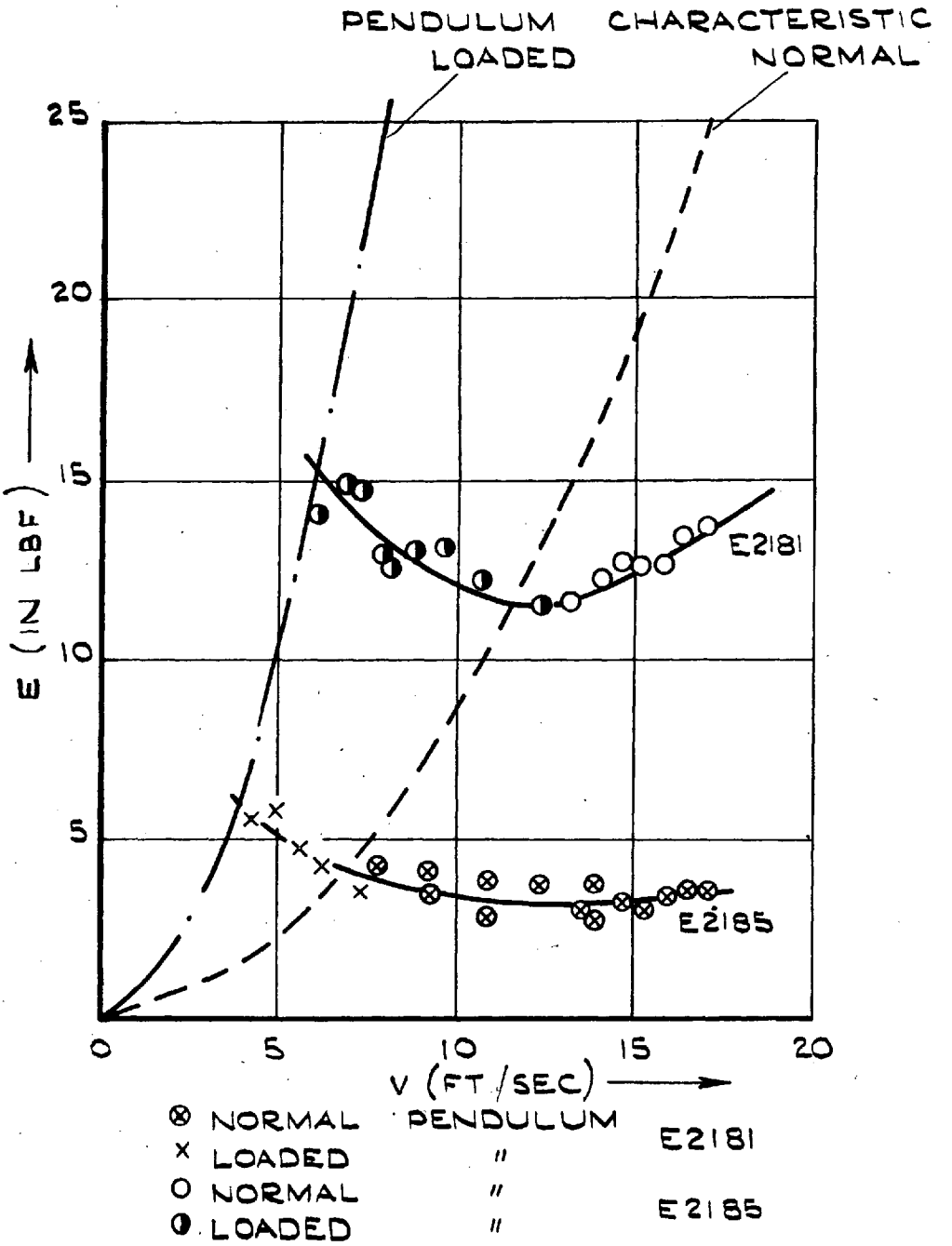

FIG. 47. VARIATION OF ENERGY TO RUPTURE WITH VELOCITY OF IMPACT.

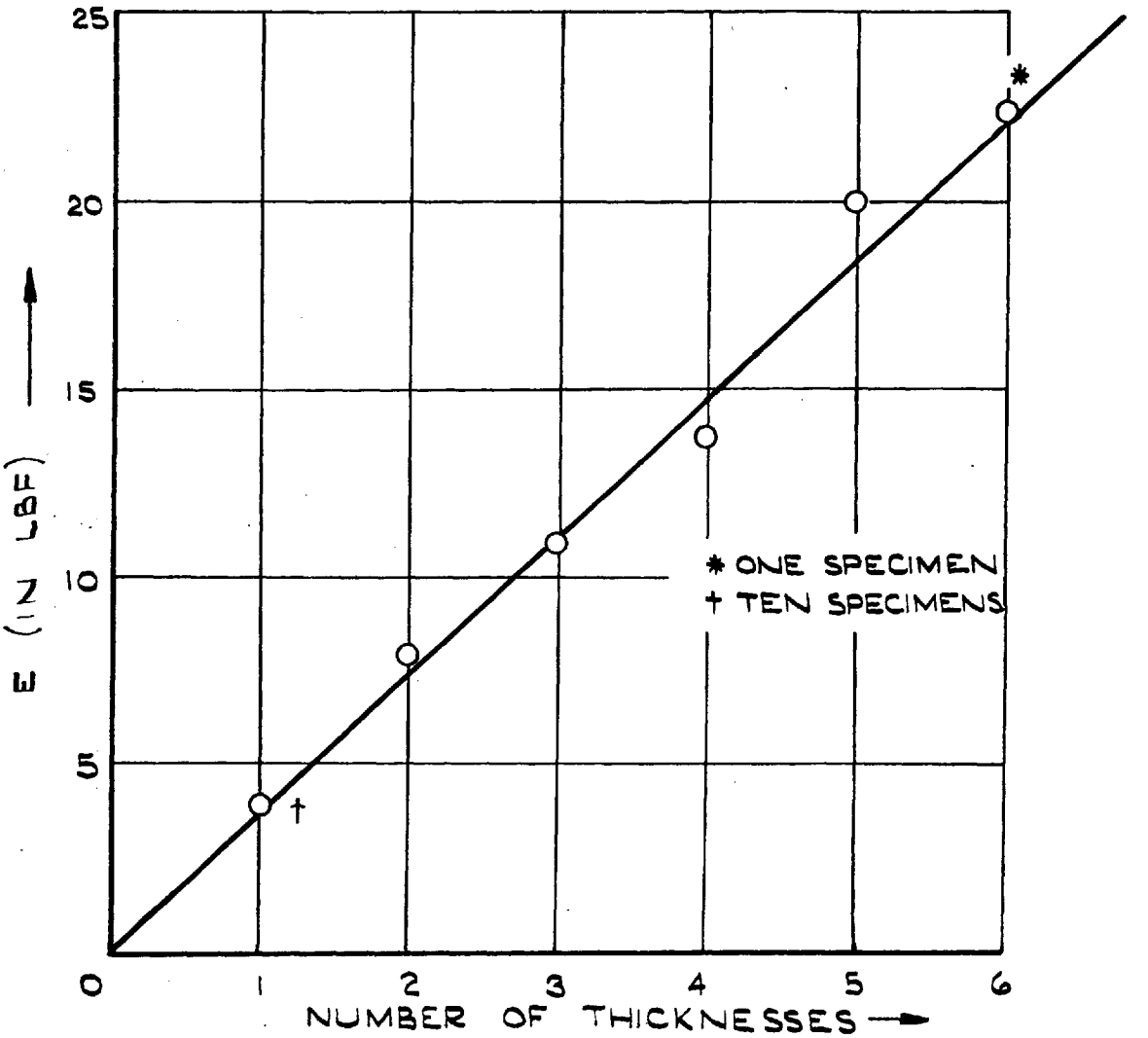

FIG. 48. MULTIPLE THICKNESS TESTS E2185
MEANS OF FIVE SPECIMENS.

a)

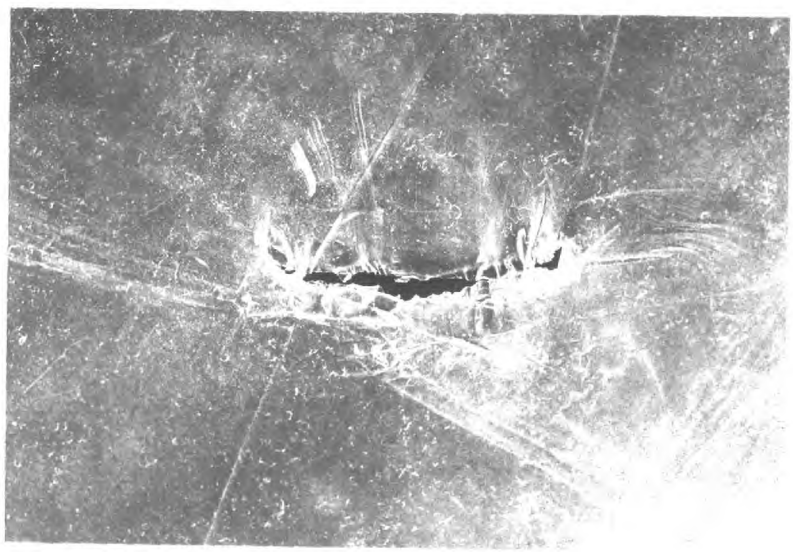

b)

FIG 49

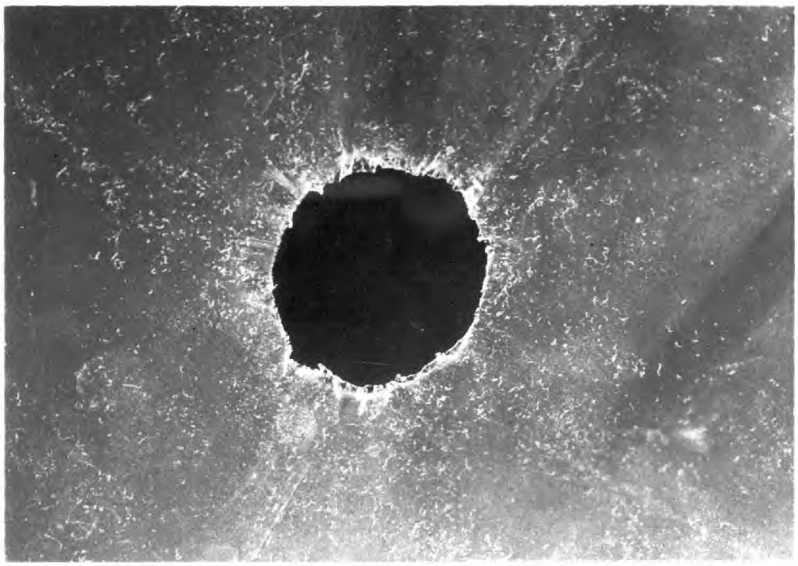

a)

b)

FIG 50

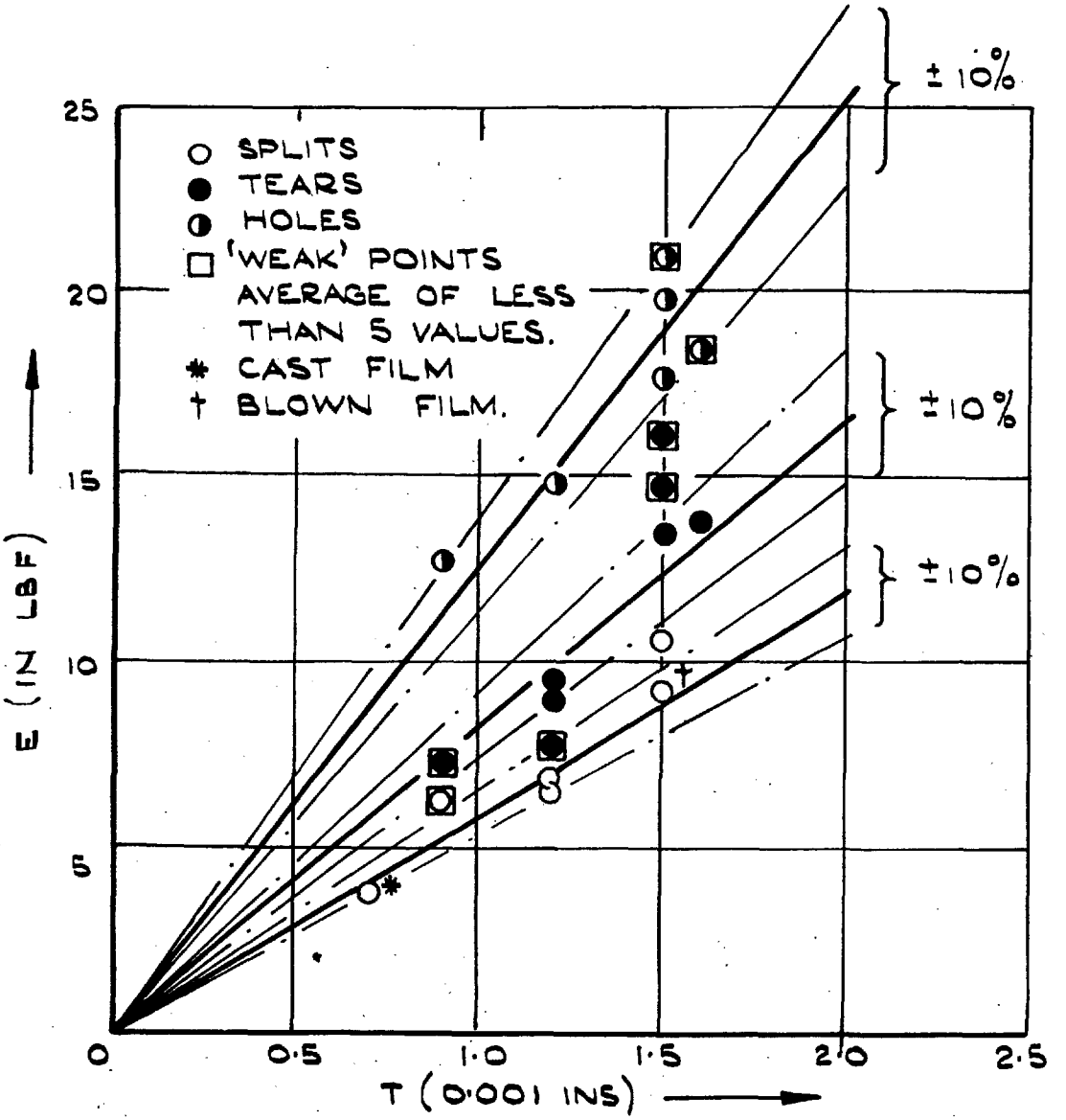

FIG. 51. ENERGY v. THICKNESS FOR IMPACT TEST.

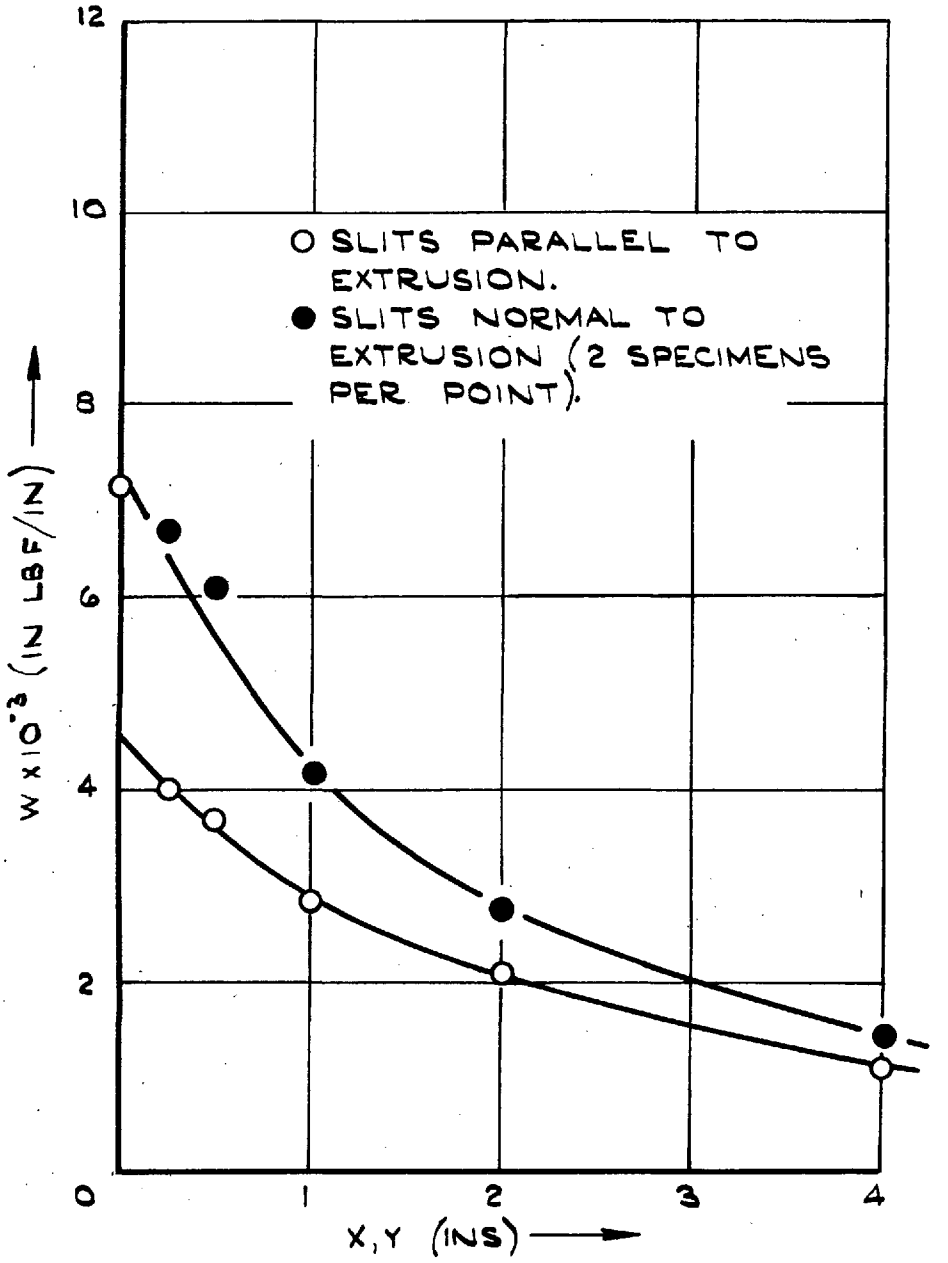

FIG. 52. ENERGY PER UNIT THICKNESS FOR SLITS AT THE IMPACT POINT E 2184 'SPLIT' MATERIAL.

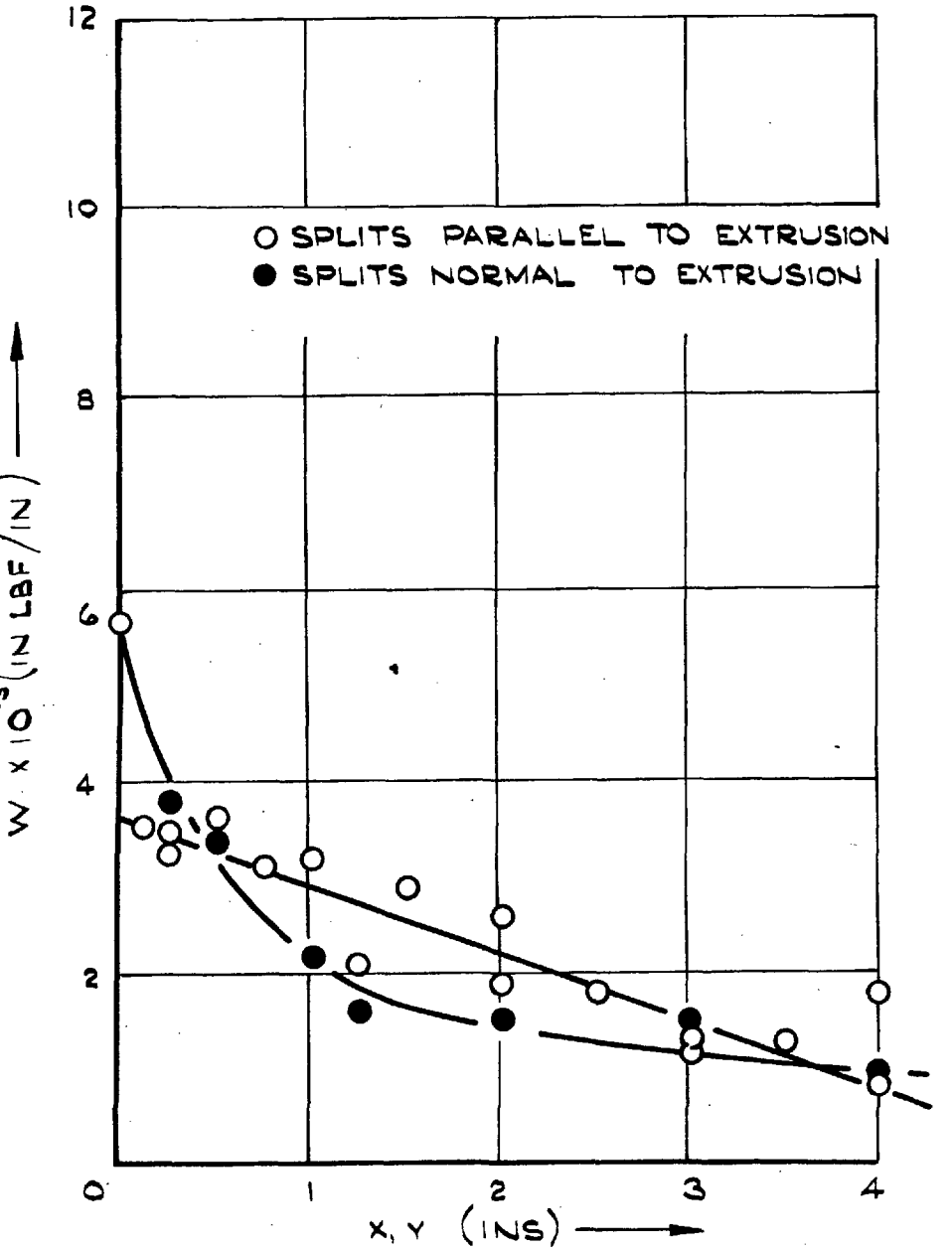

FIG. 53. ENERGY PER UNIT THICKNESS FOR SLITS AT THE IMPACT POINT E2186 'SPLIT' MATERIAL

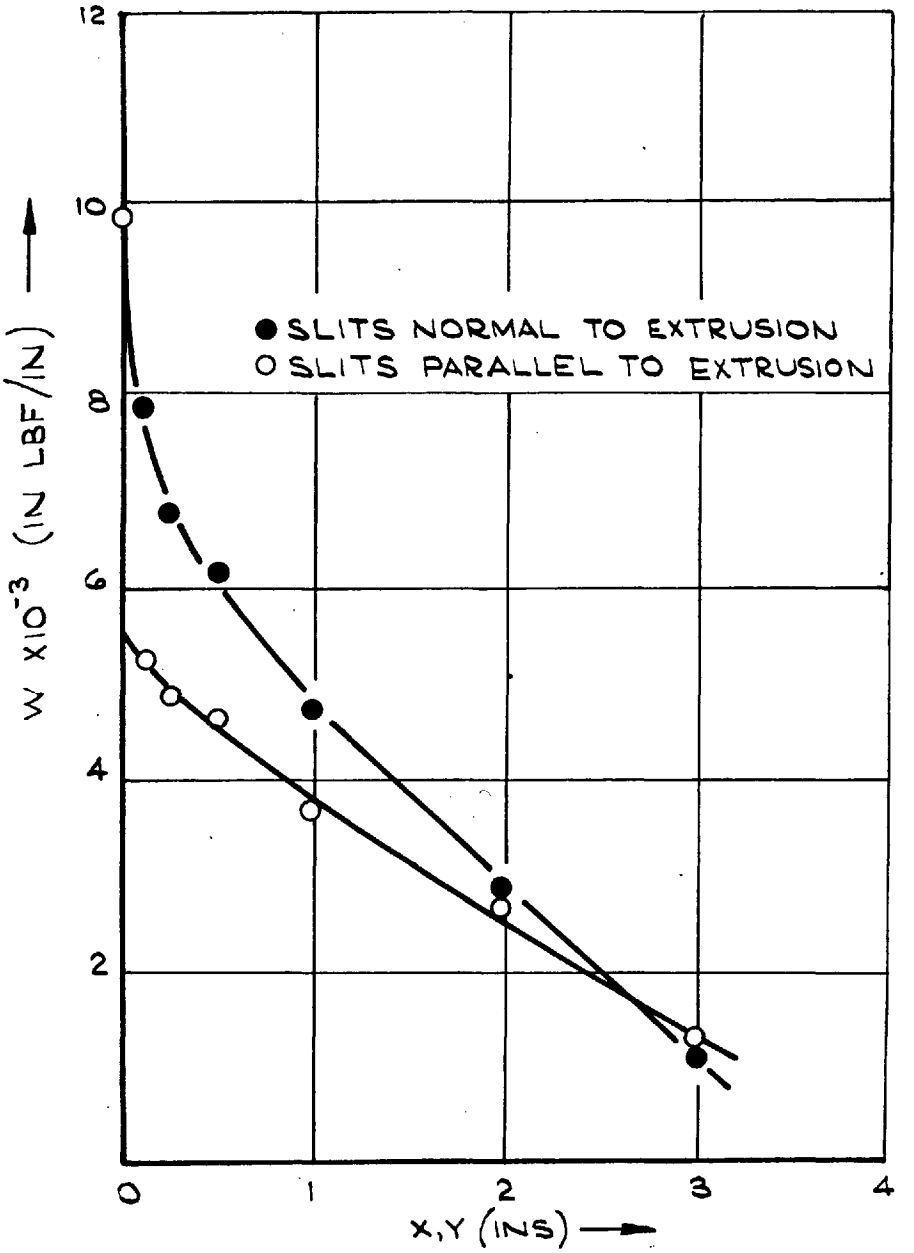

FIG. 54 ENERGY PER UNIT THICKNESS FOR SLITS AT THE IMPACT POINT E2068 'TEAR' MATERIAL.

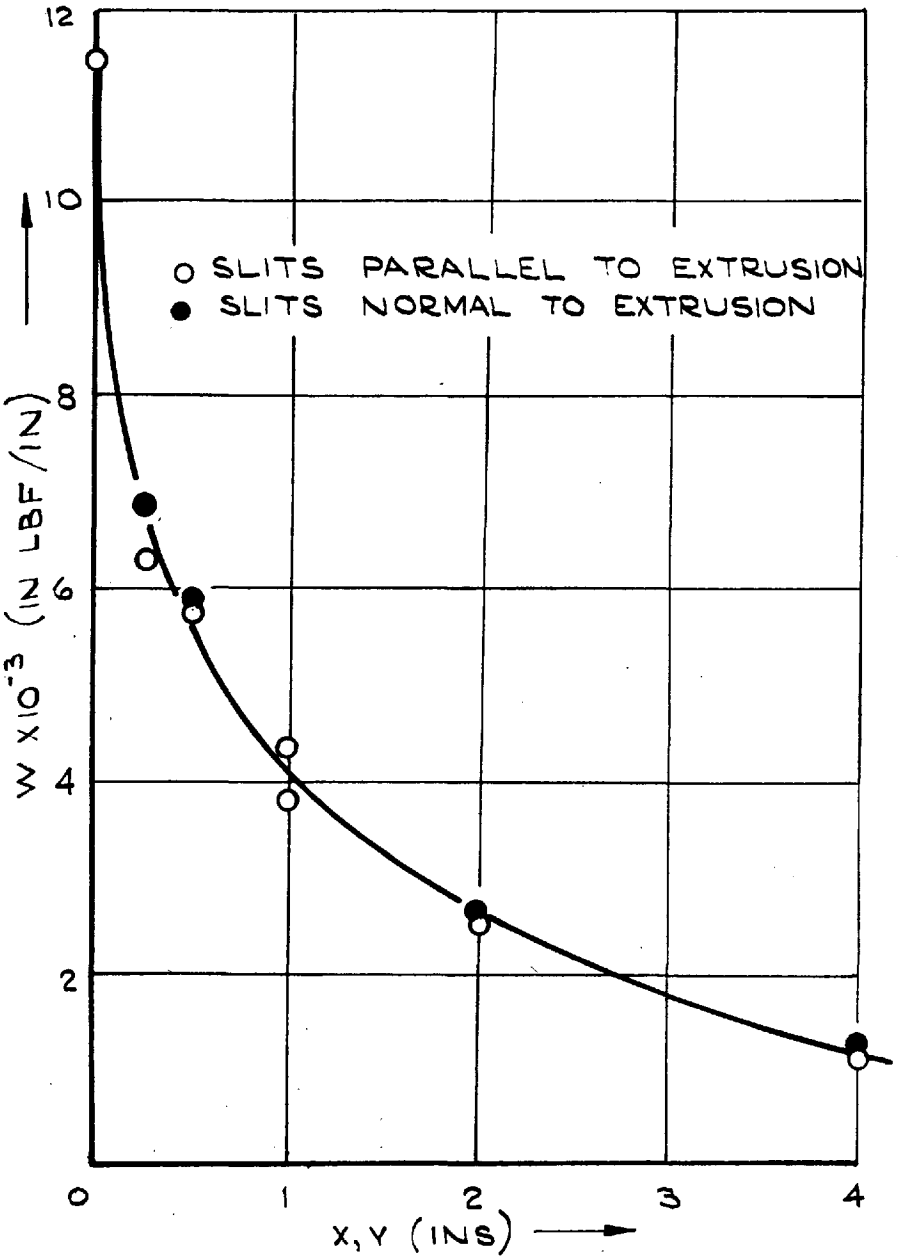

FIG. 55 ENERGY PER UNIT THICKNESS FOR SLITS AT IMPACT POINT E 2182 'HOLE' MATERIAL.

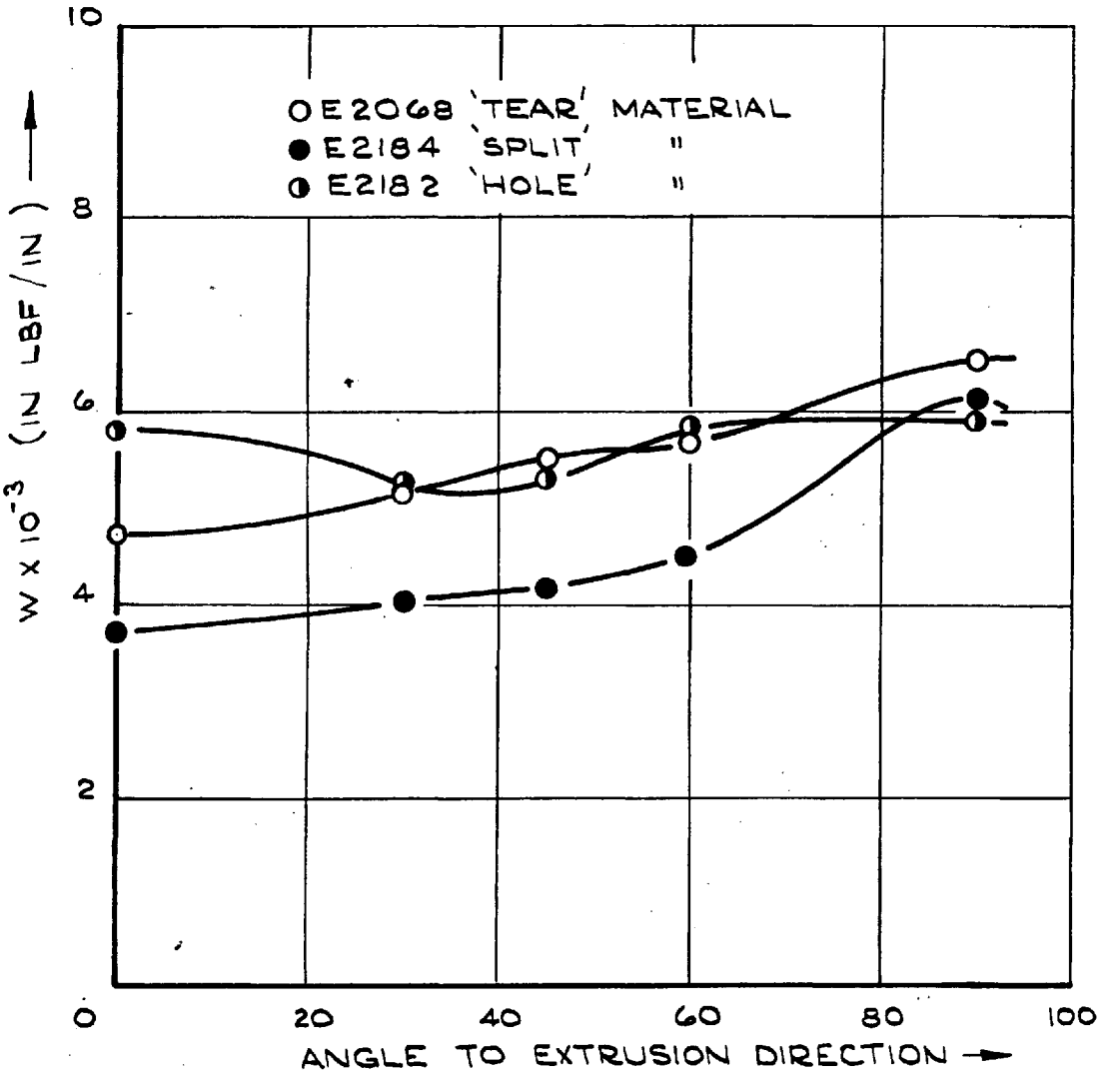

FIG.56. HALF INCH SLIT SET AT VARIOUS ANGLES TO THE EXTRUSION DIRECTION

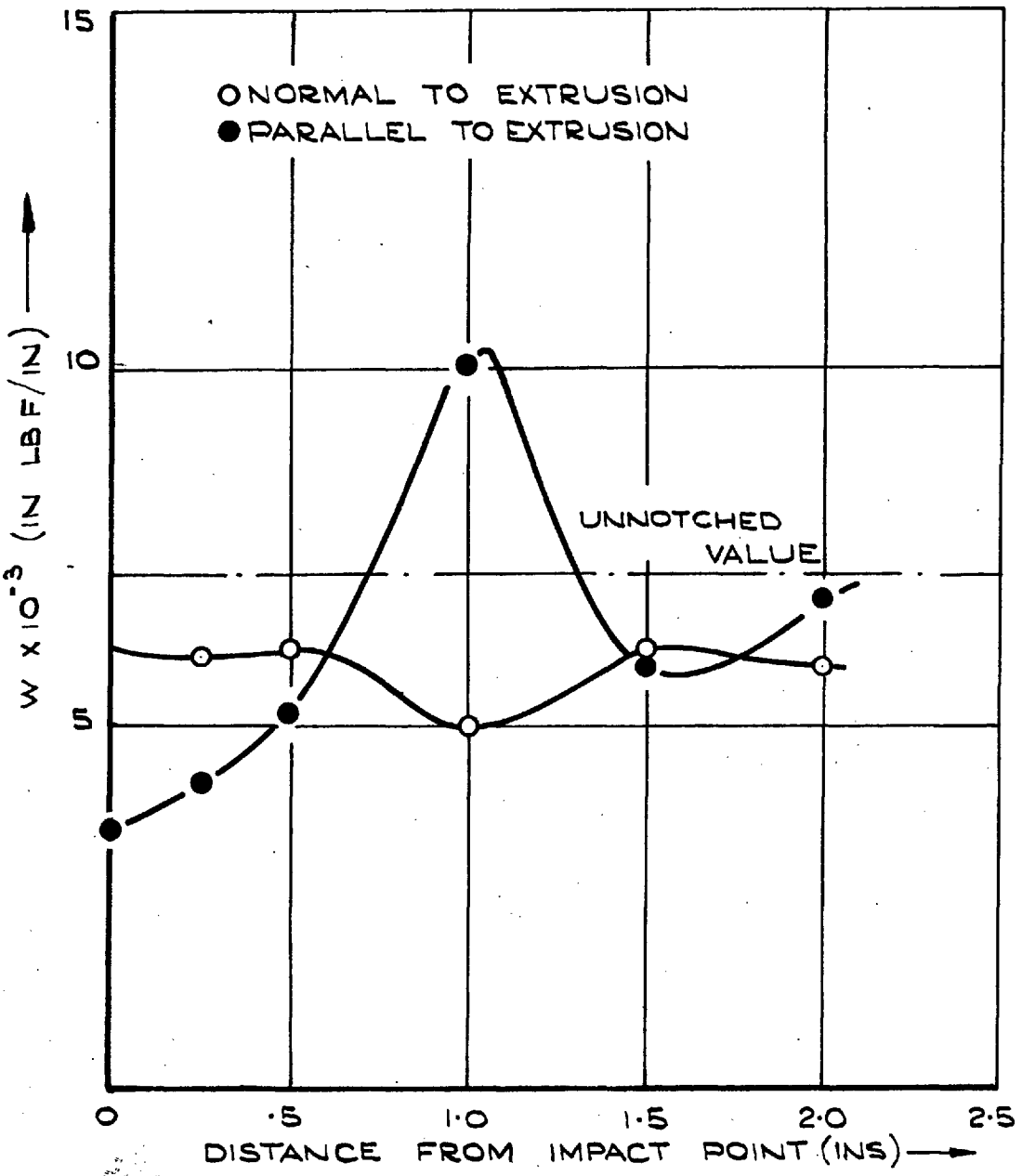

FIG.57. HALF INCH SLIT OFFSET, E2184 'SPLIT' MATERIAL.

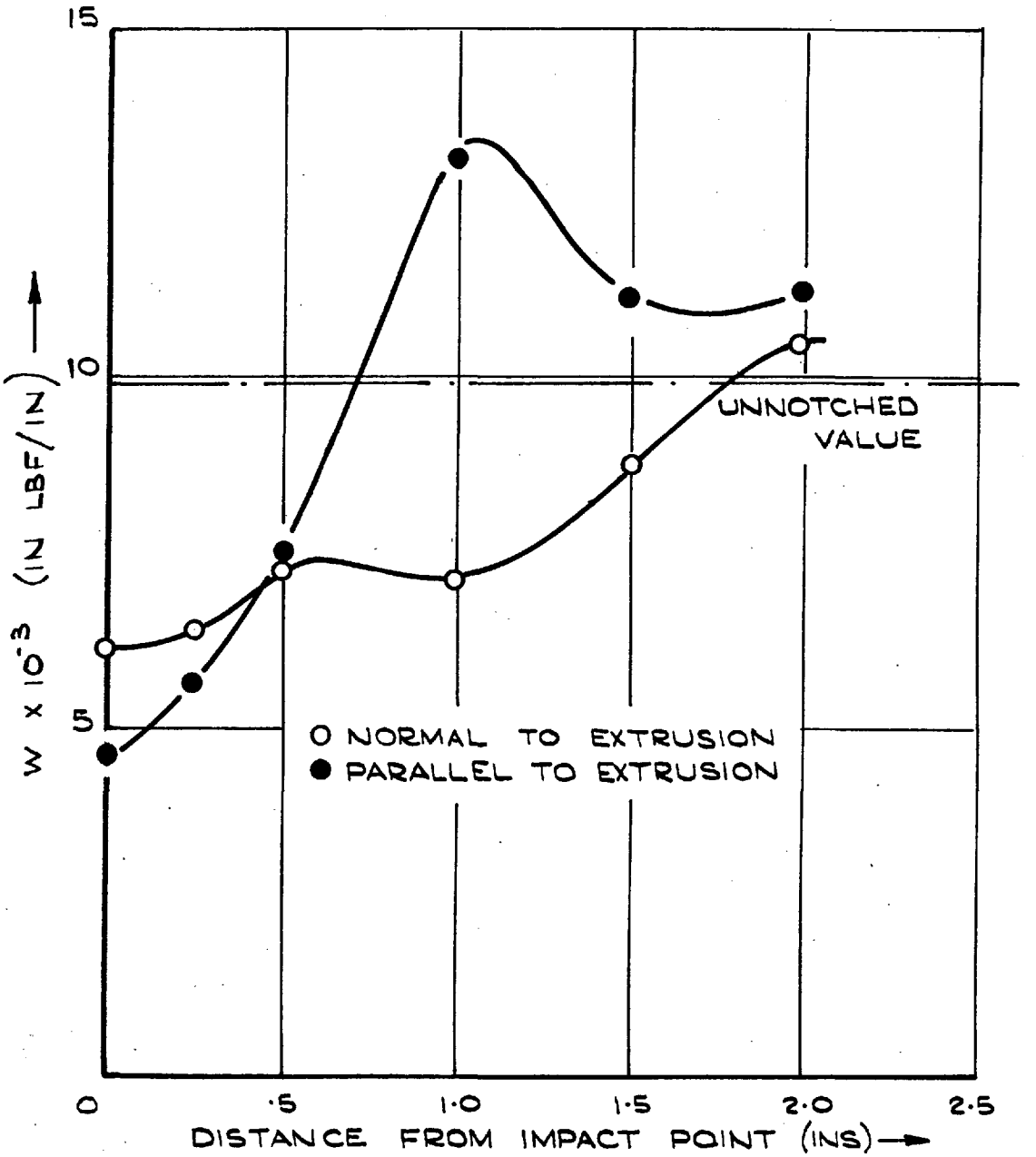

FIG. 58. HALF INCH SLIT OFFSET, E2068 'TEAR' MATERIAL.

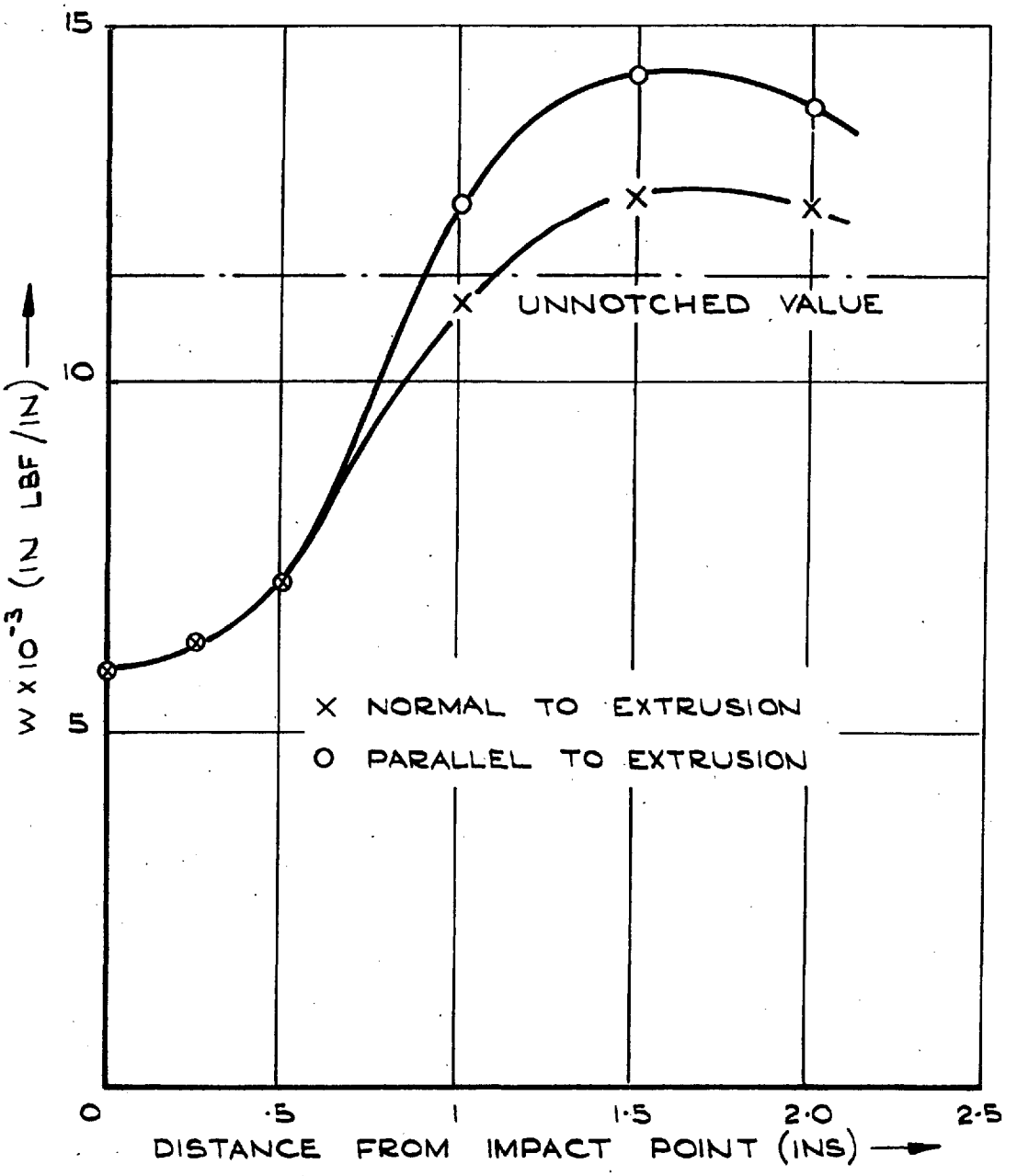

FIG. 59 HALF INCH SLIT OFFSET, E2182 'HOLE' MATERIAL.

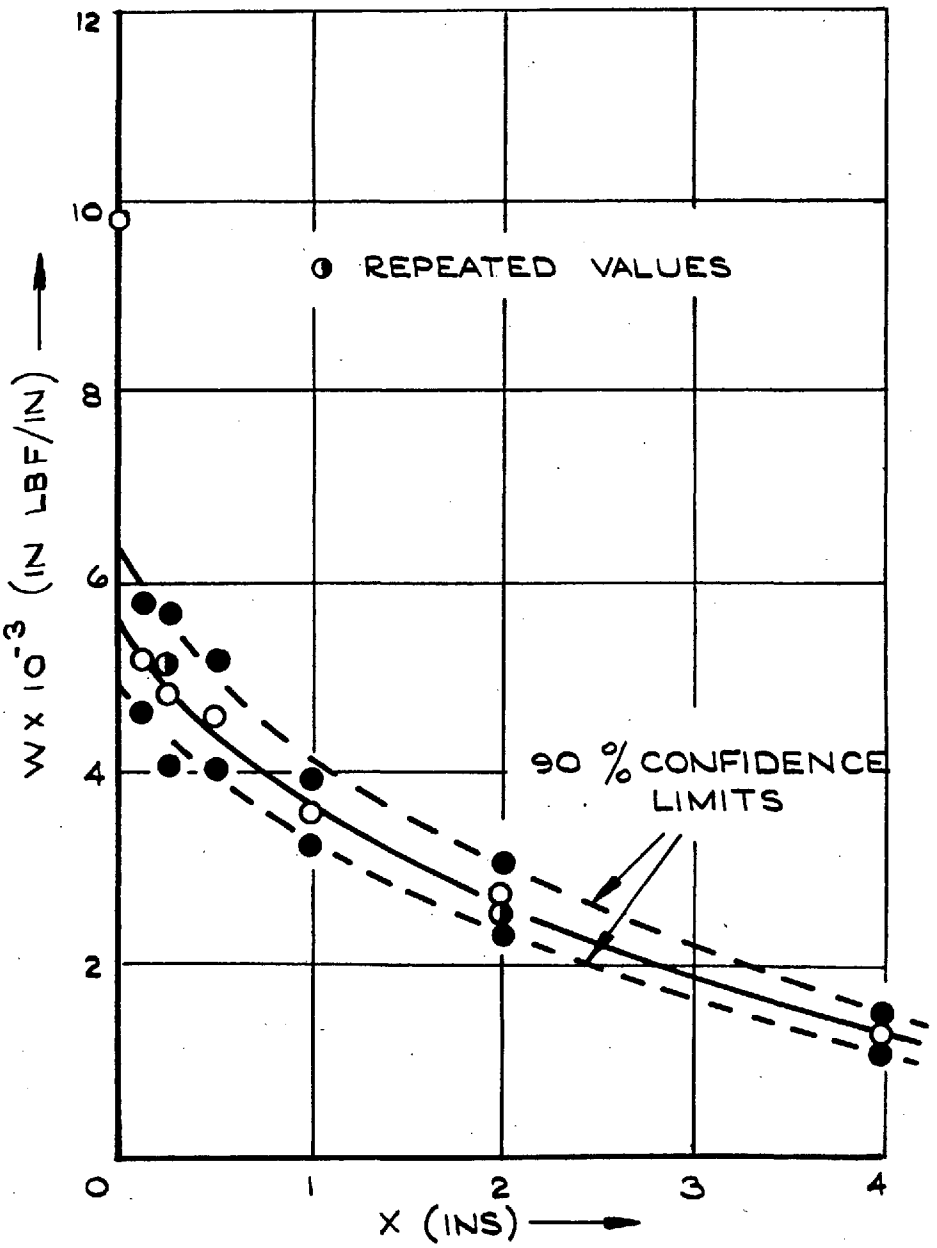

FIG. 60. ACCURACY OF SLIT TEST E 2068. SLITS PARALLEL TO EXTRUSION

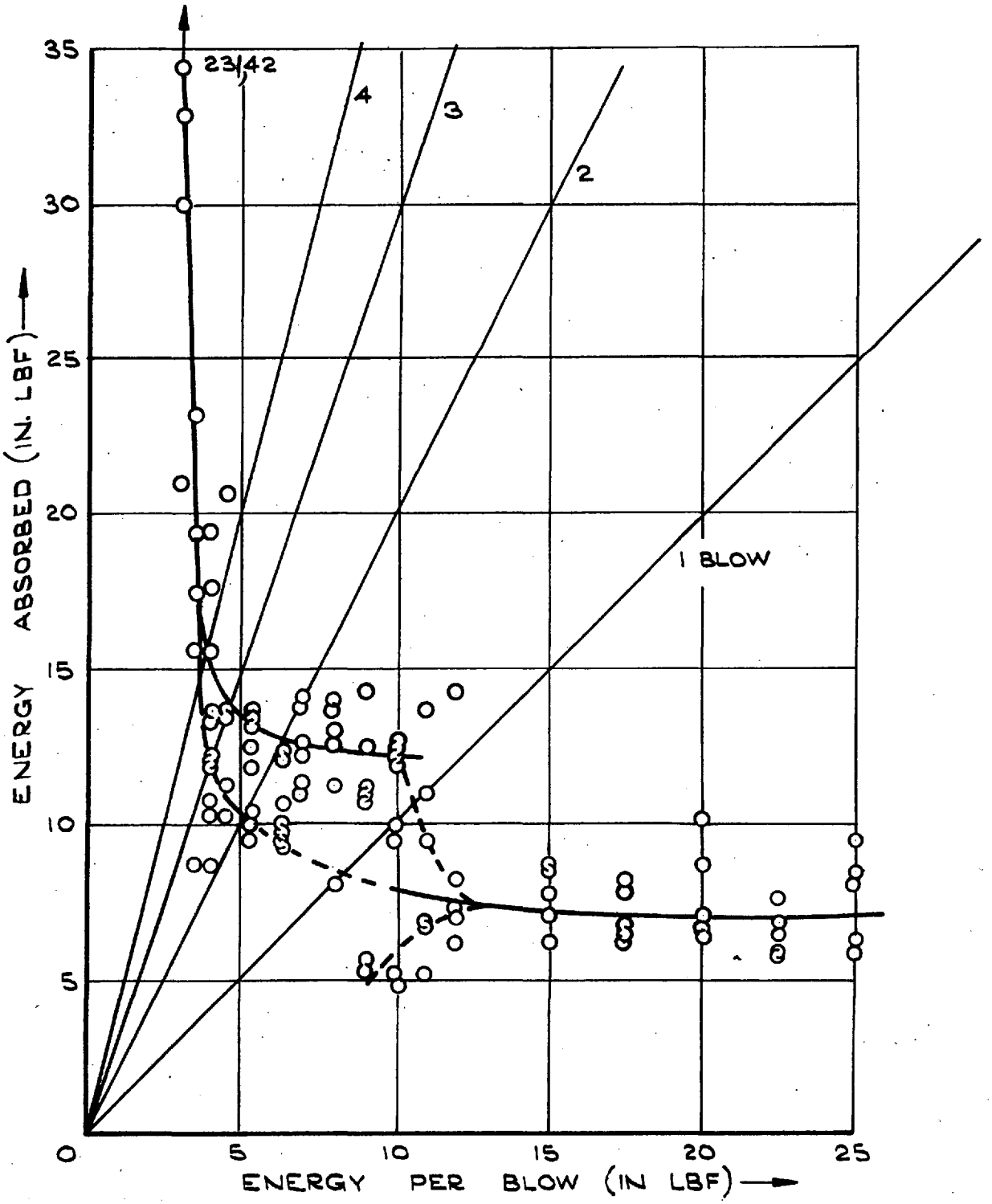

FIG. 61. REPEATED BLOW TEST FOR E 2184 'SPLIT' MATERIAL

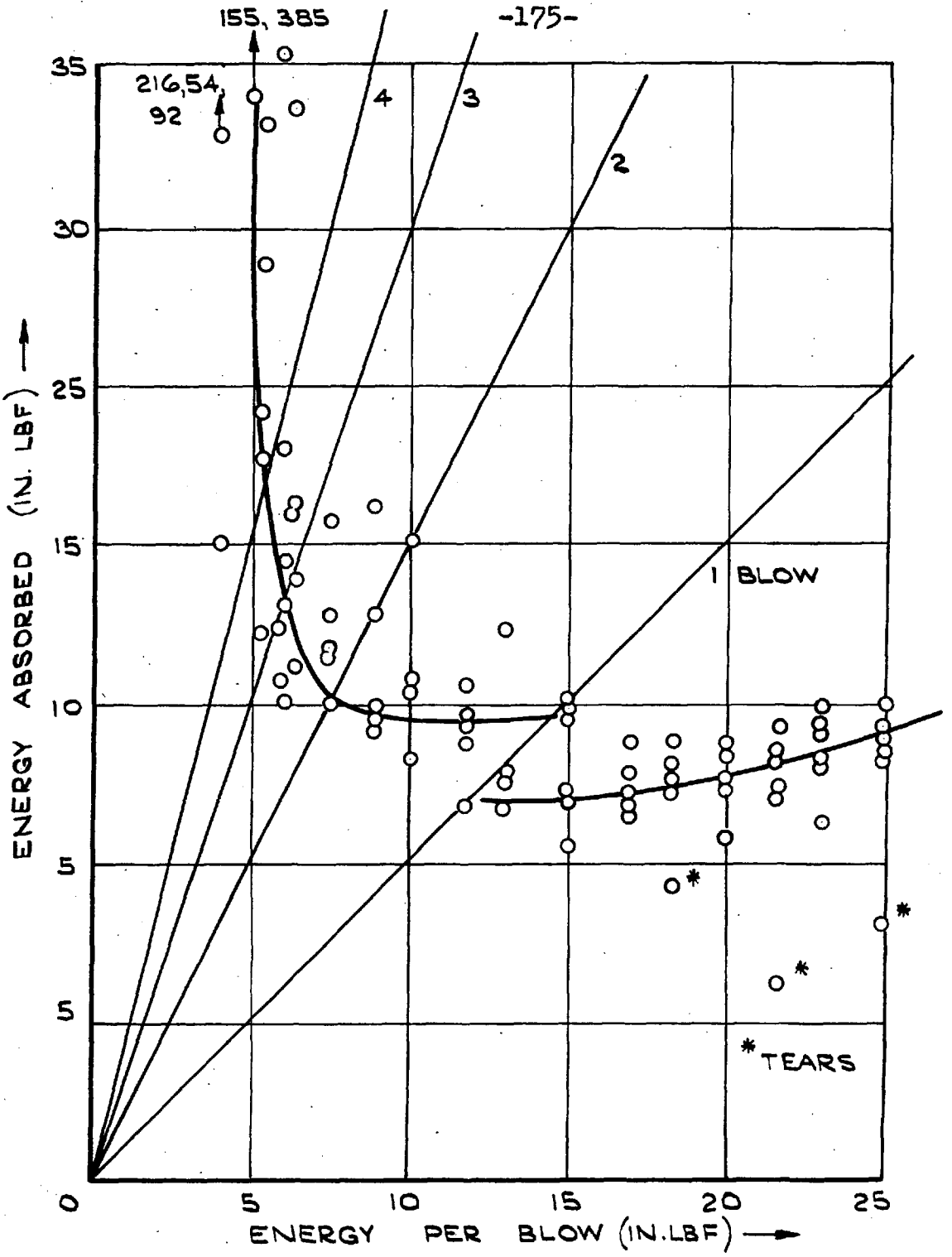

FIG. 62. REPEATED BLOW TEST FOR E2181 'HOLE' MATERIAL.

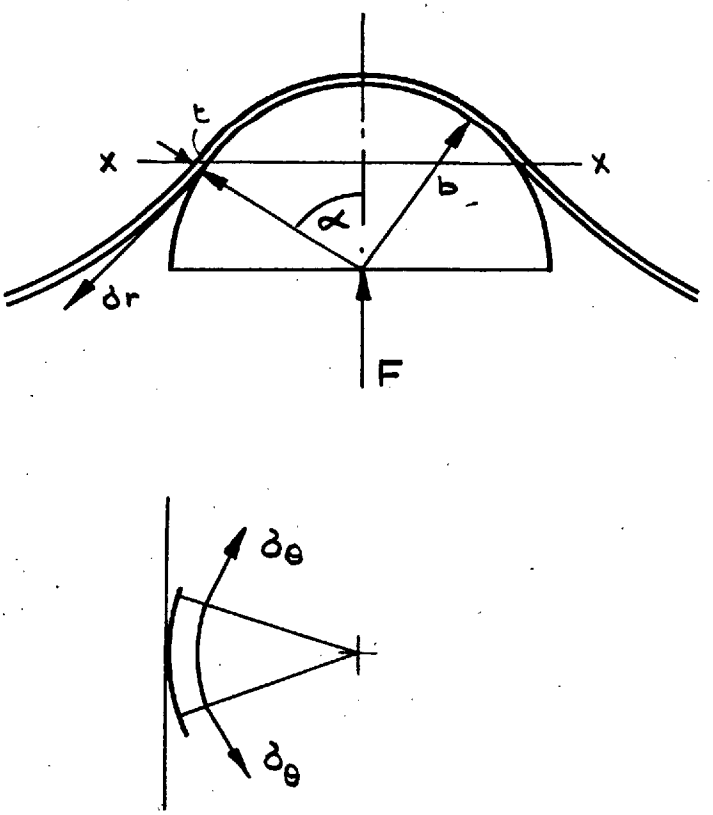

FIG. 63.

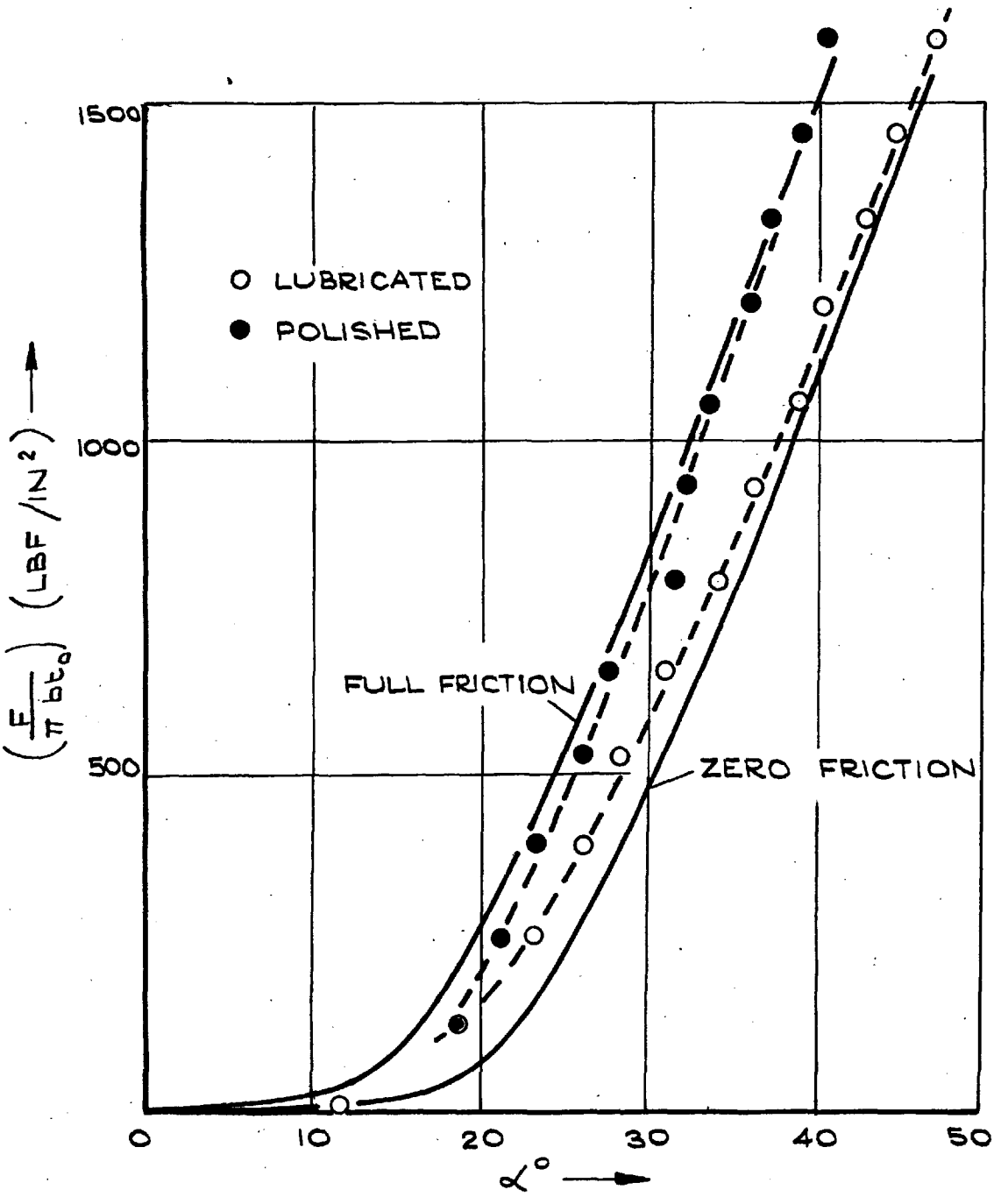

FIG. 64. SEMI-STATIC TEST E2066
FORCE VERSUS ANGLE OF OVERLAP

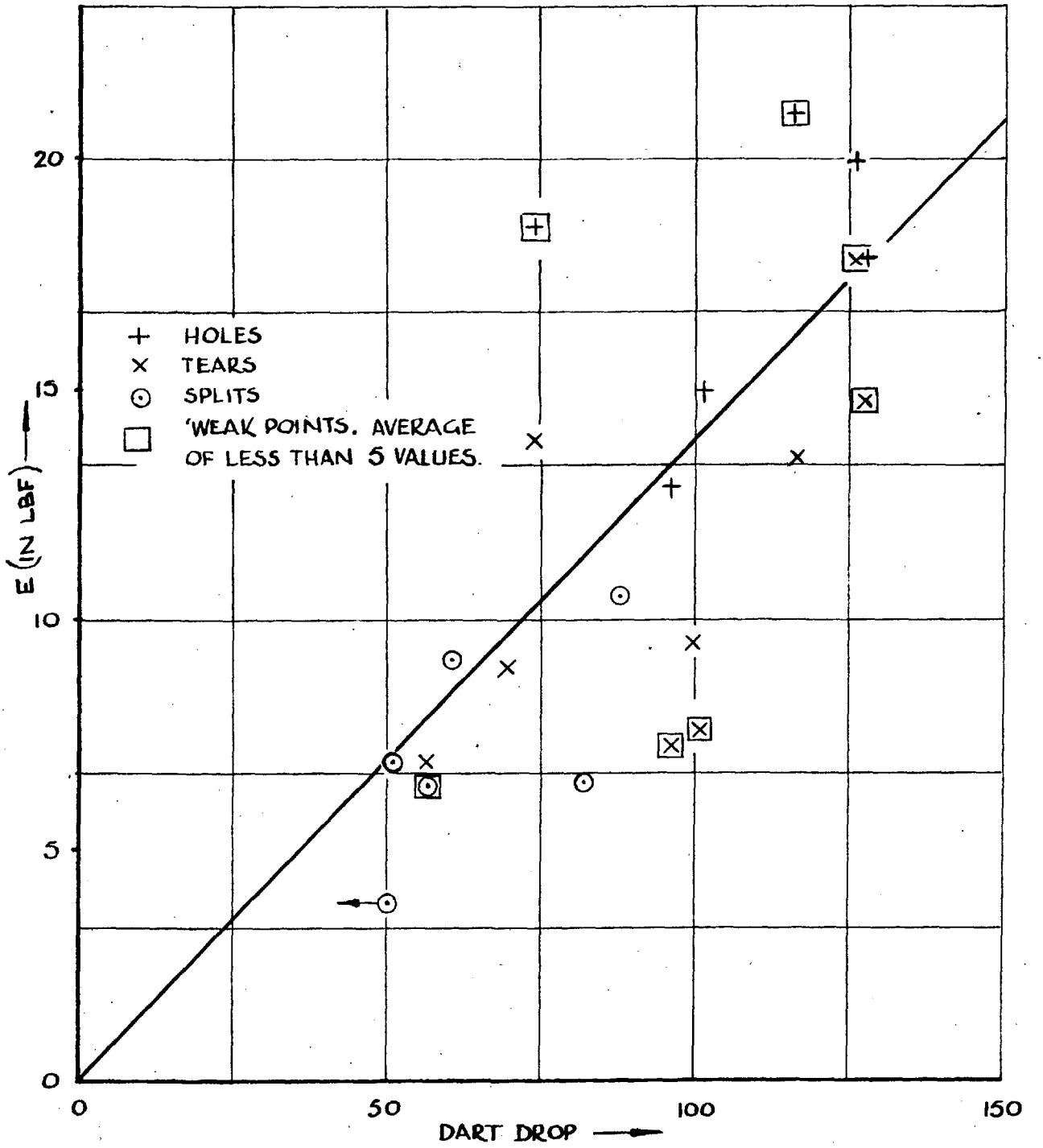

FIG. 65. ENERGY vs. DART DROP VALUE

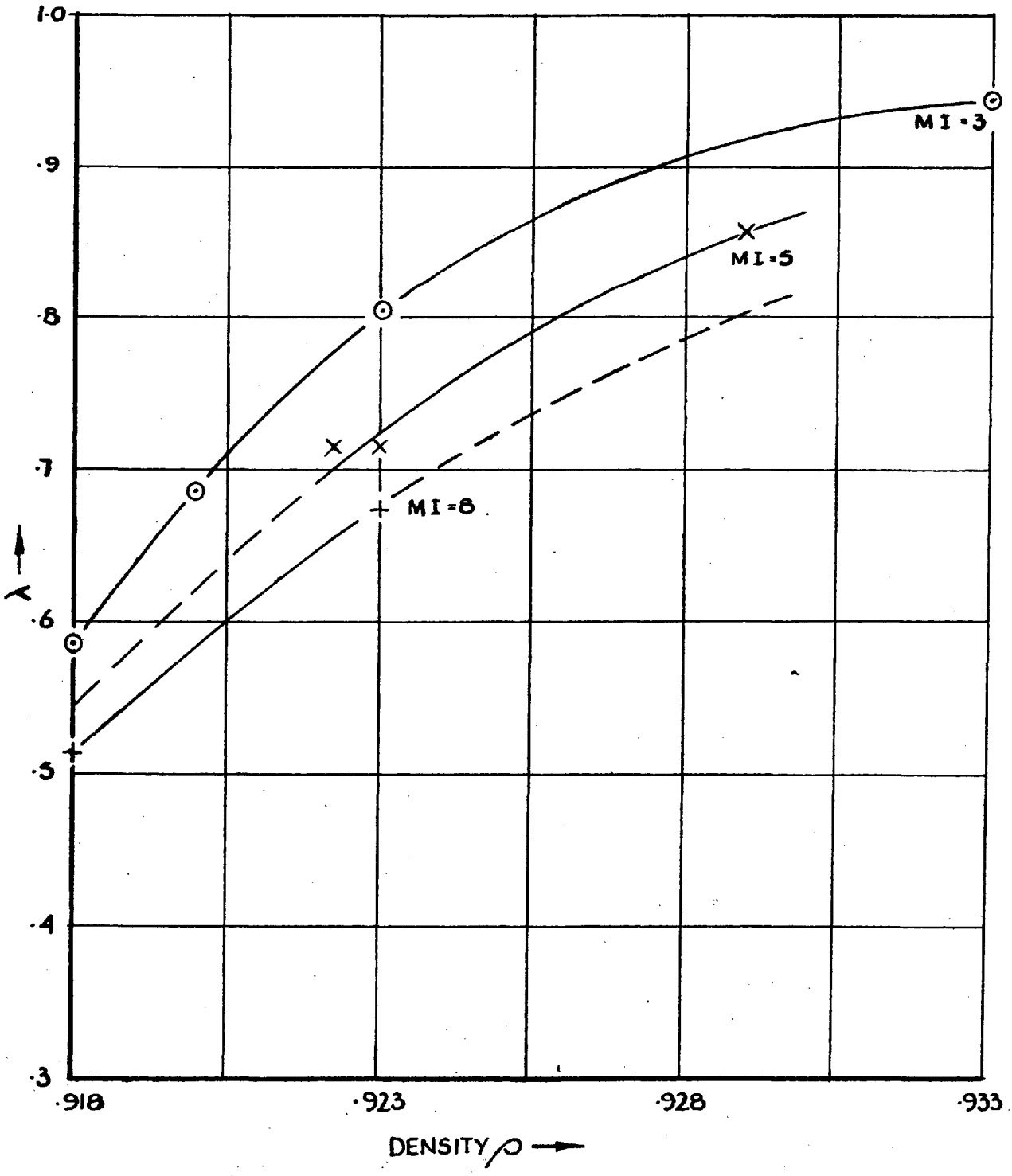

FIG. 66. λ vs. DENSITY FOR THE PLANE STRAIN COMPRESSION TEST

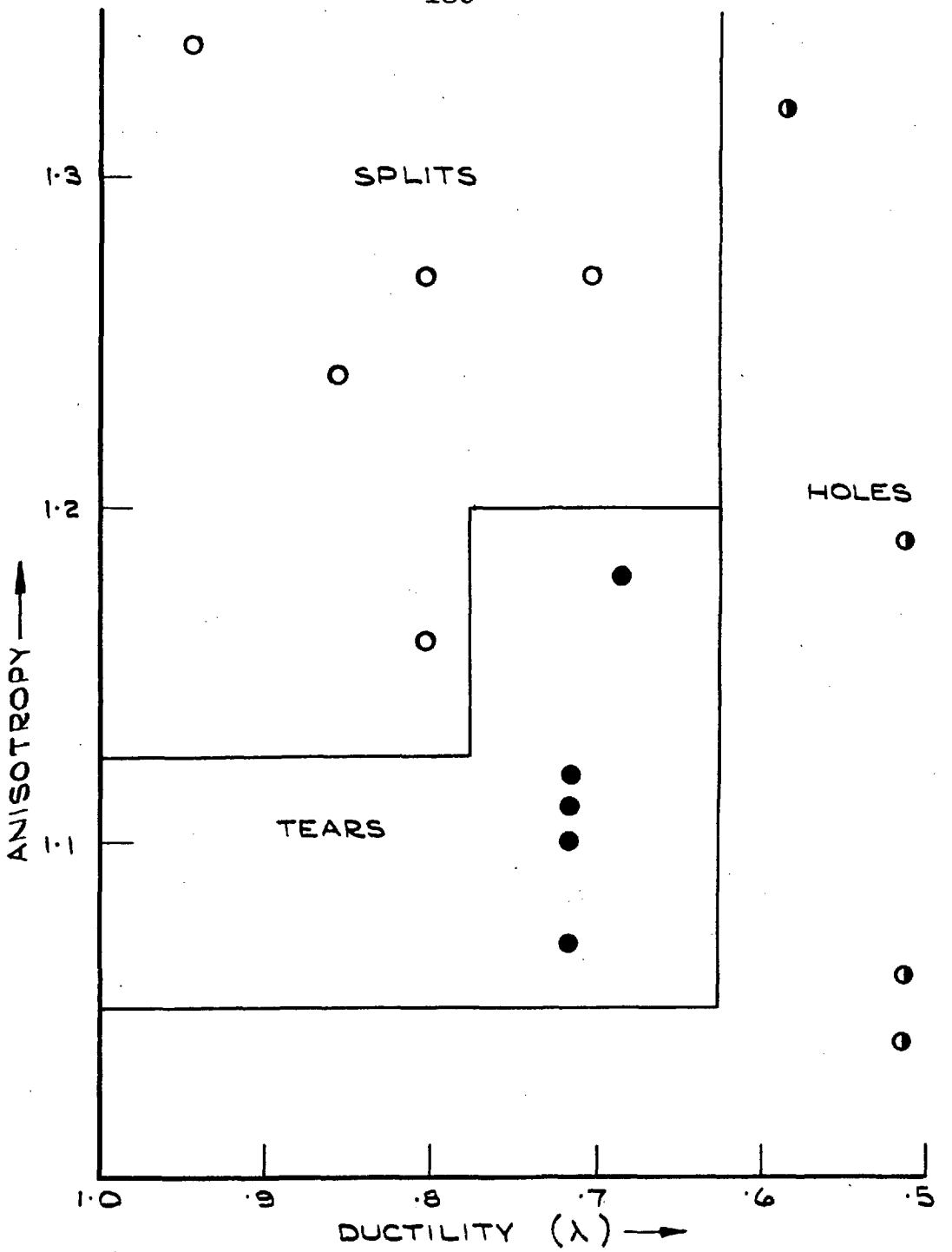

FIG. 67. RELATIONSHIP BETWEEN ANISOTROPY, DUCTILITY AND FRACTURE TYPE.

Table 2. Properties of the materials used in the Impact tests

(1) USI REF.	(2) Density	(3) Melt Index	(4) Film thickness (.001 in)	(5) Film Tensile Data Yield psi	(6) Break psi	(7) Elongation %	(8) Elmendorf Tear gms/mil	(9) Dart Drop gms F_{50}	(10) Pendulum Impact Test Split Energy lb-in	No.	(11) Tear Energy lb-in	No.	(12) Hole Energy lb-in	No.	(13) Plane Strain λ value	(14) Anisotropy factor
E2070	.923	5.0	0.9	MD1440 TD1570	2600 2340	340 560	226 105	57	6.3	2	6.7	8	-	0	.716	1.11
E2069	.923	5.0	1.2	MD1515 TD1545	2445 2225	360 550	240 118	70	-	0	9.0	10	-	0	.716	1.10
E2068	.923	5.0	1.6	MD1550 TD1565	2415 2250	420 560	175 112	74	-	0	13.9	9	18.5	1	.716	1.07
E2183	.922	5.0	1.2	1420 1470	2440 2190	390 550	185 134	100	-	0	9.5	10	-	0	.715	1.12
E2066	.929	5.0	1.5	1775 1885	2300 1850	350 575	154 147	88	10.6	10	-	0	-	0	0.856	1.24
E2064	.918	3.0	1.5	1320 1200	2670 1935	180 470	118 47	127	-	0	16.2	2	19.9	8	.589	1.32
E2184	.923	3.0	1.2	1540 1540	2500 2160	320 500	180 103	82	6.5	10	-	0	-	0	.802	1.16
E2185*	.933	3.0	0.7	1760 1670	2630 1960	380 560	144 232	50	3.8	10	-	0	-	0	.945	1.34
E2180	.918	8.0	0.9	1080 1040	1910 1610	295 400	79 67	97	-	0	7.25	4	12.8	6	.514	1.19
E2181	.918	8.0	1.2	1030 1030	1860 1790	315 460	77 62	102	-	0	7.7	2	14.9	8	.514	1.04
E2182	.918	8.0	1.5	1050 1040	1760 1660	330 435	56 69	128	-	0	14.75	1	17.7	9	.514	1.06
E2186	.929	8.0	1.2	1670 1790	2030 1600	310 540	53 142	51	6.9	10	-	0	-	0	.803	1.27
E1962**	.920	3.0	1.5	1400 1400	2950 2500	375 525	173 93	117	-	0	13.5	9	21.0	1	.685	1.18
E1963**	.924	8.0	1.5	1450 1650	1900 1500	300 375	274 130	61	9.1	10	-	0	-	0	.702	1.27

* Cast film (chill roll)

**- Blow film